

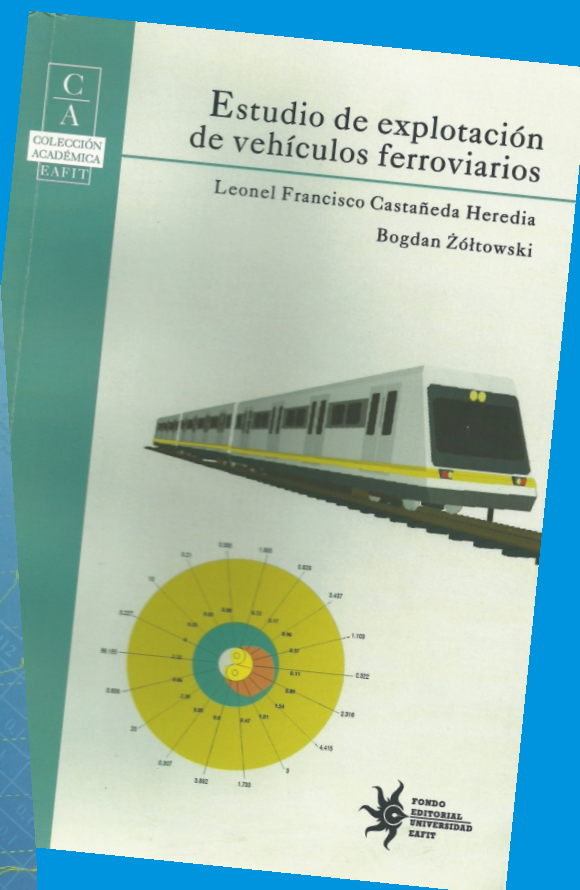
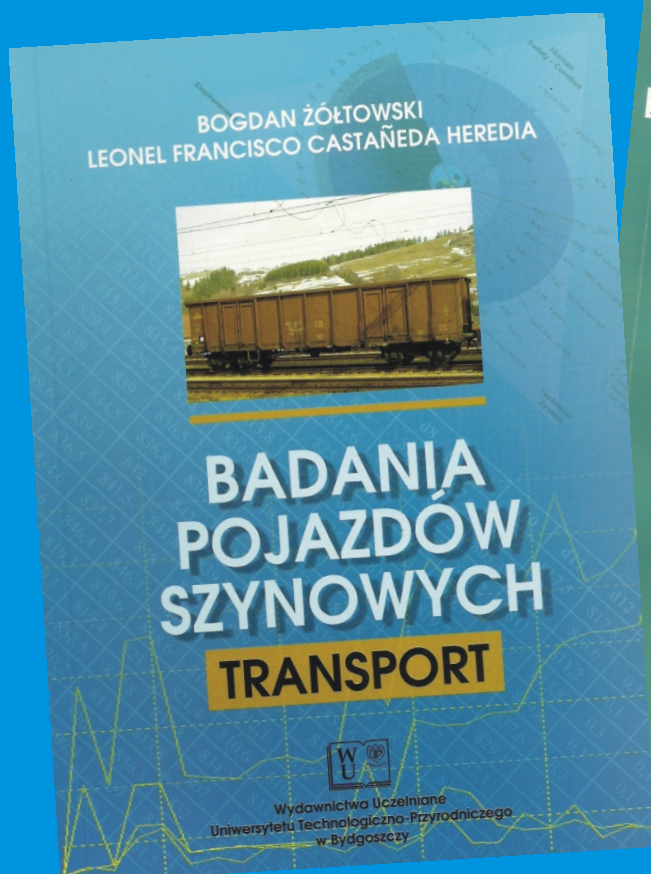


afiliowane przy

Wydziale Nauk
Technicznych
Polskiej Akademii Nauk

Diagnostyka

ISSN 1641-6414



RADA PROGRAMOWA / PROGRAM COUNCIL

PRZEWODNICZĄCY / CHAIRMAN:

prof. dr hab. dr h.c. mult. **Czesław CEMPEL** *Politechnika Poznańska*

REDAKTOR NACZELNY / CHIEF EDITOR:

prof. dr hab. inż. **Ryszard MICHALSKI** *UWM w Olsztynie*

CZŁONKOWIE / MEMBERS:

prof. dr hab. inż. **Jan ADAMCZYK**
AGH w Krakowie

prof. **Jérôme ANTONI**
University of Technology of Compiègne – France

prof. dr. **Ioannis ANTONIADIS**
National Technical University Of Athens – Greece

dr inż. **Roman BARCZEWSKI**
Politechnika Poznańska

prof. dr hab. inż. **Walter BARTELMUS**
Politechnika Wrocławska

prof. dr hab. inż. **Wojciech BATKO**
AGH w Krakowie

prof. dr hab. inż. **Lesław BĘDKOWSKI**
WAT Warszawa

prof. dr hab. inż. **Adam CHARCHALIS**
Akademia Morska w Gdyni

prof. dr hab. inż. **Wojciech CHOLEWA**
Politechnika Śląska

prof. dr hab. inż. **Zbigniew DĄBROWSKI**
Politechnika Warszawska

prof. **Wiktor FRID**
Royal Institute of Technology in Stockholm – Sweden

dr inż. **Tomasz GAŁKA**
Instytut Energetyki w Warszawie

prof. **Len GELMAN**
Cranfield University – England

prof. **Mohamed HADDAR**
National School of Engineers of Sfax – Tunisia

prof. dr hab. inż. **Jan KICIŃSKI**
IMP w Gdańsku

prof. dr hab. inż. **Jerzy KISIŁOWSKI**
Politechnika Warszawska

prof. dr hab. inż. **Daniel KUJAWSKI**
Western Michigan University – USA

prof. dr hab. **Wojciech MOCZULSKI**
Politechnika Śląska

prof. dr hab. inż. **Stanisław NIZIŃSKI**
UWM w Olsztynie

prof. dr hab. inż. **Stanisław RADKOWSKI**
Politechnika Warszawska

prof. **Bob RANDALL**
University of South Wales – Australia

prof. dr **Raj B. K. N. RAO**
President COMADEM International – England

prof. **Vasily S. SHEVCHENKO**
BSSR Academy of Sciences Mińsk – Belarus

prof. **Menad SIDAHMED**
University of Technology Compiègne – France

Prof. **Wiesław TRĄMPCZYŃSKI**
Politechnika Świętokrzyska

prof. dr hab. inż. **Tadeusz UHL**
AGH w Krakowie

prof. **Vitalijus VOLKOVAS**
Kaunas University of Technology – Lithuania

prof. dr hab. inż. **Andrzej WILK**
Politechnika Śląska

dr **Gajraj Singh YADAVA**
Indian Institute of Technology – India

prof. dr hab. inż. **Bogdan ŻÓŁTOWSKI**
UTP w Bydgoszczy

WYDAWCA:

Polskie Towarzystwo Diagnostyki Technicznej
ul. Narbutta 84
02-524 Warszawa

REDAKTOR NACZELNY:

prof. dr hab. inż. **Ryszard MICHALSKI**

SEKRETARZ REDAKCJI:

dr inż. **Sławomir WIERZBICKI**

CZŁONKOWIE KOMITETU REDAKCYJNEGO:

dr inż. **Krzysztof LIGIER**
dr inż. **Paweł MIKOŁAJCZAK**

ADRES REDAKCJI:

Redakcja Diagnostyki
Katedra Budowy, Eksploatacji Pojazdów i Maszyn
UWM w Olsztynie
ul. Oczapowskiego 11
10-736 Olsztyn, Poland
tel.: 89-523-48-11, fax: 89-523-34-63
www.diagnostyka.net.pl
e-mail: redakcja@diagnostyka.net.pl

KONTO PTDT:

Bank PEKAO SA O/Warszawa
nr konta: 33 1240 5963 1111 0000 4796 8376

NAKLAD: 500 egzemplarzy

Wydanie dofinansowane przez Ministra Nauki i Szkolnictwa Wyższego

Spis treści / Contents

M. TOUNSI, F. CHAARI, A.T. FAKHFAKH, M. HADDAR – National School of Engineers of Sfax, Tunisia ..3 Effect of camshaft eccentricity and follower backlash on the dynamic behaviour flexible cam mechanism	
Bohuš LEITNER – University of Žilina, Slovakia, Miroslav KELEMEN – Armed Forces Academy of General Milan Rastislav Štefánik, Slovakia 11 Safety enhancement and fatigue life protection of the lorry frames carrying elements by using of its real working conditions simulation	
Diego GALAR, Luis BERGES – University of Zaragoza, Spain, Jesus ROYO – ZLC Zaragoza Logistics Center, Spain..... 17 Overall Factory Vibration Level: The need for global indicators in CBM	
Tomasz BARSZCZ, Adam JABŁOŃSKI – AGH University of Science and Technology, Krakow25 Selected methods of finding optimal center frequency for amplitude demodulation of vibration signals <i>Wybrane metody znajdowania optymalnej częstotliwości nośnej w procesie demodulacji amplitudowej sygnału drgań</i>	
Anna BZYMEK, Anna TIMOFIEJCZUK – Silesian University of Technology, Gliwice.....29 Welded joint assesment on the basis of an algorithm of characteristic edge detection <i>Ocena poprawności wykonania złączy spawanych z zastosowaniem algorytmu detekcji krawędzi</i>	
Izabela KUTSCHENREITER-PRASZKIEWICZ – University of Bielsko-Biała 37 Reliability estimation in product configuration issue <i>Szacowanie niezawodności w zarządzaniu konfiguracją produktu</i>	
Tomasz GAŁKA – Instytut Energetyki, Warszawa..... 41 Correlation analysis in steam turbine malfunction diagnostics <i>Analiza korelacji w diagnozowaniu uszkodzeń turbin parowych</i>	
Andrzej NIEWCZAS – Technical University of Lublin, Daniel PIENIAK – Main School of Fire Service Warsaw, Agata M. NIEWCZAS – Medical University of Lublin 51 Method of evaluation of degradation of bio-mechanical tooth-composite filling system <i>Metoda oceny degradacji systemu biomechanicznego zęb - wypełnienie kompozytowe</i>	
Wojciech JAMROZIK – Silesian University of Technology at Gliwice 59 An example of surface fault estimation on the basis of super-resolution approach <i>Przykład estymacji wad powierzchniowych z zastosowaniem nadrozdzielczości</i>	
Zenon SYROKA – Uniwersytet Warmińsko – Mazurski w Olsztynie 65 Próbkowanie sygnałów diagnostycznych. Część V. Próbkowanie sygnałów o nieograniczonym paśmie za pomocą nieklasycznych jąder <i>Sampling of the diagnostic signals. Part V. Signal sampling with infinite frequency band using non clasical kernels</i>	
Nadanie "Medalu im. Profesora Stefana Ziembę" profesorowi dr. hab. inż. Bogdanowi ŻÓŁTOWSKIEMU 71	
Warto przeczytać / Worth to read 73	

EFFECT OF CAMSHAFT ECCENTRICITY AND FOLLOWER BACKLASH ON THE DYNAMIC BEHAVIOUR FLEXIBLE CAM MECHANISM

M. TOUNSI, F. CHAARI, MS. ABBES T. FAKHFAKH, AND M. HADDAR

Mechanical Systems Dynamic Research Unit, National School of Engineers of Sfax, Sfax, Tunisia

e-mail: tounsienis@yahoo.fr

Summary

A cam follower system is modelled in this work. The equation of motion and the eigenfrequencies are recovered. The computation of the dynamic response is made by mean of combined implicit Newmark-Newton Raphson algorithm. Moreover, dynamic behaviour of the follower train is analysed in presence of an eccentricity in the camshaft and backlash between the follower rods and its guide.

Key words: Cam, follower, dynamic response simulation, camshaft eccentricity, follower backlash.

INTRODUCTION

A cam follower system may be defined as a machine element having a curved outline or a curved groove, which, by its oscillation or rotation motion, gives a predetermined specified motion to another element called the follower. The cam has a very important function in the operation of many classes of machines, especially those of the automatic type, such as printing presses, shoe machinery, textile machinery, gear-cutting machines, screw machines, and automobiles. The performance of such cam follower systems can be evaluated by the precision of the follower motion. In high-speed cam follower mechanism, high precision of the follower motion become increasingly important especially in automatic machines. Several studies have yielded a vast literature on this topic [1-4]. Backlash errors or wear of the parts of the cam-follower system can cause an excessive vibration and noise [5, 6]. Dynamic analysis of cam-follower system have been of great interest by several researchers to investigate the possible factors which cause the deviation of the follower output from the desired one. Kim and Newcombe [7, 8] investigated the combined effects of three sources of errors: geometric inaccuracy, kinematic errors and dynamic effects. Grewal and Newcombe [9] studied the effect of machining errors of the contact surfaces on the motion of the follower. By an experimental study Norton [10, 11] investigated the effect of variation in manufacturing tolerance on the dynamic performance of eccentric and double dwell cams. Rao [12] developed relationships between the design parameters of the follower train for minimum flexibility error and optimum sensitivity synthesis of cam mechanisms. Wu and Chang [13, 14] presented an analytical method for analysing the mechanical errors of disk cam mechanisms with a flat-faced follower. In a recent work Wu and Chang [15] developed a computerized method based on the concept of the simulated higher-pair contact analysis to perform the

tolerance analysis of disk cam mechanisms with roller follower.

All of geometric, kinematics errors and dynamic effects may influence the dynamic behaviour of the cam follower mechanism [16, 17, 18]. In this work, a dynamic analysis of a cam-follower mechanism with translating follower is performed. The system is modelled with seven-degrees-of-freedom model. The developed model includes the possibility of having a camshaft eccentricity error or a backlash between the follower rod and its guide. The paper is organized in the following manner: in section 2 the cam follower model is presented, the equation of motion and the parametric expression for the cam profile are developed. Section 3 is devoted to numerical simulations of the dynamic response with and without errors.

1 ANALYTICAL FORMULATION

1.1 The cam follower system model

In this work, the adopted model is derived from that developed by Kim and Newcomb [8]. This model with seven-degrees-of-freedom include nonlinear contact between cam and follower, flexible camshaft bearing and follower rod (figure 1). M_{eq} is the mass of the follower; x_i and y_i represent respectively the horizontal and vertical displacement of the camshaft and the follower. h , is the programmed motion machined on the cam. Suitable dampings are introduced in parallel with stiffness. Applying Lagrange formulation yield to the equation of motion [8]:

$$M \ddot{q} + C \dot{q} + K q = F(t) \quad (1)$$

with $q = \langle y_1, y_2, y_3, y_4, x_1, x_2, x_3 \rangle^T$ is the vector of degrees of freedom

M is the mass matrix, K is the stiffness matrix, C is the damping matrix and F is the nonlinear time varying force vector.

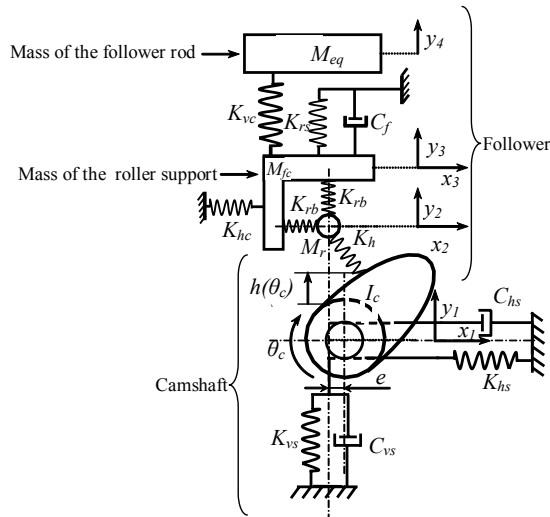


Fig. 1. Schematic representation of the cam-follower dynamic model

1.2 Parametric expression for the cam profile

In order to investigate how the manufacturing, assembling and wear errors affecting the dynamic behavior of the cam follower system, the analytical expressions for the theoretical cam profile should be determined. Figure 2 shows a disk cam mechanism with offset translating roller follower. The concept of velocity instant center is used to recover the cam profile [19-21].

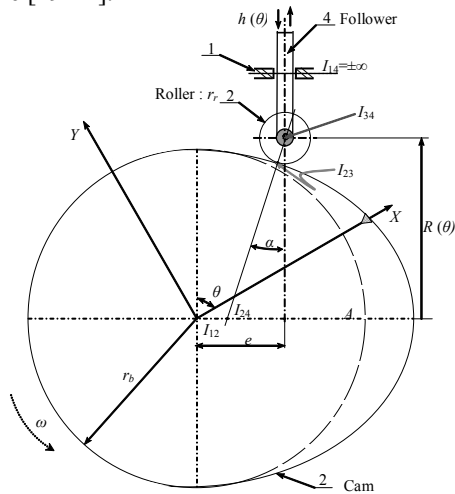


Fig. 2. Cam disk with an offset translating roller follower

The instant center between link i and j is denoted by I_{ij} , the theoretical offset reference point is denoted by A .

The links are numbered in the following way:

The ground link is numbered as 1, the cam as 2, the follower roller as 3 and the follower rod as 4.

The pressure angle, α , the nominal displacement of the follower, $h(\theta)$, the theoretical follower offset and the camshaft angular velocity, $\omega = d\theta/dt$, can be related from rigid body kinematic [21].

The velocity of instant center I_{24} is given by:

$$V_{I_{24}} = \frac{dR(\theta)}{d\theta} \omega \quad (1)$$

The displacement function of the follower can be expressed as:

$$R(\theta) = \sqrt{(r_b + r_r)^2 - e^2} + h(\theta) \quad (2)$$

Here, r_b is the radius of the base circle, r_r is the radius of the follower roller and e is the offset.

When the instant center I_{24} is assumed to be on link 4, this velocity is given as:

$$V_{I_{24}} = dh/dt \quad (3)$$

From the triangle $I_{24} A I_{34}$, the pressure angle α can be expressed as:

$$\alpha = \tan^{-1} \left(\frac{I_{12} I_{24} - e}{R(\theta)} \right) \quad (4)$$

The parametric vector equations of the theoretical cam profile coordinates are [22]:

$$R_T(\theta) = \begin{Bmatrix} R_T(\theta) \\ R_T(\theta) \end{Bmatrix} = I_{12} I_{23} \quad (5)$$

$$I_{12} I_{23} = \begin{Bmatrix} R(\theta) \cos \theta - e \sin \theta - r_r \cos(\theta - \alpha) \\ R(\theta) \sin \theta + e \cos \theta - r_r \sin(\theta - \alpha) \end{Bmatrix}$$

1.3. Modeling of cam-follower defect

Parts cannot be made to ideal or design dimensions because inaccuracies are inherent in manufacturing process. In this section we recognize this imperfection as errors.

For the purpose of studying the effects of manufacturing or assembling errors, two defect cases are considered. Firstly, an eccentricity error between the camshaft and its bearing is considered. This analysis will be done by considering a disk cam with in line translating follower and an offset translating follower. Secondly, a backlash error between the follower rod and its support is considered.

1.3.1. First case (Eccentricity error of the camshaft bearing)

In this case we assume that we have an eccentricity on the camshaft. The eccentricity expresses the difference between the theoretical and the real rotational axis (figure 3a). This defect is introduced by adding a transmission error modeled as displacement on the line of action between the cam and the roller. Figure 4 show a schematic diagram of the eccentricity error of a disk cam with an offset translating roller follower. The introduction of this displacement in the equation of motion yields to an exciting force. As a result, an amplitude modulation of the contact force between the cam and the follower in the vertical direction is expected [23].

$$F(t) = \Delta e_c(t) K_h \quad (6)$$

$$\Delta e_c(t) = \overline{\Delta e_c} \sin(\omega t + \zeta) \quad (7)$$

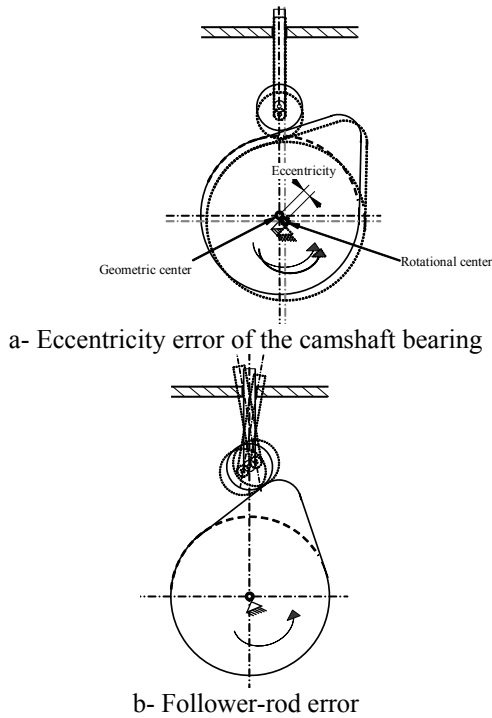


Fig. 3. Schematic representation of the cam-follower errors

This eccentricity error provides a pressure angle and an offset variation ($\Delta\alpha$ and Δe). The instantaneous contact point varies from I_{23} to I'_{23} with corresponding angle θ , (Here the deviation of eccentricity is exaggerated for clarity purposes). From the parametric vector $R_T(\theta)$ of the theoretical cam profile coordinates given in equations 5, the new position vector $R_T^*(\theta)$ of the contact point I'_{23} in term of the cam rotation angle can be expressed as:

$$R_T^*(\theta) = \begin{Bmatrix} R_{T_x}^*(\theta) \\ R_{T_y}^*(\theta) \end{Bmatrix} = I_{12}^* I_{23}^* \quad (8)$$

$$I_{12}^* I_{23}^* = \begin{Bmatrix} R^*(\theta) \cos \theta - e^* \sin \theta - r_r \cos(\theta - \alpha^*) \\ R^*(\theta) \sin \theta + e^* \cos \theta - r_r \sin(\theta - \alpha^*) \end{Bmatrix} \quad (9)$$

Where

$$e^* = e \pm \Delta e_x \quad (9)$$

$$R^*(\theta) = \sqrt{(r_b + r_r)^2 - e^{*2}} + h(\theta) \quad (10)$$

The pressure angle which depends of the new position vector will be expressed as follow:

$$\alpha^* = \tan^{-1} \left(\frac{I_{12}^* I_{24}^* - e^*}{R^*(\theta)} \right) \quad (11)$$

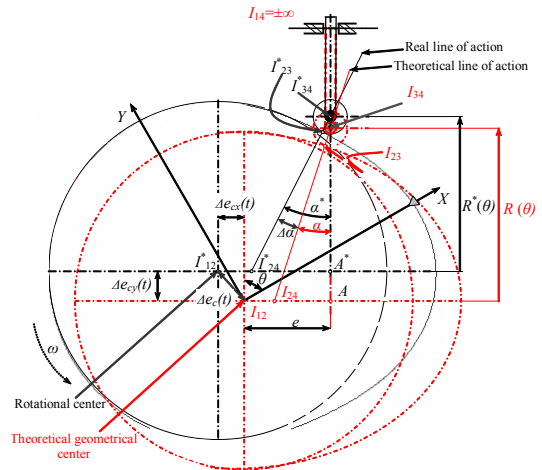


Fig. 4. Schematic diagram of the eccentricity error on the disk cam with an offset translating roller follower

1.3.2. Second case (Follower-rod error)

In this case we assume that we have a backlash error between the follower rod and the frame. This backlash error expresses the additional clearance caused by tolerances (figure 3b). Figure 5 show a schematic diagram of a backlash error between the follower rod and the frame on the disk cam with an offset translating roller follower in the two extreme cases. Because of a backlash error between the follower rod and the frame two defect positions of the follower can be observed depending on the period rising or return. These two defects position will provide follower direction change, a pressure angle and an offset variation ($\Delta\alpha$ and Δe).

This effect is introduced by adding a transmission error modeled as a displacement of the follower-roller-support in horizontal direction. Which yield to an exiting force in then horizontal direction of the bearing.

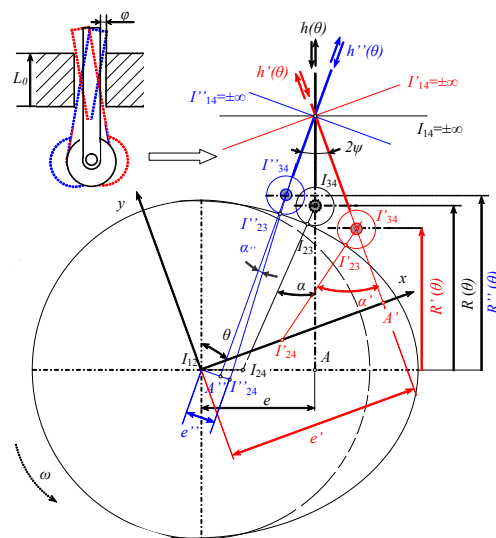


Fig. 5. Schematic diagram of a backlash error between the follower rod and the frame on the disk cam with an offset translating roller follower

The instantaneous contact point varies from point I_{23} to point I'_{23} or I''_{23} with corresponding angle θ . The new position vectors $R'_T(\theta)$ and $R''_T(\theta)$ in the two limit cases in term of the cam rotation angle can be expressed as:

$$R'_T(\theta) = \begin{Bmatrix} R'_{T_x}(\theta) \\ R'_{T_y}(\theta) \end{Bmatrix} = I_{12}I'_{23}$$

$$I_{12}I'_{23} = \begin{Bmatrix} R'(\theta)\cos\theta - e'\sin\theta - r_r\cos(\theta - \alpha') \\ R'(\theta)\sin\theta + e'\cos\theta - r_r\sin(\theta - \alpha') \end{Bmatrix} \quad (12)$$

$$R''_T(\theta) = \begin{Bmatrix} R''_{T_x}(\theta) \\ R''_{T_y}(\theta) \end{Bmatrix} = I_{12}I''_{23}$$

$$I_{12}I''_{23} = \begin{Bmatrix} R''(\theta)\cos\theta - e''\sin\theta - r_r\cos(\theta - \alpha'') \\ R''(\theta)\sin\theta + e''\cos\theta - r_r\sin(\theta - \alpha'') \end{Bmatrix} \quad (13)$$

$$e' = e + \Delta e \quad \text{and} \quad e'' = e - \Delta e$$

$$\psi = \tan^{-1}\left(\frac{2\varphi}{l_0}\right) \quad (14)$$

Then the two positional vectors can be expressed by:

$$R'(\theta) = \sqrt{(r_b + r_r)^2 - e'^2} + h(\theta) \quad (15)$$

and,

$$R''(\theta) = \sqrt{(r_b + r_r)^2 - e''^2} + h(\theta) \quad (16)$$

The pressure angles in the two limit positions are:

$$\alpha' = \tan^{-1}\left(\frac{I_{12}I'_{24} - e'}{R'(\theta)}\right) \quad (17)$$

and

$$\alpha'' = \tan^{-1}\left(\frac{I_{12}I''_{24} - e''}{R''(\theta)}\right) \quad (18)$$

2. NUMERICAL SIMULATIONS

In this section, results from simulation performed with healthy cam-follower system are compared with those computed with system having errors. The profile of the cam is computed by using modified trapezoidal curves (table 1). The parameter of the cam follower system are given in table 2 and the natural frequency are given in table 3. The rotational speed of the camshaft is 750 rpm.

Table 1. The cam's motion curves

	Follower motion			
	Dwell	Rise	Dwell	Return
Cam angle interval	0 ~ 30°	30° ~ 180°	180° ~ 210°	210° ~ 360°
Name of the curve		Modified trapezoidal		Modified trapezoidal

Table 2. The cam-follower system parameters

Mass (Kg)	$M_{eq}=1.36, M_f=0.340, M_{fc}=0.07$
Linear damping coefficients (N.sec/m)	$C_{vs}=C_{hs}=750, C_f=0.08,$
Linear stiffness (N/m)	$K_{vs}=K_{hs}=2.6 \cdot 10^8, K_{rb}=K_{hc}=K_f=2.5 \cdot 10^8, K_{rs}=1.4 \cdot 10^4, K_{vc}=1.7 \cdot 10^8, K_h=1.9 \cdot 10^8,$
Spring initial deformation K_{rs} (mm)	$\delta_{rs}=13$
Follower total rise (mm)	$h_{max}=10$
Diameter of cam base circle (mm)	$2R_a=60$
Diameter of follower roller (mm)	$2R_1=16$
Follower offset (mm)	$e=10$

Table 3. Natural frequency of the system (Hz)

f_{01}	f_{02}	f_{03}	f_{04}
2447	2447	5711	12777
f_{05}	f_{06}	f_{07}	
13990	17009	17009	

2.1. Healthy case

In this study a disk cam with an offset translating follower is considered. Fig. 6 and 7 show respectively the variation of the contact force and the effect of flexibility on the follower acceleration.

It is well observed that contact force is time varying and periodic at the cam rotational period $T_r=0.08$ s. Also there are fluctuations much more observed on the rise period than in the return period because of the greater acceleration fluctuation produced by the modified trapezoidal motion. Furthermore the contact force between the cam and the roller is variable according to the position of the follower and depends on the particular combinations of K_{rs} spring force and positive or negative inertia forces that occur. Figure 8 show the camshaft bearing amplitude acceleration, this acceleration reaches its maximum amplitude around f_{01} and at $2/5 f_{01}$. We think that $2/5 f_{01}$ is induced by the parametric resonance caused by the time varying Hertzian stiffness whose spectrum is presented in fig 9.

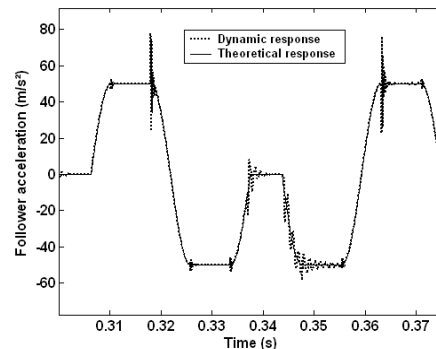


Fig. 6. Dynamic and theoretical response of the follower acceleration over one period

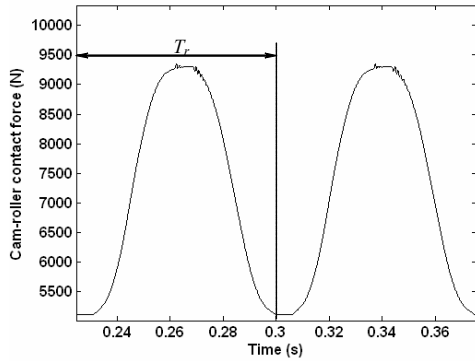


Fig. 7. Variation of the contact force

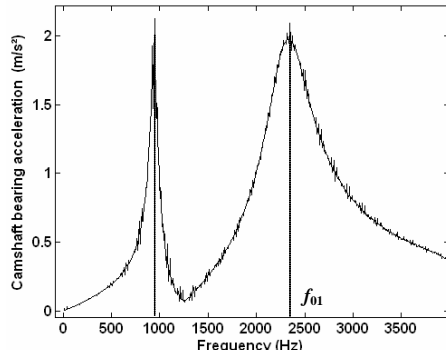


Fig. 8. Frequency response of the camshaft bearing acceleration

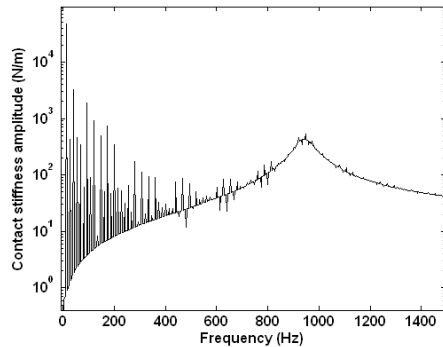


Fig. 9. Frequency response of the contact stiffness cam-roller

2.2. Defect cases

In this study two defect cases are considered. In the first one, we will consider an eccentricity of 10 μm on the camshaft. In the second case, a backlash of 10 μm between the follower rod and its frame is considered.

2.2.1. First case (eccentricity error)

Figure 10 shows the effect of the eccentricity error on follower acceleration. It is well noticed that the amplitude of the follower acceleration has increased especially on the dwell period where the follower reach its maximum value. As for the contact force (figure 11) we can observe the same phenomena. On the other hand, the camshaft bearing acceleration presents an amplitude modulation compared with the healthy case (figure 12).

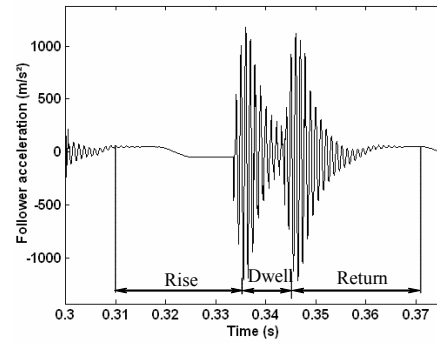


Fig. 10. Effect of an eccentricity error on the follower acceleration

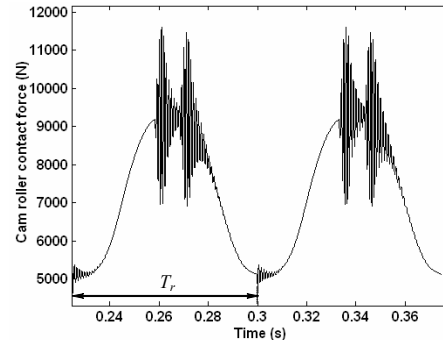


Fig. 11. Effect of the eccentricity error on the contact force

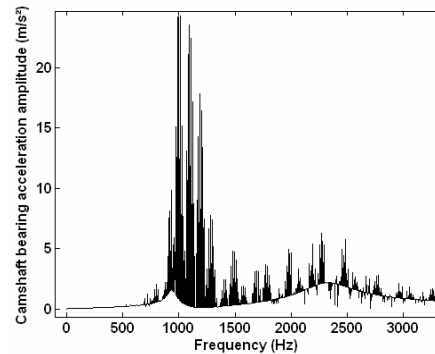


Fig. 12. Frequency response of the camshaft bearing acceleration for an eccentricity error

2.2.2. Second case (follower backlash error)

In this case amplitude of the follower acceleration (figure 13) and the contact force (figure 14) have increased especially on the two dwell periods when the follower reaches its maximum ($h = h_{max}$) and its minimum value ($h = 0$). This can be explained by the fact that the existence of the backlash allow the follower rod to oscillate in the two lateral directions. Figure 15 show the camshaft bearing acceleration which present an amplitude modulation compared with the healthy case, however this modulation is less important than for the eccentricity error case.

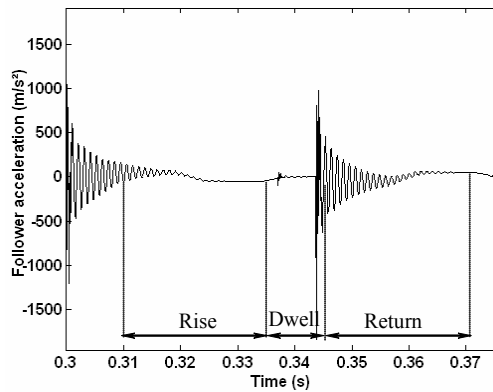


Fig. 13. Effect of backlash follower error on the follower acceleration

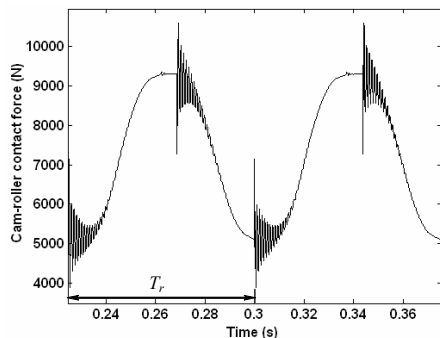


Fig. 14. Effect of a follower backlash error on the contact force

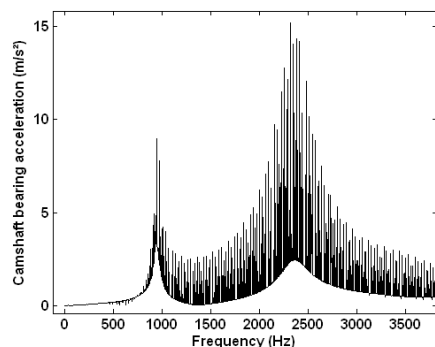


Fig. 15. Frequency response of the camshaft bearing acceleration for a follower backlash error

3. Conclusion

In this paper, seven degrees of freedom of a cam follower system is modeled and simulated in order to look at its dynamic behavior in presence of an eccentricity and a follower backlash errors induced by manufacturing imprecision and wear of the part of the cam follower system. It was shown that the flexibility of the system affects the dynamic behavior of the system. In fact, fluctuations are observed in the follower accelerations: when the errors are introduced, the fluctuations of the follower acceleration become greater and this will produce higher vibration levels included by amplitude modulation phenomenon.

Reference

- [1] H. A. Rothbart : *Design, dynamic and accuracy*. Wiley New York, Edition 1956.
- [2] M. P. Koster: *Effect of flexibility of driving shaft on the dynamic behaviour of a cam mechanism*. J. Eng. Ind, (1975), 595-602.
- [3] F. Giordana, V. Rognoni, G. Ruggieri: *On the influence of measurement error in the kinematic analysis of cam*. Mech. Mach. Theory, 14 (1979), 327-340.
- [4] J. L. Wiederrich, B. Roth: *Cams and Cam Mechanisms* (J. Recs Jones, Ed.). pp. 1-15. Mechanical Engineering.
- [5] M. N. AMBARDEKAR, K. N. GUPTA: *Stochastic optimal control of vibrations of a high-speed cam-driven mechanism*. Mech. Mach. Theory, 25 (1990), 59-68.
- [6] P. D. Lin, J. F. Chen, *Analysis of errors in precision closed-loop mechanisms*. J. Mech.Des. ASME, (1992).
- [7] H. R. Kim, W.R. Newcombe: *Stochastic error analysis in cam mechanisms*. Mechanism and Machine Theory, 1978, 13, 631-641.
- [8] H. R. Kim, W. R. Newcombe: *The effect of cam profile errors and system flexibility on cam mechanism output*. Mechanism and Machine Theory, 1982, 17, 57-72.
- [9] P. S. Grewal, W. R. Newcombe: *A comparative study of cam motions for high-speed semi-rigid follower cam systems*. Mech. Mach. Theory, 23 (1988), 121-133.
- [10] R. L. Norton: *Effect of manufacturing method on dynamic performance of cams- an experimental study*. Part I Double Dwell Cams. Mech. Mach. Theory, 23 (1988), 191-199.
- [11] R. L. Norton: *Effect of manufacturing method on dynamic performance of cams- an experimental study*. Part II Double Dwell Cams. Mech. Mach. Theory, 23 (1988), 200-208.
- [12] A. C. Rao: *Minimum flexibility error and optimum sensitivity synthesis of cam mechanisms*. Mech. Mach. Theory, 14 (1979), 209-214.
- [13] L-I. Wu, W-T. Chang: *Analysis of mechanical errors in disk cam mechanisms*. J. Mech. Eng. Scie. IMech 219 part C (2005), 209-224.
- [14] W-T. Chang, L-I. Wu: *Mechanical error analysis of disk cam mechanisms with flat-faced follower*. J. Mech. Sci. Tech, 20 (2006), 345-357.
- [15] W-T. Chang, L-I. Wu: *Computerized tolerance analysis of disk cam mechanisms with a roller follower*. Springer. Eng. Comp, 25 (2009), 247-260.
- [16] V. Niola, G. Quaremba, M. Ceccarelli: *On the Effect of Dynamical Behaviour of Cam-Follower System Damaged on Contact Surface*, WSEAS Trans. On Circuits and Systems, 3, (2004), 599-602.
- [17] Y. A. Yao, H. S. Yan, C. Zhang: *A variable speed method for reducing residual vibrations in elastic cam-follower system*. J. Dyn. Sys. Meas. Cont. Trans. ASME, 125 (2003), 480-482.

- [18] T. L. Dresner, P. Barkan: *New methods for dynamic analysis flexible single input multi input cam follower systems*. J. Mech. Des., 117 (1995), 150-155.
- [19] J. K. Davidson: *Calculating cam profiles quickly*, Machine design (1978) 151-155.
- [20] L-I. Wu: *Calculating conjugate cam profiles by vector equations*, J. Mech. Eng. Science, 217 (10) (2003), 1117-1123.
- [21] L-I. Wu, C-H. Liu, K-L. Shu, S-L. Chou: *Disk cam mechanisms with a translating follower having symmetrical double rollers*, Mech. Mach. Theory, 44 (2009), 2085-2097.
- [22] W-T. Chang: *Analysis of mechanical errors in planar cam mechanisms and its applications*. PhD dissertation. National Tsing Hua University, Hsinchu.
- [23] T. Hidaka, Y. Terauchi, K. Dohi: *On the relation between the run-out errors and the motion of the center of sun gear in a Stoeckicht planetary*. Bull JSME 22 (1979), 748-754.

SAFETY ENHANCEMENT AND FATIGUE LIFE PROTECTION OF THE LORRY FRAMES CARRYING ELEMENTS BY USING OF ITS REAL WORKING CONDITIONS SIMULATION

Bohuš LEITNER¹, Miroslav KELEMEN²

¹University of Žilina, Faculty of Special Engineering,
Department of Technical Sciences and Informatics,
ul.1.mája 32, 010 26 Žilina, Slovakia
E-mail: Bohus.Leitner@fsi.uniza.sk

²Armed Forces Academy of General Milan Rastislav Štefánik,
Demänová 393, Liptovský Mikuláš, Slovakia
E-mail: rektor@aos.sk

Summary

The goal of this paper will be to present FEM application in the TATRA 815 lorry frame structure fatigue life estimation. Structure critical nodes from the fatigue damage point of view have been found and analyzed. Analysis of the particular traffic states influence on the fatigue damage cumulation is going to be presented too.

Keywords: working conditions, dynamic analysis, cumulative damage, computer simulation, fatigue life prediction.

1. INTRODUCTION

The goal of this paper is to present the selected results of the computer simulation analysis of the lorry frames fatigue damage. This simulation concentrates to the most important aspects which are typical for transport means working conditions, using of the obtained computational models for a working exciting simulation of a real lorry structure, dynamic analysis of the vehicle critical parts stress under the influence of typical working conditions, the fatigue life prediction of the analyzed vehicle most exposed parts. During the computational simulation of the chosen vehicle (TATRA 815 S2 – Fig. 1) under the modelled conditions of its service, it was necessary to consider that it is a kind of vehicle whose traffic conditions are determined mainly by the influence of the following aspects: roadways and terrain surface unevenness and traffic velocity.



Fig. 1. Tatra 815 S2

2. ANALYZING PARTS OF VEHICLE

It is well known from the technical publications and from the similar performed analyses of the various transportation vehicles kinds, that the most loaded lorry parts are their bearing members (bearing frames, subsidiary bearing structures) and axles. They carry the loads occurred at the interaction of the vehicle instantaneous weight influence and roadways surface undulation influence in synergy with chosen traffic velocity. This is the reason why the presented description is oriented mainly to these structure entities. Vehicle TATRA 815 S2 as lorry undercarriage consists of a frame, a subsidiary frame (Fig. 2), front and back hangers composed of axels with wheels, cushioning, own brakes and an axle control operating machinery, a control and a brakes machinery.

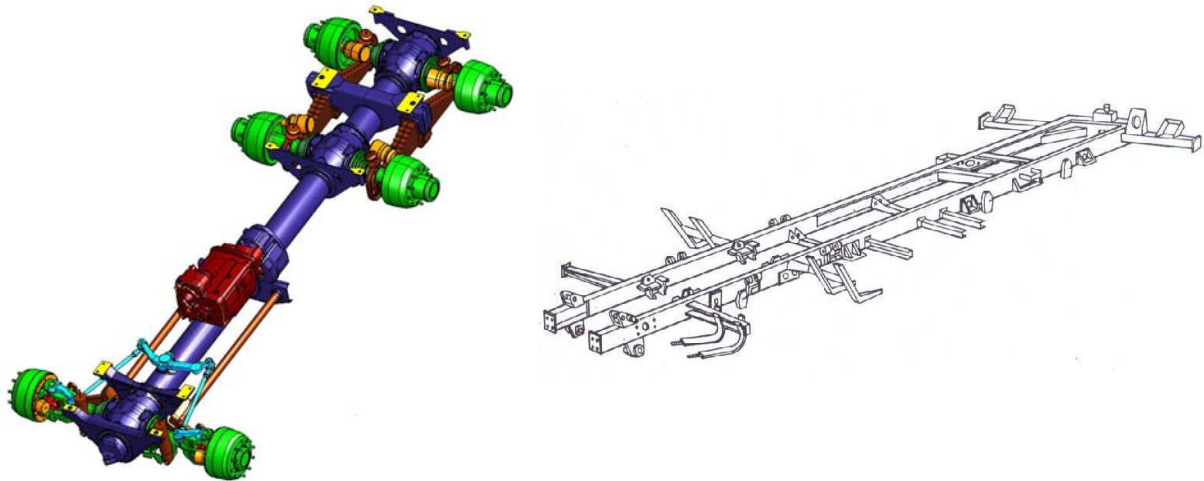


Fig. 2. Three-dimensional model of TATRA 815 S2 lorry undercarriage and subsidiary ladder frame

The main vehicle bearing part is formed by a spinal frame, to which a subsidiary ladder frame for bodywork assessment, a driving-gear and a sleigh is mounted. The spinal frame consists of particular axle gear-boxes, an additional gear-box, front and back joining piece, front and back bearing tube and transoms. Connecting of the mentioned parts is realized by using of flanges and bolted connections. The subsidiary ladder frame welded from longitudinal "U" shapes is mounted on the transoms by bolted connections. The "U" shapes are going through all the vehicle length and are interconnected by transoms. A cab, an engine together with a clutch, a sleigh, a reel, bumpers, draw-bar equipment etc. are mounted on transoms, brackets and holders of the subsidiary ladder frame.

3. COMPUTATIONAL MODEL OF THE VEHICLE

Computational FEM model of the TATRA 815 S2 vehicle was built-up in package COSMOS/M in cooperation with Tatra Kopřivnice Company in Czech Republic.

In general, its applied realization consisted of several consequential phases:

- *geometry model generation,*
- *definition of elements, their cross-section constants and material characteristics,*
- *generation of final element mesh,*
- *definition of boundary conditions,*
- *setting of acting load,*
- *computing and verification of results.*

Beam elements of the Beam3D type, mass elements of the Mass type, axial spring boundary elements of the Bound type together with damping units were used for generation of finite-element model of the analysed vehicle. Generated model of the vehicle is presented on the Fig. 3.

Elements No. 21, 79 and 250 are extremely stressed (Fig. 3), as ensued from the graphical representation of performed strain analysis results and from the next performed analyses output files. Particular examined elements can be shortly characterized as follows

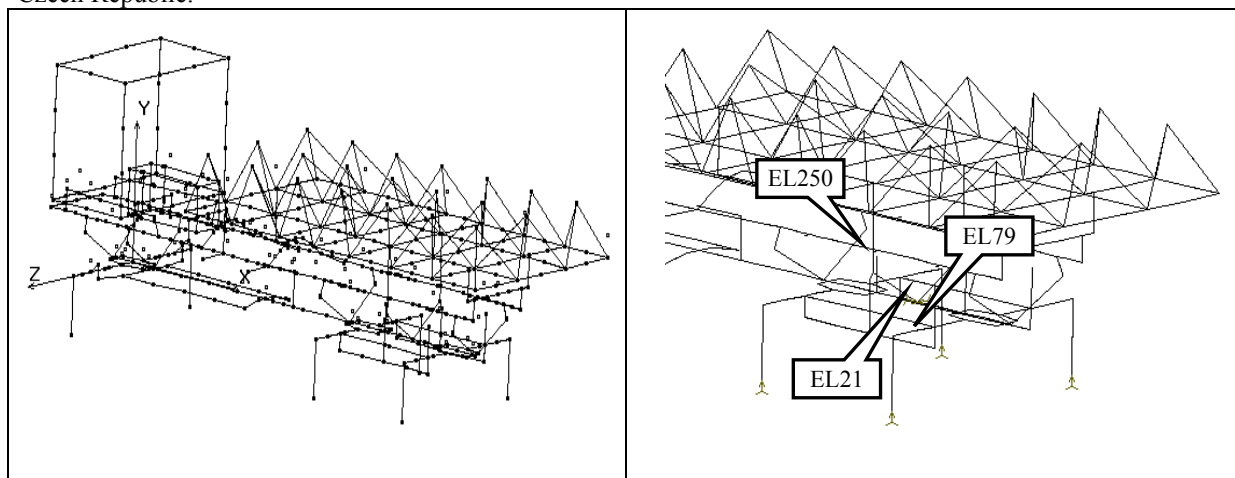


Fig. 3. Finite-element model with definition of chosen vehicle critical parts location

- a) **Element 21** – part of the vehicle bearing spinal frame, specifically the back bearing tube, structural material – steel 11 523, shape according to Fig. 4a,
- b) **Element 79** – part of the formed thick-walled bridge tube of the right central half-axle, structural material – steel 11 523, tube shape according to Fig. 4b,
- c) **Element 250** – the longitudinal truss part of the subsidiary bearing frame, approximately in the middle between both back axles, “U” shape 250x100x7, structural material – steel 11 523, element shape according to Fig. 4c.

Computational model of vehicle was excited by random function representing stochastic surface undulations of different quality roadways and relatively aggressive terrain conditions. Starting surface undulations of chosen (reference) roadway and terrain parts, identified on the base of valid roadway surface classifications were obtained by experimental measurements.

Performed experiments always resulted into one realization of the stochastic vertical unevenness course of the different quality roadway surfaces. Because of the experimental measurements difficulty and necessity to use more realisations of the stochastic vertical unevenness behaviours for each surface class, it was more effective to use for the stochastic unevenness behaviour mathematic modelling the application of Monte Carlo method [3].

On the base of the mentioned mathematical mechanism, the needed amount of the stochastic

undulation function realizations for chosen segments was generated. These function realisations properly described roadways and terrain surface undulations, where the examined vehicle moved by the appropriate prescribed velocity

4. THE COMPUTATIONAL PREDICTION OF A LORRY FRAMES FATIGUE LIFE

It is well known that vehicle reliability in operation, in particular its no-failure operation and lifetime is a dominant property for the vehicles as the typical representative of the dynamically stressed complex mechanical structures. These properties gain importance continually. Obviously it relate to the transport velocity raising, the structure parts weight reduction, the computational safety constants decreasing, the new construction materials development and application, etc.

Various vehicles operational failure cause analyses definitely prove that the fatigue process as the dynamic stress consequence assists in nearly all cases. During the simulation, the dynamical analysis often ends at the modal-spectral structure properties determination, or at its stochastic oscillation solving only from the rigid body oscillation point of view, as for example vehicle vibration, swinging, rolling etc. If the potential response acquisition is needed too, the problems related to problem size can often occur. This means enormous requirements for the computer performance and the available operating memory size..

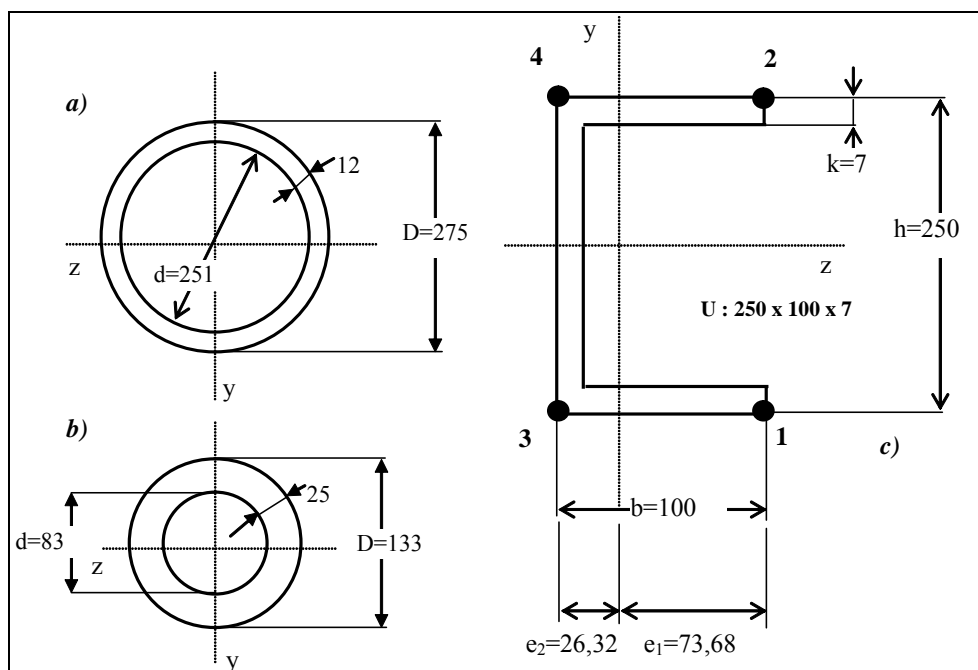


Fig. 4. Cross-sections of the analysed critical parts

Fatigue life "computation" or rather "estimation" in fact differs from the value achieved during the real machine operation. This is caused mainly by the problems related to exact determination of external load characteristic parameters, which affect the structure during operation. Fatigue strength values are not available for the specific nodes of structure but mainly only for the material samples representing the perfect status, which occurs in the real operation conditions only rarely.

Considerations about the problem solution possibilities of the fatigue life estimation can be simply reduced to the four basic tasks [1]:

- *selection of the structure critical locations, that will become the subject of the additional analysis,*
- *stress determination in the chosen critical locations and its "post-processing" using the methods suitable for the lifetime estimation,*
- *design or examination of the used construction material properties on the base of the chosen material characteristics,*
- *selection of the suitable computational procedure – theorem of the fatigue damage cumulation – which effectively join the material characteristics to the operational stress characteristics.*

Application result of the suitable fatigue damage cumulation theorem is the lifetime estimation quantified value of the analysed critical part of the examined structure. Rajcher's theorem was used for the fatigue damage computations in the identified critical parts of the TATRA vehicle. This theorem defines the fatigue damage in the critical location of the components induced per one second and is expressed by the following equation [2]

$$D_s = \frac{\Gamma \cdot \left(\frac{w}{2} + 1\right) \cdot \left[2 \cdot \int_0^{\infty} f^{\frac{w}{2}} \cdot S(f) df \right]^{\frac{w}{2}}}{N_c \cdot \sigma_c^w} \quad (1)$$

where w is exponent of S/N curve, σ_c is fatigue limit, N_c is limit number of cycles to failure, f is frequency, $S(f)$ is spectral power density of the stress loading process and $\Gamma \cdot \left(\frac{w}{2} + 1\right)$ is gamma function value.

Time until the next failure can be expressed (in hours) as follows [2]

$$T = \frac{1}{3600 \cdot D_s} = \frac{N_c \cdot \sigma_c^w}{3600 \cdot f_e \cdot (2 \cdot s_\sigma^2)^{\frac{w}{2}}} \cdot \Gamma \cdot \left(\frac{w}{2} + 1\right) \quad (2)$$

It is obvious that all the process can be realized only by means of the computer technique efficient enough.

The approach in practice is that after import or calculation of the process spectral power density values the process standard deviation and process effective frequency of the probability density will be determined.

The practical application of the presented process was realized by the program created in the MATLAB environment. The worked computational program *FATIGUE.M* was used at the fatigue life computational estimation of the structure in the selected critical locations under the chosen characteristics of the lorry operating conditions. In the application the following material parameters defining the fatigue properties were used: *slope of S/N curve* w , *fatigue limit* σ_c , *limit number of cycle* N_c and *yield limit* R_e which gain the following values for the particular elements

$$\text{EL 21: } w = 5,8, \quad N_c = 3 \cdot 10^6, \\ \sigma_c = 190 \text{ MPa}, \quad R_e = 355 \text{ MPa};$$

$$\text{EL 79: } w = 5,8, \quad N_c = 3 \cdot 10^6, \\ \sigma_c = 190 \text{ MPa}, \quad R_e = 355 \text{ MPa};$$

$$\text{EL 250: } w = 5,8, \quad N_c = 3 \cdot 10^6, \\ \sigma_c = 190 \text{ MPa}, \quad R_e = 355 \text{ MPa}.$$

Value σ_c , was during this process reduced according to the stress average value and also according to factors affecting the fatigue limit (shape, size, stress concentration in the score, treatment quality etc.) [4].

From the influence analysis of the chosen operational condition characteristics it was determined, that the impact of the roadway surfaces from the 1st to 4th class on the analysed vehicle parts fatigue damage level is nearly negligible. Therefore only a simulated loading process generated only from the stress behaviour originating during the vehicle operation on the 5th class roadways and in the terrain was further applied.

On the base of the statistically determined percentage expression of the analysed vehicle operation particular mode appearance (Tab.1), the critical vehicle parts operation stress processes were created as the implication of the operation loads effect evoked by the analysed lorry operation on the 5th class roadways and in the terrain.

Tab. 1. Percentage ratio estimation of the selected vehicle operation modes occurrence

	5. class				terrain			
Velocity [km/h]	20	40	60	80	10	20	30	40
Estimation ratio [%]	10	10	10	10	15	20	15	10

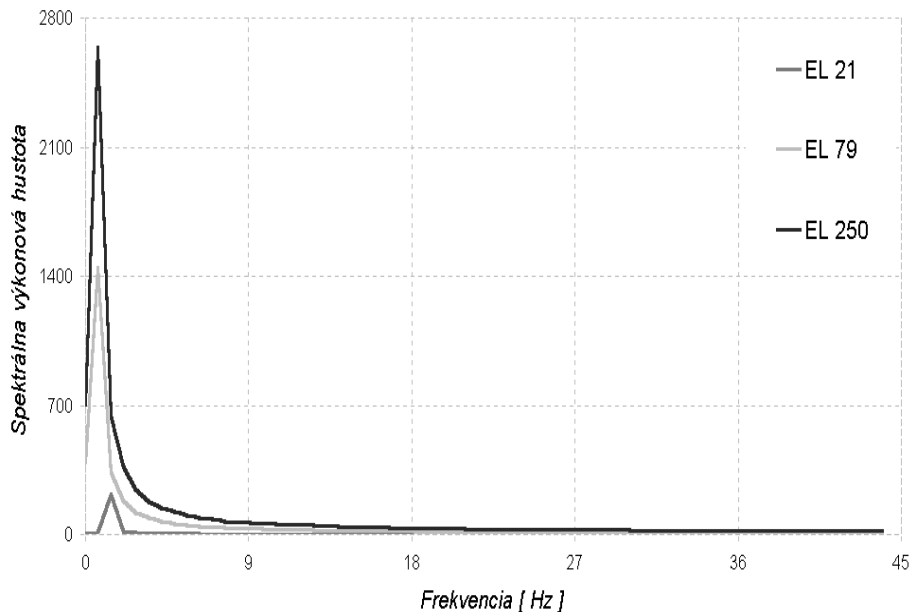
SVH centrovanej zložky napätí v kritických miestach
(Kategória 5, $v = 80$ km/h)

Fig. 5. Stress PSD in the critical elements at the selected surface quality and velocity

Tab. 2. Estimated fatigue life values of the vehicle critical parts during its real operating conditions

Element	EL 21	EL 79	EL 250a	EL 250b	EL 250c	EL 250d
Predicted Fatigue Life [in hours]	27 251	19 095	10 743	11 961	595 720	66 133

Obtained stresses behaviour in the particular critical elements of the TATRA vehicle structure were constituted by the 200.000 discrete values representing roadway or terrain distance with overall length 50 km.

The selected power spectral stress density behaviour in the analyzed elements under the chosen velocity and specific roadway class are for the illustration displayed on the Fig. 5. These stress PSD behaviour in all the three determined critical locations of vehicle structure were used as inputs for the worked *Fatigue.m* program.

The critical vehicle parts lifetime estimations were its output. The obtained fatigue life estimations of the particular critical elements are listed in Tab. 2.

On the base of performed analyses and comparisons, it is possible to state that in term of the selected operation condition characteristics influence evaluation on the transport vehicle components dynamic stress level, both examined transport vehicle operation condition characteristics (roadway and terrain unevenness and operational velocity) have significant influence on the vehicle critical parts stress.

It is obvious that it was not possible to analyse all the actuating characteristics and factors of the typical lorry operating conditions. Therefore it is necessary to understand the proposed paper as the contribution to the solution of the problem related mainly to the operational processes modelling and computer simulation.

5. CONCLUSIONS

From the realized calculations, it is possible to state that the analysed TATRA 815 S2 lorry structure is sufficiently dimensioned from the fatigue damage point of view. The goal of the paper was mainly to

- present the methodology of the fatigue life prediction based on the modelling of the working conditions most important factors,
- show the possibilities of the available software optimal use based on the FEM in order to obtain the results needed to the fatigue life prediction,
- verify the suggested computational approach on the specified lorry structure.

REFERENCES

1. Melcher R.: *Structural Reliability Analysis and Prediction*. Second edition. John Wiley & Sons, 1999.
2. Růžička M.: *Kritéria a postupy při posuzování únavové pevnosti a životnosti konstrukcí*, ČVUT, Praha 1999. On web: http://mechanika.fs.cvut.cz/sources_old/pzk/obsah.html).
3. Leitner B.: *Modelling and Simulation of Transport Machines Working Conditions by using of Autoregressive Models*. In: Academic Journal "Mechanics, Transport, Communications", Issue 1/2007, Article No. 0079, VTU of Todor Kableshkov, Sofia, Bulgaria, 10 pp. Www: < <http://mtc-aj.com/php/welcome.php?lang=gb> >.
4. Leitner B.: *Risk Factors in Process of Fatigue Life and Safety Estimation of Technical Systems*. In: Zbornik radova, Nacionalna konferencija: Upravljanje vanrednim situacijama", Univerzitet u Nišu, Fakultet Zaštite Na Radu, Niš, Serbia 2007, p. 179-186.

This work has been supported by the grant project VEGA No.1/0430/09.

OVERALL FACTORY VIBRATION LEVEL: THE NEED FOR GLOBAL INDICATORS IN CBM

Diego GALAR¹, Luis BERGES¹, Jesus ROYO²

¹Manufacturing Engineering and Advanced Metrology Group
Aragon Institute of Engineering Research (I3A), University of Zaragoza, Zaragoza, Spain
Department of Engineering Design and Manufacture
School of Engineering
University of Zaragoza, Zaragoza, Spain

²ZLC Zaragoza Logistics Center
Institute for Research in Logistics, Zaragoza

Summary

When we do predictive maintenance, including vibration analysis, rotating machinery, we anticipate many times a catastrophic failure that without this technology, would be difficult to locate and make unsafe our system functionally. This analysis is done individually machine to machine, point to point which prevents us from having a parameter that quantifies the overall status of all rotating machinery of a plant or department.

Key words: vibration, speed, acceleration, predictive maintenance, CBM, data collector, indicator.

INTRODUCTION

It is very common, the uses of non-destructive testing for diagnosis of machinery, which failure modes are not enough to file a hidden pathology visible to the operator. The non-detectability of these faults has extended the use of these technologies in particular the analysis of vibration, very successful in rotating machinery. This has made large investments in equipment gauges, many hours of training to operators and engineers to interpret data and a radical change in the planning of maintenance. Breakdowns are reduced significantly and the non planned actions too, being replaced by interventions result of the predictive inspections. It is therefore important the correctness of these predictions because of the high cost is an intervention in labour, parts and lost production. It is considered a successful program that avoids costs of intervention with these inspections, but unfortunately in most cases repairs are made useless because of false alarms. The dynamics of the systems tells us that a perfect rotating machine must not vibrate, being this failure mode an anomaly. But this statement is partially true in the industrial world. Most machines suffer from failures from the day of their operation due to:

- installed incorrectly machines
- poor operating conditions
- poor design or machine manufacturing defects
- adjacent machinery with problems transferred to the reference machine.

This means that in the case of vibration, we find machines, which since its installation vibrate due to faulty benches, incorrect installation, improper piping design, hydraulic imbalances by use products

are not allowed to pump etc. In the case of machines with spent operating time, the above issues have been able to generate a vibration pattern hardly changed and that we must contemplate when planning any repairs because the inherent level of reliability has been reduced in the machine. The values of vibration of such equipment are therefore not zero and comparative analysis we can create false alarms, being higher than the other machines in environment or are in gangs of dissatisfaction if we follow vibration standards. We therefore created in the analysis of the plant a distorting element, because we think the machine is in poor condition when vibration due to a defective bench can be sustained over time with minimal damage to the machine itself and almost never justifies the investment that often has little impact. It is therefore proposed in this article, an average parameter value of vibration for rotating machinery, so that we can display the severity of the vibration of machines, groups of machines or entire plants, with an overall indicator, without false alarms that we can create with the strict application of the standard point to point.

1. POINTS OF MEASUREMENT AND CALCULATION OF AVERAGE MACHINE VIBRATION

The intention of the indicators described in this article is to obtain a set of parameters and templates easy to reach without a specific diagnosis, to detect an anomaly in the operation of a plant or an area with a number of rotating machines. That is why we calculate the average level of machine vibration, and then calculate the average level of vibration of the

plant. In the case of machines composed of elements that rotate at a speed only, as in Figure 1, the parameters to consider are:

- power (in kw)
- speed (usually measured in rpm or revolutions per minute)
- average vibration of the points of measurement (mm / s)

The points of vibration measurement, to collect data easier to analyze, are proposed by [1] with special emphasis on the collection of data in horizontal, vertical and axial. The orientation of each point of measurement is an important consideration in configuring the database for analysis. There is an optimal orientation for each measurement point of the machine in a predictive maintenance program. If only we could take a radial measurement, must be oriented in the plane (vertical or horizontal) that provides the highest vibration amplitude. For continuity, each machine must be clear of the train the shaft of entry and exit of driver and driven machine. The measurement points should be numbered sequentially starting with the main driver. This is illustrated in Figure 1. Any numbering convention may be used, but must be consistent in this way will provide the following benefits:

1. Immediate identification of the location of a point during the analysis and diagnosis.
2. The cluster of points per axis allows the analyst a clear view of the problems in each component.

In the case of electric motors, we will have two points of measurement, corresponding to the housing of the bearings. At each point, it is normal to take two measurements, in a horizontally and vertically, reflecting different pathologies vibration obtained in two different directions, despite being the same pocket. It allows the analyst a clear view of the problems in each component.

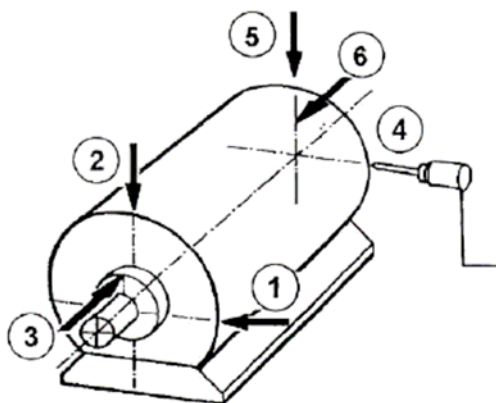


Fig. 1. Measurement points in an electric motor

Point 1 is also called NCS measure (acronym Non Coupling Side). In Section 1, we have measures in 1H Horizontal and Vertical 1V.

In Figure 2 correspond to:

- 1H: Point 4

- 1V: Point 5

Section 2 will be called the CS (acronym Coupling Side). Again we find 2H and 2V whose correlation:

- 2H: Point 1
- 2V: Point 2

Respect to the axial measurement, reflected in the figure, can be taken in 1 or 2 in the graph represented by 3 and 6 (because the measure is the same) but by accessibility of the sensor is used in point 6 of the figure, which is commonly known as 1A, to be located at the cashier and 1 being the axial direction of rotation. Besides an important detail of the measure 1A, which is no risk to the operator that measures the vibration, not to approach any mobile device discovered. Which measure 3, which would be called 2A, it is close to the motor shaft and the coupling and the risk of entrapment and amputation. In an electric motor therefore average vibration is:

$$V_{average} = \frac{V_{1H} + V_{1V} + V_{2H} + V_{2V} + V_{1A}}{5} \quad (1)$$

Where $V_{1H}, V_{1V}, V_{2H}, V_{2V}, V_{1A}$, the values of vibration velocity (measured in mm / s) at the points previously selected. In the case of more complex machines, that is coupled to fan motors or pumps, but having a single speed, it would act similarly, but taking into account that the two points of the engine are joined by two other housings for the pump bearings of the same, which will call 3 and 4.

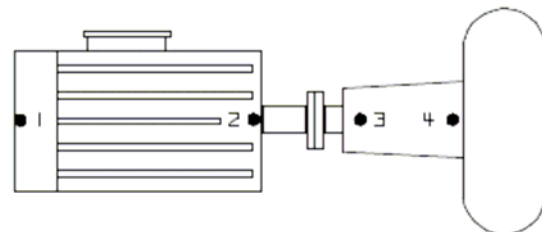


Fig. 2. Measurement points in an electric motor coupled to a centrifugal pump.

Again, we find the 3H and 3V and the 4H and 4V. It will be interesting to take the measurement 4A for a coupling in the middle of the train. The reason to take 4A, instead of 3A, is the safety of the operator, knowing that we are talking about the same vibration.

Therefore, the average vibration machines such a coupling and four bearings operating at the same speed will be:

$$V_{average} = \frac{V_{1H} + V_{1V} + V_{2H} + V_{2V} + V_{1A}}{10} + \frac{V_{3H} + V_{3V} + V_{4H} + V_{4V} + V_{4A}}{10} \quad (2)$$

Being

$V_{1H}, V_{1V}, V_{2H}, V_{2V}, V_{1A}, V_{3H}, V_{3V}, V_{4H}, V_{4V}, V_{4A}$ vibration speed in the points. In the case of machines with multiple speeds, it is interesting to ponder the vibration of each point depending on the speed at which the element rotates at the same treadmill. It should be remembered that the frequency of rotation of the machine is an important parameter, since the acceleration of the vibration increases with the square of the frequency of rotation and speed of vibration increases linearly with increases in the frequency of rotation, [2]. Therefore, the most common machines with different speeds, i.e. motor-gear train fans and pumps with pulleys and belts, we calculate a speed weighted average, for obtaining an average value that reflects the criticality of element that we look and do not mask high-frequency amplitudes with low frequencies which clearly do not pose the same risk factor. How to perform measurements on trains coupled machines is described in ISO 7919-3 [3], this policy helps us in the case of rotating machines that have a relatively rigid casing and / or heavy compared to its rotational mass, often considering which has a flexible shaft rotor. In this case, the vibration should be assessed with greater sensitivity if the measures are carried out on rotating elements and not on the static components of the machine.

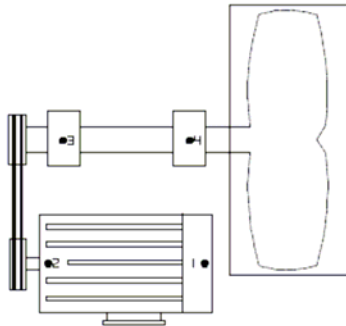


Fig. 3. Fan belt driven

In the simple case of a fan driven by belt where:

v_{motor} is the speed at which the motor rotates

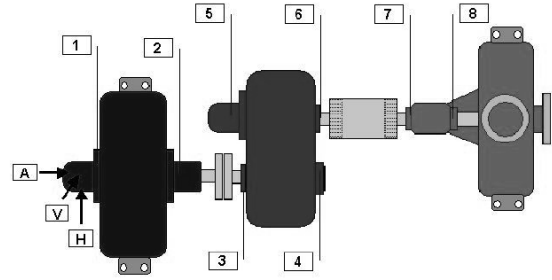
v_{fan} is the speed at which the fan rotates.

Assuming that the transmission through the pulleys is different from 1:1, i.e. the pulleys are of different size and thus the speeds are also different, the vibration is:

$$V_{average} = \frac{v_{motor} (V_{1H} + V_{1V} + V_{2H} + V_{2V} + V_{1A})}{5v_{motor} + 5v_{fan}} + \frac{v_{fan} (V_{3H} + V_{3V} + V_{4H} + V_{4V} + V_{4A})}{5v_{motor} + 5v_{fan}} \quad (3)$$

In this case, we are again with a four-bearing machine. Some configurations have more points of measurement; it is the case of a driver (motor or turbine) with a gearbox and pump. In this

configuration, we find eight bearings, with their pockets as shown in Figure 4:



1	Turbine Non Coupling Side	5	Gearbox Low Speed Non Coupling Side
2	Turbine Coupling Side	6	Gearbox Low Speed Coupling Side
3	Gearbox High Speed Coupling Side	7	Pump Coupling Side
4	Gearbox High Speed Non Coupling Side	8	Pump Non Coupling Side

Fig. 4. Details of the measuring points on a machine train: turbine-gear-pump

In the case of the figure, a turbine coupled to a gearbox and a pump to this, we measure the following points:

- Turbine 1A, 1H, 1V, 2H, 2V
- Gearbox 3H, 3V, 4^a, 4H, 4V, 5^a, 5H, 5V, 6H, 6V
- Pump 7A, 7H, 7V, 8H, 8V

Naming:

$v_{turbine}$, is the speed at which the steam turbine rotates

v_{pump} , is the speed at which the pump rotates.

Therefore, average vibration of this machine is:

$$V_{average} = \frac{v_{turbine} (V_{1H} + V_{1V} + V_{2H} + V_{2V} + V_{1A})}{10v_{turbine} 10v_{pump}} + \frac{v_{turbine} (V_{3H} + V_{3V} + V_{4H} + V_{4V} + V_{4A})}{10v_{turbine} 10v_{pump}} + \frac{v_{pump} (V_{5H} + V_{5V} + V_{6H} + V_{6V} + V_{5A})}{10v_{turbine} 10v_{pump}} + \frac{v_{pump} (V_{7H} + V_{7V} + V_{8H} + V_{8V} + V_{7A})}{10v_{turbine} 10v_{pump}} \quad (4)$$

We can therefore generalize the expression of the average vibration as follows:

$$V_{average} = \frac{\sum_{i=1}^n v_i V_i}{\sum_{i=1}^n v_i} \quad (4)$$

Where v_i is the speed associated to the i point,

V_i represents the speed of vibration measured at the point i, where n is the total points measured: horizontal, vertical and axial, not the pockets of the bearings. This overall vibration measure of a

machine, allows a first assessment. In the above analysis, we obtained 20 measures vibration velocity at different points, which give us an idea of the deterioration of the elements located in these positions. Normally, when we classify a machine according to the degree of severity of the vibrations that suffers, we are guided by the highest vibration that appears, this being a serious error in the creation of false alarms. Many machines in its period of maturity or due to poor installation have bench problems or structures that support the joint, as can be seen in Figure 5.



Fig. 5. Rotating machines with a weak bench

Therefore, when calculating the severity of the vibration by the highest value we are creating a false alarm almost permanent, because there are particularly critical points, as the supports of the pump on the side of the coupling, which normally vibrates from its installation. This support, in the analysis correspond to the points 3H and 3V (especially 3H) and lead a vibration much higher than the rest of the machine due to poor support or bolt, which by this vibration, are dropping. For that reason, the analysis of severity mentioned, this vibration partially masks the state of the machine, because despite being a vibration, it is very difficult to remove it in the machinery of a certain age. With the average vibration value of machine, this discordant, is softened by the rest of the machine measurements, and we obtain a value more in line with reality, with which to assess the severity of that vibration.

3. VIBRATION SEVERITY

The most common value used to display the severity are the peak and RMS, [5], being the second most widely used and included in the existing rules. Thus, ISO defines as "severity of the

vibration, the higher value of the RMS amplitude of vibration velocity obtained in the frequency range 10-1.000 Hz and measured at predetermined points of the structure (usually measures at the top of the bearings or the supports). The most common rule is ISO 10816 [6], which is now considered to assess the status of machines. It applies to machines with rotating rigid rotors and flexible rotors with rotating machinery, where the vibration of the bearing cap is indicative of the behaviour of vibrating shaft. This rule is studying global vibration without bands. The data required for implementation, are the overall level of vibration at speed (effective value RMS) in a frequency range between 10 and 1,000 Hz (vibration severity to ISO).

The criterion for acceptable vibration severity in each class of machines referred to is reflected in Table 1.

Table 1. Severity of vibration according to ISO 2372/ISO 10816

VIBRATION SEVERITY PER ISO 10816						
	Machine		Class I small machines	Class II medium machines	Class III large rigid foundation	Class IV large soft foundation
	in/s	mm/s				
Vibration Velocity Vrms	0.01	0.28				
	0.02	0.45				
	0.03	0.71		good		
	0.04	1.12				
	0.07	1.80				
	0.11	2.80		satisfactory		
	0.18	4.50				
	0.28	7.10		unsatisfactory		
	0.44	11.2				
	0.70	18.0				
0.71	28.0		unacceptable			
1.10	45.0					

As shown in the table, the severity of vibration is divided into four ranges: Good, Satisfactory, Unsatisfactory or Unacceptable and four types of machines depending on the power installed, CLASS I, II, III and IV. To use ISO 2372, simply classifying the machine to be considered within the relevant class and, once obtained, the total value (RMS) vibration between 600 and 60,000 RPM (that band of 10 to 1000 Hz), we can locate in the table the level of severity of your machine. In general, it is generally considered that the severity of vibration of the machine remains unchanged if you have the same value of RMS velocity amplitude of vibration in the frequency range 10 - 1000 Hz. To illustrate the applicability of this indicator and its relationship with the severity of the vibration, take a machine like described one above, consisting of a steam turbine of 400kW, a gearbox (4000RPM speed input and output rate 1300 RPM) and a centrifugal pump coupled to the gearbox.

The values obtained by data collectors, can be of two types, the first is the peak value, useful if the subject of the sensor and the measure is not contaminated, otherwise, the collectors estimate the root mean square value of velocity vibration during

the exposure time to the sensor (which also value and support the relevant regulations). This value is known as quadratic value RMS (Root Mean Square). If we look, the two highest steps on the machine are 23.6 and 35.5 mm / s. With these values taken to the 10816 standard for machines greater than 75kW, as is the case (CLASS III) we find the power of this machine, much in the unacceptable range, almost the full scale. Looking in depth at the location of these measures so alarming, we see that occur in the 7H and 8H, which correspond to the horizontal of the pump, excessive measures which are not equivalent in their vertical 7V and 8V, so imbalances that are discarded and other pathologies of a certain severity. It is therefore clear that it is due to a bench defect or minor structural rigidity.

Table 2. Data from vibration of the machine

DATA CBM turbopump					
	Rotation Speed (RPM)	Equipment	Measurement point	Units	Value
Steam turbine	4000	Turbine	1A	mm/s	2.3
	4000	Turbine	1H	mm/s	1.8
	4000	Turbine	1V	mm/s	2.4
	4000	Turbine	2H	mm/s	2.8
	4000	Turbine	2V	mm/s	2.2
Gear Box	4000	Reductor	3H	mm/s	4.7
	4000	Reductor	3V	mm/s	9.4
	4000	Reductor	4A	mm/s	16.7
	4000	Reductor	4H	mm/s	9.1
	4000	Reductor	4V	mm/s	16.0
	1300	Reductor	5A	mm/s	11.9
	1300	Reductor	5H	mm/s	6.6
	1300	Reductor	5V	mm/s	8.9
	1300	Reductor	6H	mm/s	15.0
	1300	Reductor	6V	mm/s	18.1
Pump	1300	Pump	7A	mm/s	13.9
	1300	Pump	7H	mm/s	23.6
	1300	Pump	7V	mm/s	5.9
	1300	Pump	8H	mm/s	35.5
	1300	Pump	8V	mm/s	7.4

Conversely, if we calculate the parameter proposed average vibration, with appropriate weighting for the speed in each zone so far obtained is 8.68 mm / s, much more rational and placing the machine in the range limit between satisfactory and unsatisfactory, while minimizing the effects of structural vibration and eliminating false alarms in the monitoring. Hence, we can generalize the use of the average vibration parameter for a full factory or area of analysis. The expression of the parameter proposed OFVL (Factory Overall Vibration Level) therefore is:

$$OFVL = \frac{\sum_{i=0}^n P_i V_i}{\sum_{i=0}^n P_i} \tag{5}$$

Where V_i is the average of the vibration machine i has been calculated as above, P_i the power on the i -machine and n the number of machines included in the search for the global average value of vibration. With these data we can also calculate the average power installed per machine:

$$P_{media} = \frac{\sum_{i=0}^n P_i}{n} \tag{6}$$

4. CALCULATION OF OFVL

This parameter is easy to calculate manually, but when the plants take on a certain size and the number of rotating machines is high, should be made systematic and automated as far as possible. All plants that have a predictive program perform measurements with three different types of equipment, [7]:

- Collectors of absolute value.
- Collectors and spectrum analyzers.
- Continuous monitoring.

The measurement equipment is automatically connected to the computer system in the post-measurement and downloaded all data. Being better the quality of monitored continuously vibration by the repetitiveness of the process. The basic vibration meters, do not often have memory or is very small, so there are values to be scored in the appropriate medium. After entering all the data, the calculation of the parameter is very simple, because the datasheets in the machine analysis software, often have the power and frequency of rotation of the elements and they are capable to make rapid exports to spreadsheets where speeding up the process. Measurement systems in companies with high level of monitoring, due to the criticality of some elements can certainly achieve a complex structure, which can include several pieces of equipment described, with several dozen accelerometers as described by [9]. These systems respond to the need to measure acceleration, velocity or displacement, in a very large fleet, with different criticality, rotation speeds and power. This is where you need a connection or interface between the entire system of CBM and CMMS installed in the plant, necessarily existing, as proposed by [8]. This gives us the OFVL parameter is calculated by the CMMS, and incorporated into the indicator panel control of maintenance team. This parameter is not for immediate intervention, because that is the task of

continuously monitor or routes that will yield the state machinery and the necessity of stopping, repairs or replacements. This parameter will allow us to see the trend of the vibration and thus the overall success of the predictive, reaching as far as possible to the minimum levels of the same or what is the status of reliability inherent in the system. Obviously, this parameter plant has some correlation with the indicators with the indicators proposed by some authors as [10], to measure the success of implementing a predictive maintenance program. So at the beginning of the program, while the overall vibration decreases, the number of hours spent PMP (Predictive Maintenance Programme) increasing to stabilize these two parameters. Also reducing the overall vibration plant will strongly correlates with the reduction of failures and thus the frequency of the same. Simplifying, we can observe that as decreases the overall value, increases the MTBF to be both achieved in the so-called reliability of the system, aiming to achieve the same inherent reliability.

5. CONCLUSIONS

The need for indicators, appear when we try to use a score card, as a way of management different than the current one. As organizations use indicators in the maintenance function, they realize that they can be used to define the strategy and achieve consensus on it, communicate the strategy throughout the organization, align personal goals and the departments, aims to link long-term and annual maintenance budgets, identify and align strategic initiatives, regular and systematic reviews, and obtain feedback for the strategy and improve it. The indicators serve to refocus the management system and link short term with long-term strategy, linking the maintenance function with other functions of the organization, especially, production. The results should eventually translate into financial technical achievements, leading to the maximization of the value created by the company. The proper use of maintenance indicators, allows you to select an optimal frequency of maintenance and inspection, inventory levels, management and optimization of budgets, contracts and technical proposals. It will help us to consider, objectively, the impact they bring with them different modes of failure on operations, production, safety and environment, thus helping to reduce production costs and maximizing the value of the cycle equipment life, increasing the benefits. The OFVL is configured as one indicator

of high importance when assessing the success of PDM, and the quantification of the tendency of the state machinery. The OFVL, basic numerical indicator will allow us to compare the value of vibration of the plant with the specific machine or with the same manufacturing plant, for analysis or sectorial comparative tests of different machines for the same purpose. We are also permitted under current regulations, documenting the overall state of the plant and set a trend that marked the PM policy, corrective and overhauls, and we can relate this parameter with other parameters controlling the maintenance function.

REFERENCES

- [1] Mobley R.: *Vibration fundamentals*. Butterworth-Heinemann. USA 1999.
- [2] Mosquera M., De la Victoria M.: *Las vibraciones mecánicas y su aplicación al mantenimiento predictivo*. Centro de Altos Estudios Gerenciales ISID. Caracas 2001.
- [3] ISO 7919-3, *Mechanical vibration. Evaluation of machine vibration by measurements on rotating shafts*. Part 3: Coupled industrial machines.
- [4] Kumaraswamy S., Rakesh J.: Standardization of Absolute Vibration Level and Damage Factors for Machinery. *Health Monitoring. Proceedings of VETOMAC-2*, Mumbai, 2002.
- [5] W. de Silva C.: *Vibration: fundamentals and practice*. CRC Press LLC, USA, 1999.
- [6] ISO 10816-3, *Mechanical vibration. Evaluation of machine vibration by measurements on non-rotating parts. Part 3: Industrial machines with nominal power above 15 kW and nominal speeds between 120 r/min and 15000 r/min when measured in situ*.
- [7] Girdhar P.: *Practical Machinery Vibration Analysis and Predictive Maintenance*. Elsevier. Oxford 2004.
- [8] Peters R. W.: *Maximizing Maintenance Operations for Profit Optimization: The Journey to Maintenance Excellence*. The Maintenance Excellence Institute. Raleigh, North Carolina 2002.
- [9] Reeves C. W.: *The Vibration Monitoring Handbook*. Coxmoor Publishing, USA 1998
- [10] Wireman T.: *Developing Performance Indicators for Managing Maintenance*: Industrial Press, USA 2005.



Dr. Diego GALAR Pascual is Phd in Industrial Engineering and Telecommunication Engineer from the University of Saragossa, he has taught at several universities including the University of Saragossa or the European University of Madrid, ANANTASA technical director, director of academic innovation and subsequently pro-vice-chancellor at the Universidad San Jorge. He is currently a researcher in the department of design and manufacturing engineering from the University of Saragossa.)



Dr. Luis BERGES Muro is PhD. in Industrial Engineering, and professor at the University of Saragossa. He has played numerous positions such as Vice Chancellor for Infrastructure of the University of Saragossa, Director of the Office of Research Results Transfer from University of Saragossa. Director Precision Mechanical Services, University of Saragossa, Board Member and Chairman of the Government Commission on Culture and Education of the Association of Industrial Engineers of Aragon and La Rioja. Professor of many degrees and postgraduate degrees currently serves as Director of Engineering Department of Design and Manufacture, University of Saragossa.



Dr. Jesús ROYO Sánchez is PhD in Industrial engineering, professor at the University of Saragossa. in numerous degrees and postgraduate courses. He has been Director of industrial management post degree taught in Saragossa, currently serves as Director of the Institute of Logistics participated by the Government of Aragon , University of Saragossa and MIT (Massachusetts Institute of Technology)

SELECTED METHODS OF FINDING OPTIMAL CENTER FREQUENCY FOR AMPLITUDE DEMODULATION OF VIBRATION SIGNALS

Tomasz BARSZCZ, Adam JABŁOŃSKI

AGH University of Science and Technology, Dept. of Mechanical Engineering and Robotics
Al. Mickiewicza 30, 30-059 Kraków, Polska, e-mail: tbarszcz@agh.edu.pl

Summary

The paper concerns the subject of the optimal center frequency selection for the amplitude demodulation, which is a principal tool for detection of bearing faults. In the first part, existing methods along with their advantages and drawbacks are discussed. A special attention is paid to methods implementing kurtosis-based estimators. In following sections, the authors demonstrate a novel method based on the so called "max-med" estimator. The method is validated on a real signal containing a bearing fault signatures.

Keywords: machine diagnostics, amplitude demodulation, kurtosis, median, Protrugram.

WYBRANE METODY ZNAJDOWANIA OPTYMALNEJ CZĘSTOTLIWOŚCI NOŚNEJ W PROCESIE DEMODULACJI AMPLITUDOWEJ SYGNAŁU DRGAŃ

Streszczenie

Tematyka artykułu dotyczy optymalnego wyboru częstotliwości nośnej w procesie demodulacji amplitudowej, która jest podstawowym narzędziem detekcji uszkodzeń łożysk. Pierwsza część pracy przedstawia obecnie używane metody wskazując ich zalety oraz wady, ze szczególnym uwzględnieniem metod bazujących na kurtozie. W kolejnych częściach pracy autorzy ilustrują nową metodę z wykorzystaniem operatora „max-med” (od ang. *maximum-median*). Działanie zaprezentowanej metody jest weryfikowane na sygnale rzeczywistym zawierającym komponenty generowane przez uszkodzone łożysko.

Słowa kluczowe: diagnostyka maszyn, demodulacja amplitudowa, kurtoza, mediana, Protrugram.

1. INTRODUCTION

The amplitude demodulation has been a successful technique in diagnostics of rotating machinery over the years. The development of fast processors has enabled the engagement of highly-memory-consumption signal processing methods with a minor time consumption cost. One of such method is based on narrowband envelope spectra calculated via Hilbert Transform in the frequency domain [1]. The authors have successfully used the method to develop a number of diagnostic algorithms employed in commercial monitoring and vibration system [2].

One of the major advantage of this method is the ability to create a basis for determination of an optimal band for signal demodulation. Frequently, resonance frequencies tend to overlap one another, which complicates the selection of a single frequency band. The authors have proposed the estimator based on kurtosis of the envelope spectrum (in contrary to typical approach, where the kurtosis is used for time signals [3]). In contrast to other techniques engaging kurtosis-based estimators, the method presented in the paper takes advantage of the "max-med" estimator, which emphasizes the presence of characteristic frequencies and its

harmonics, and as a result, it provides an aid to the selection of the optimal band for demodulation.

2. EXISTING METHODS

2.1. Db direct spectrum comparison

A comparison of frequency spectra is a relatively old, yet valuable technique for determination of significant spectrum changes. The comparison may be carried out by plotting a difference between a younger and older data. In this matter, spectral regions where amplitude has risen are emphasized. However, the method has got two major drawbacks. Firstly, it is relatively poorly accurate. Secondly, the selection of the optimal spectrum calculation technique from commonly available (*fft*, *psd*, *cpb*, etc.) is not obvious, and may lead to different results depending on a selected spectrum calculation technique.

2.2. Fast Kurtogram

Fast Kurtogram is a relatively new tool, presented by Antoni in 2008 [4]. The tools illustrates the kurtosis-based estimator values representing the peakiness of the filtered envelope time signals for a defined combination of center frequencies and

bandwidths. The result of the tool for a single vibro sample is a 2D colormap, where colors represent the kurtosis levels. The main drawback of the method is a high sensitivity to random extraneous components, which can give ambiguous results.

Another version of a kurtogram-based methods was presented by Zimroz in [5,6], where the optimal center frequency (indirect) detection algorithm is divided into “starting” and “ending” frequency. Even though the presented results are satisfactory, once again the kurtosis-based estimator shows the tendency to point out misleading frequency intervals, as stated by Zimroz. One of the solutions is the synchronous averaging, but it may cause the loss of information as well [5].

2.3. Spectrogram

Spectrogram is one of the most common time-frequency analysis map, which illustrates how the spectral density of the signal varies with time. The technique may enable to select the frequency range, where the damped impulses from local faults occur [5]. A spectrogram may be calculated from a sequence of band-pass filters (obsolete) or via STFT (short-time Fourier transform). The latter one is accomplished by breaking up the time signal into intervals (usually overlapping), and calculating the power spectrum for each part. Main drawbacks of the method include: i) the knowledge of the number of intervals into which the signal is to be divided, ii) complicated and time-consuming calculation, iii) frequently challenging interpretation of the resultant color map.

2.4. Protrugram

The Protrugram is a tool developed by the authors in 2009 for optimal center frequency selection [3]. The tool illustrates the kurtosis values of spectral amplitudes of narrowband envelope signals calculated in the frequency domain via Hilbert transform. In the algorithm, the selected bandwidth (as a function of the sought characteristic frequency) is shifted by a defined step (100Hz default), and the narrowband envelope spectrum is recalculated. At each step (i.e. for each center frequency), the kurtosis from all spectral amplitudes is calculated, and is stored in a vector as a single scalar value.

As a result, these kurtosis values are plotted as a function of the center frequency. The major drawback of the method, which is to be overcome in this paper, is the negative influence of harmonic components on the final estimator's value, which in practice is expected to behave in an opposite manner.

3. ENHANCED ALGORITHMS

3.1. Algorithm description

The aforementioned Protrugram algorithm is based on kurtosis values calculated from amplitudes

of positive frequencies of a number of narrowband envelope spectra. This solution has the disadvantage of gathering all signal signatures “into a single pot”. If the envelope spectrum is not masked by superfluous components, e.g. fundamental harmonics, the method works fine. However, in many cases, the envelope spectrum (even narrowband) will include superfluous components, which may ruin the Protrugram algorithm. One of solutions to the problem is to add an extra step, i.e. an “extraction criterion” to the algorithm.

The authors propose such enhancement to be oriented towards extraction of sought characteristic frequencies from a defined set, which implies a knowledge of the machine kinematic configuration data. Once a particular characteristic frequency is on the spotlight, for a current narrowband envelope spectra, a set of neighborhoods of possible harmonic lines is selected. Next, for each harmonic line, a ratio of the maximum amplitude value of the selected region to the median value of all current narrowband spectrum amplitudes is calculated, and may be multiplied by a weighing function, for instance proportional to the harmonic index, in order to highlight the presence of higher harmonics. It is worth stating that a kurtosis-based estimator may not be used as a selection criterion, since it is a function of number of samples. Therefore in practice, kurtosis estimators require relatively large number of samples, which is contradictory to the idea of single-peak spectral detection.

As endorsed by a many publications [5, 7], it is of additional benefit to emphasize the presence of higher harmonic components, as opposite to the Protrugram criterion, where the presence of additional harmonics lowered the estimator's ultimate value. Finally, it needs to be stated firmly that following algorithm requires a knowledge of the machine kinematics, namely the set of characteristic frequencies.

3.2. Algorithm steps

The algorithm is as follows:

1. Calculate FFT from a given time signal $x(t)$
2. For a starting center frequency f_i , select amplitudes from a defined bandwidth BW , and calculate a narrowband envelope spectrum NES_i via Hilbert transform
3. For each frequency f_i from the set F , select the intervals on NES_i of neighboring samples up to the k th harmonic of f_i
4. Calculate the sum of the weighted (weighing function equal to m) ratios of the maximum values of amplitudes from selected interval to the median value of all amplitudes of the current NES_i :

$$Q(NES_i, f_i) = \sum_{m=1}^k \left\{ \frac{\max[amp(m \cdot f_i - \delta, m \cdot f_i + \delta)]}{median[amp(NES_i)]} \cdot m \right\} \quad (1)$$

where:

- δ - half of the bw (i.e. local NES_i bandwidth as opposed to the global BW)

NES_i - consecutive narrowband envelope spectrum.
 The parameter rewers actually to the center current frequency CF
 amp - spectral amplitudes of $x(t)$

5. Repeat point 3 for all $f_j \in F$
6. Shift the BW by a defined step towards the sampling frequency and repeat points 2-5
7. Plot the resultant *max-med* vector as a function of center frequencies, creating an array:
 $PQ \sim f(Q(NES_i, f_j)) \quad (2)$

The center frequencies on the horizontal axis for the largest values on the vertical axis represent frequencies, for which the modulating components are most clearly visible when demodulated. Note that it is most probable to anticipate high Q values for relatively high frequencies, i.e. over 2 kHz.

3.3. Algorithm block diagram

Fig. 1 presents the block-diagram representation of the algorithm:

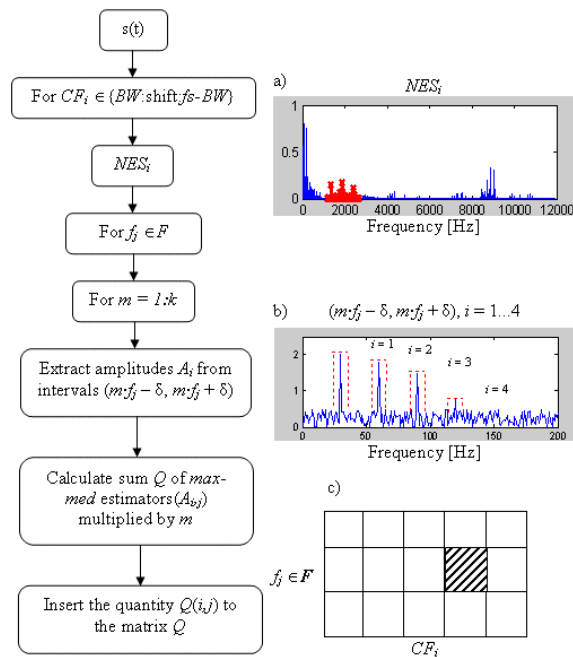


Fig. 1. Block diagram of the proposed algorithm
 a) Scaled amplitude spectrum (positive frequencies only) with a marked i -th demodulated band. b) I -th narrowband envelope spectrum with marked harmonic lines of the j -th characteristic frequency. c) An illustration of the representation of a single $Q(i,j)$ scalar value.

A single hatched area represents a degree of a signal-to-noise ratio for a given characteristic frequency f_j demodulated at a center frequency CF_i in terms of a sum of weighted kurtosis-based estimators.

Note that the weighing function is linear and equal to the harmonic's number. In consequence, the presence of higher harmonics will be emphasized by

the algorithm. For instance, if for a given f_j at NES_i , the max-med values equal to $k_{i,j} = \{11, 7, 3, 2\}$, the resultant $Q(i,j)$ will be calculated as $\sum(11 \cdot 1, (7 \cdot 2), (3 \cdot 3), (2 \cdot 4)) = 42$ (dimensionless).

4. VALIDATION

The algorithm's performance is demonstrated on a real vibration signal on a test rig, with the bearing outer race fault. The signal was recorded with sampling frequency equal to 24 kHz. The data acquisition time was 10 seconds. The characteristic frequency was calculated as follows:

$$BPFO = S \frac{N_r}{2} \left(1 - \frac{R_d \cos \phi}{P_d} \right) \quad (3)$$

where:

- $N_r = 14$
- $\phi = 0^\circ$
- $R_d = 7.94 \text{ mm}$
- $P_d = 45.4 \text{ mm}$

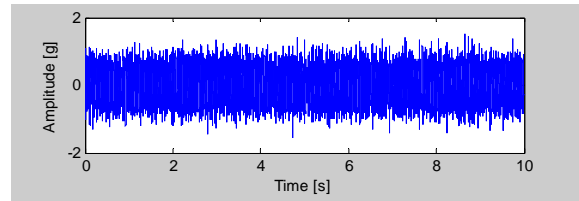


Fig. 2. Time view of the studied signal

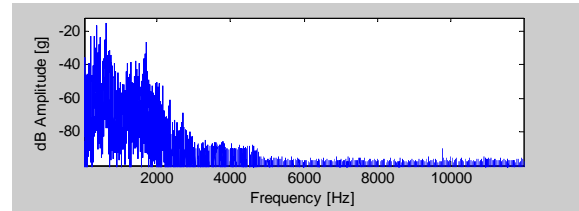


Fig. 3. Amplitude spectrum of the studied signal

Note that both, the time view of the signal as well as the amplitude spectrum do not display a clear information about the fault signature. However, the Fig. 4, presenting the result of the max-med plot, displays unambiguously the presence of harmonic components modulating 4kHz wave.

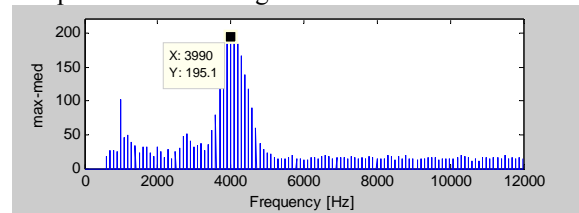


Fig. 4. Max-med plot of the signal under validation. Optimal center frequency equals 3990 Hz

Note: for the clarity of the algorithm, a single characteristic frequency was defined, i.e. $F = \{f_i\}$. If F contained more than one element, i.e. the algorithm was implemented for a multi-element set of characteristic frequencies, the figures may be plotted “one on the top of another”, which is surely readable for up to a dozen figures at one time.

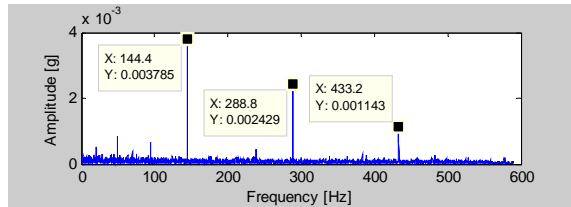


Fig. 5. Narrowband envelope spectrum of the signal for optimal parameters pointed out by the max-med algorithm

The Fig. 5 presents the narrowband envelope spectrum calculated from the band given by the max-med method. The figure clearly shows existence of strong harmonics related to the outer ring fault.

4. SUMMARY

The presented method demonstrates the possible enhancement of the optimal center frequency selection method via a novel “max-med” estimator. The technique enables a more robust selection alternative to existing methods, including Fast Kurtogram and Protrugram, both based on the kurtosis-based estimator.

The authors have shown that kurtosis-based estimators are not feasible for detailed spectral “scanning”, since they by definition require large number of samples. The method is yet to be empirically developed in terms of the optimal neighborhood selection δ as a function of the signal length and the sampling frequency, as well as the weighing scale as a function of the number of harmonic lines. Further research concerning the multi-component analysis (e.g. gear meshing frequencies with sidebands) will be conducted by the authors as well.

The paper was supported by the Polish Ministry of Science and Higher Education as the research project no N504 347436.

REFERENCES

- [1] Ho D., Randall R. B., *Optimization of bearing diagnostic techniques using simulated and actual bearing fault signals*, Mechanical Systems and Signal Processing. Volume 14, Issue 5, 2000, Pages. 763-788
- [2] Jabłoński A.: *Development of algorithms of generating an envelope spectrum of a vibration signal in the frequency domain for rolling element bearing fault detection*, MSc thesis, AGH

University of Science and Technology, Kraków, 2008.

- [3] Barszcz T., Jabłoński A.: *A novel method for the optimal band selection for vibration signal demodulation and comparison with the Kurtogram*. Submission MSSP09-209 (Mechanical Systems and Signal Processing).
- [4] Antoni J.: *Fast computation of the kurtogram for the detection of transient faults*. Mechanical Systems and Signal Processing. Volume 21, Issue 1, January 2007, Pages 108-124
- [5] Zimroz R.: *Optymalizacja wyboru szerokości pasma w demodulacji sygnału do wykrywania uszkodzeń lokalnych w elementach maszyn górniczych*. Badawcze Laboratorium Diagnostyki i Wibroakustyki, Zakład Systemów Maszynowych Instytutu Górnictwa PWr.
- [6] Bartelmus W., Zimroz R.: *Optymalny zakres częstotliwości w procedurze demodulacji amplitudy w zastosowaniu do uszkodzeń lokalnych*. Diagnostyka 1(37), 2006.
- [7] Mayoof N. F.: *Beating Phenomenon of Multi-Harmonics Defect Frequencies in a Rolling element Bearing: Case Study from Water Pumping Station*. World Academy of Science, Engineering and Technology 57, 2009.



Tomasz BARSZCZ pracuje jako adiunkt w Katedrze Robotyki i Mechatroniki. Zajmuje się diagnostyką maszyn oraz systemami monitoringu i diagnostyki. Jest autorem 4 książek i ponad 60 publikacji. Opracowane przez niego systemy pracują na ponad stu kilkudziesięciu instalacjach.



Adam JABŁOŃSKI jest absolwentem Wydziału Inżynierii Mechanicznej i Robotyki AGH oraz Central Texas College, USA. Obecnie inżynier diagnosta w EC Systems i doktorant WIMiR, AGH. Zajmuje się przetwarzaniem sygnałów dla potrzeb diagnostyki maszyn.

WELDED JOINT ASSESMENT ON THE BASIS OF AN ALGORITHM OF CHARACTERISTIC EDGE DETECTION¹

Anna BZYMEK, Anna TIMOFIEJCZUK

Department of Fundamentals of Machinery Design, Silesian University of Technology
44-100 Gliwice, ul. Konarskiego 18a, tel. (32) 237 10 63, fax (32) 237 13 60,
anna.bzymek@polsl.pl , anna.timofiejczuk@polsl.pl

Summary

Research presented in the paper concerns a part of the software applied in a vision system designed for welding process diagnostics. In the system one infrared camera and two CCDs were applied. All procedures included in the image analysis module were limited to operations performed within distinguished ROIs (Region Of Interest), the areas around ROIs were omitted. The goal of the analysis was to obtain series of image features that could be a background for recognition abnormalities of the welding process and faults of the weld. Procedures elaborated within the framework of the described research were focused on the application of two algorithms realized correspondingly, they were: scanning operations, and procedures of identifying characteristic edges of the welded joints. Presented research were elaborated in Department of Fundamentals of Machinery Design of Silesian University of Technology within the framework of PW-004/ITE/10/2006 project.

Keywords: quality assessment, welded joint, image analysis, edge detection.

OCENA POPRAWNOŚCI WYKONANIA ZŁĄCZ SPAWANYCH Z ZASTOSOWANIEM ALGORYTMU DETEKCJI KRAWĘDZI

Streszczenie

Prezentowane badania dotyczą części oprogramowania opracowanego dla celów systemu przeznaczonego do diagnostyki procesu spawania. System składa się m.in. z dwóch kamer CCD i jednej kamery termowizyjnej. Na podstawie analizy wyróżnionych obszarów zainteresowania (ROI) ze zdjęć rejestrowanych w trakcie procesu spawania, wyznaczono zbiór cech, które mogą stanowić podstawę do wnioskowania o niezgodnościach spawalniczych powstających podczas spawania oraz o stabilności procesu. Wyniku przeprowadzonych badań opracowane zostały dwa algorytmy: tzw. skanowania połączenia w celu wyznaczenia profilu jasności oraz procedury umożliwiające identyfikację krawędzi charakterystycznych dla konkretnych niezgodności. Badania zostały przeprowadzone w Katedrze Podstaw Konstrukcji Maszyn w ramach projektu PW-004/ITE/10/2006

Słowa kluczowe: poprawność wykonania, złącze spawane, analiza obrazów, detekcja krawędzi.

1. INTRODUCTION

Vision systems are more and more often applied as integral parts of manufacturing processes. Among numerous examples of their applications the assessment of the welding processes is one of faster developing directions of these systems. The most important applications are aimed at analysis of these

processes as well as the estimation of welded joint correctness on-line [1] [4] [10]. In such cases, the achievement of the system application is strongly related not only to appropriate parameters of a hardware part but also to procedures of image processing and analysis [2] [3] [5] [7] [11] [12]. There are different approaches to this process assessment. The majority of them are based on

¹ Scientific work financed from resources assigned to science in the years 2006-2008 as a research project

applications of cameras acquiring images within visible range of the radiation. However, the observation of the welded joint by means of an infrared camera becomes more and more popular [6]. Information extracted on the basis of image analysis, both infrared and regular images, lets us estimate the welded joint quality and thereby the process.

Presented research concerns the part of the software applied in a vision system designed for the welding process diagnostics. Procedures have been elaborated in Department of Fundamentals of Machinery Design of Silesian University of Technology within the framework of PW-004/ITE/10/2006 project.

In Fig. 1 the vision system consisting of two CCDs and one infrared camera, industrial PC, and

the lightening has been presented during operation in an automotive industry company [1] [5].

2. RESEARCH PROBLEM

A concept of the elaborated system and information concerning the realization of its parts have been described in [1]. The core of the system was an image analysis module. An idea of the application of selected image analysis methods in the system was based on an assumption that observation of the welding arc with the use of the system and the analysis of acquired images performed afterwards, could provide us with the information about stability of the arc and through this – the stability of the welding process. Such approach was described in [3] [5] in details.

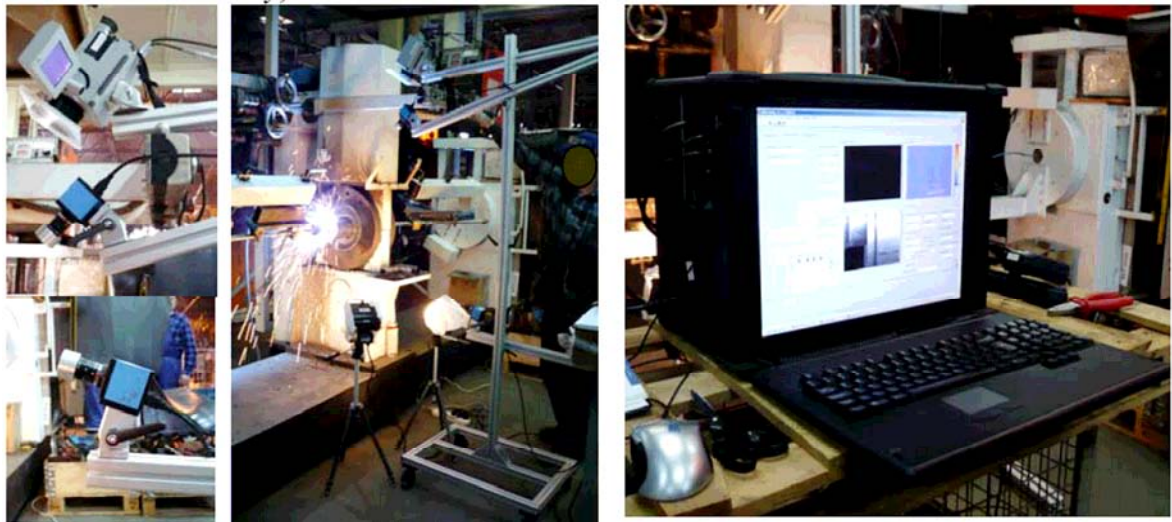


Fig. 1. Research stand.

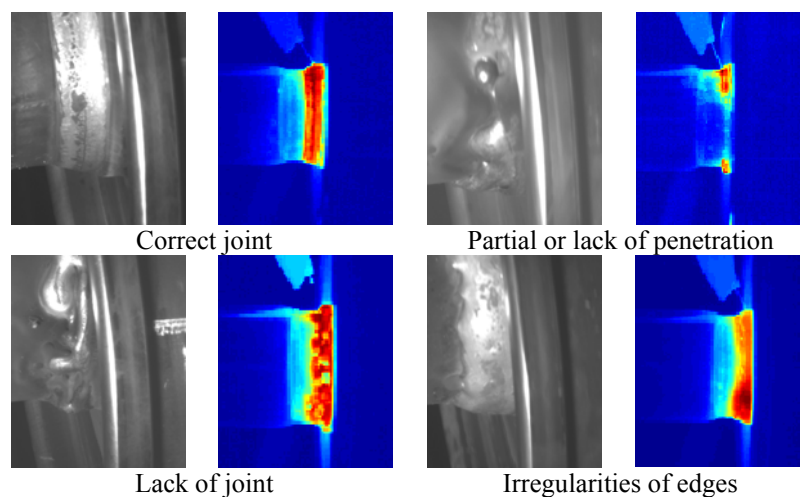


Fig. 2. Examples of images of correct and faulty joints.

The second assumption let us state that on the basis of results of the analysis of images of the welded joints acquired with the use of the CCD and infrared camera, it was possible to estimate the quality of the welded joint. In the system one infrared and two CCDs were applied. Examples of images acquired with the use of both cameras have been presented in Fig. 2. There are examples of a correct joint and three faulty joints in these images. All procedures included in the image analysis module of the system were limited to operations performed within distinguished ROIs (Region Of Interest), the areas around ROIs were omitted. The goal of the analysis was to obtain series of image features that could be a background for recognition abnormalities of the welding process and faults of the weld. A simplified scheme of the system

consisting of several modules has been shown in Fig. 3.

An approach presented in the paper concerns a part of the system which is the module of processing and analyzing images. Input images were required by module of image recording. Results of the procedures of image processing and analysis were sent to modules of recognition and inference modules. Applied techniques were focused on images of the welded joint acquired by means of one of two CCDs during observations of the welding process. Since the majority of faults being detected manifest themselves on the surface and along borders of joints, procedures of image analysis were required to be very sensitive. Taking into account characteristic forms of the faults two kinds of algorithms have been applied.

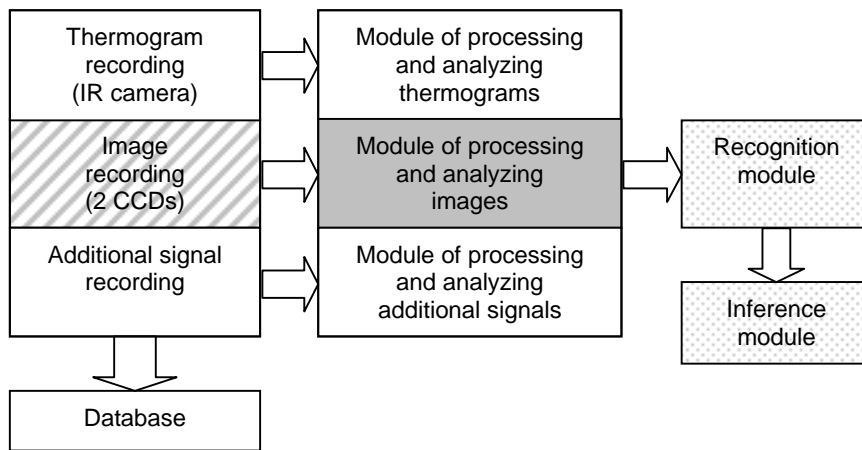


Fig. 3. Examples of images of correct and faulty joints.

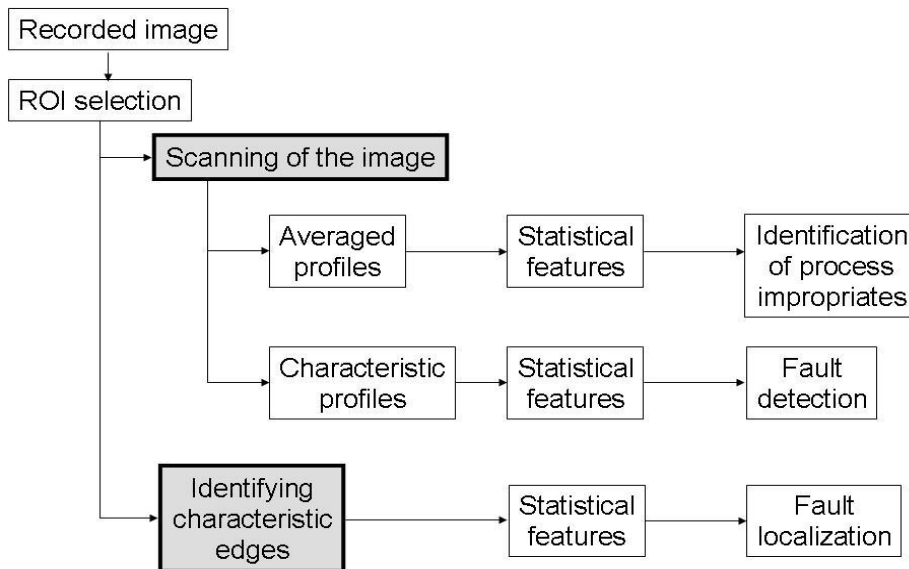


Fig. 4. Scheme of the application of the algorithms and their results.

3. PROCEDURES APPLIED IN THE RESEARCH

Procedures elaborated within the framework of the described research were focused on the application of two algorithms that realized correspondingly:

- scanning operations,
- identifying characteristic edges of the welded joints.

A scheme of the application of these algorithms as well as further operations performed with the use of results of the algorithms (blocks on the right) have been presented in Fig. 4.

In both cases the goal of their application was to look for outstanding areas or artifacts in the analyzed image. Both algorithms were performed for ROIs automatically distinguished from analyzed images.

3.1. Scanning operations

The first of the applied algorithms consisted in observation of the changes of the intensity level along straight lines moved over the welded joint in two perpendicular directions. As results brightness profiles along distinguished straight lines were calculated.

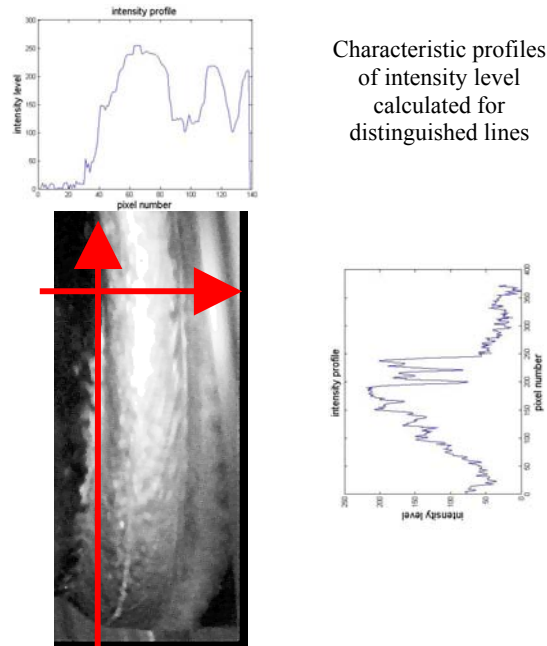


Fig. 5. Scheme of the application of the scanning algorithm

The averaged profiles were used for evaluation of additional features that were used during recognition and inference phases. These features have been not described in the paper. Positions of the characteristic profiles and connection between these profiles let us detect a fault of the joint and roughly estimate its localization and size. The approach enabled us also to identify the width of the weld face and estimate rectilinearity of its edges.

Employment of these scanning methods made it possible to identify such welding faults like: concavity of the weld, metal spattering as well as partial or lack of penetration. An example of the application of this procedure has been presented in Fig. 5. In the image there has been presented an exemplary image representing a faulty joint with lack of penetration.

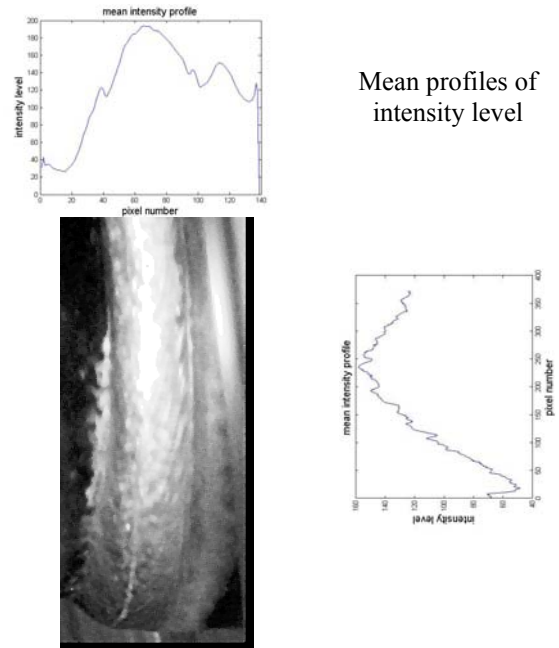


Fig. 6. Scheme of the application of the scanning and averaging algorithm

As the result of this algorithm profiles in two selected perpendicular direction have been estimated (Fig. 5). Moreover, series of such profiles have been also subjected to an averaging procedure (Fig.6).

3.2. Identifying characteristic edges of welded joint

The second algorithm was elaborated in order to precisely estimate faults identified in the first stage. The main idea of this approach was to identify and distinguish characteristic edges in a selected area of the image. As results of several testing approaches and numerous experiments, the elaborated algorithm was based on detection of short straight sections that represented fragments of edges of the welded joint, with the use of function in LabView [8] [9].

On the basis of these line it was possible to estimate the continuity of the whole edge and variations of its shape. In order to determine the shape of the edges, coordinates of line endpoints in each section were calculated. These values let us calculate characteristic coefficients that corresponded to fault kinds and their precise dimensions. As in case of the previous algorithm, described operations were performed for ROI representing a selected part of the image. A scheme of the application of the procedure has been presented in Fig. 7.

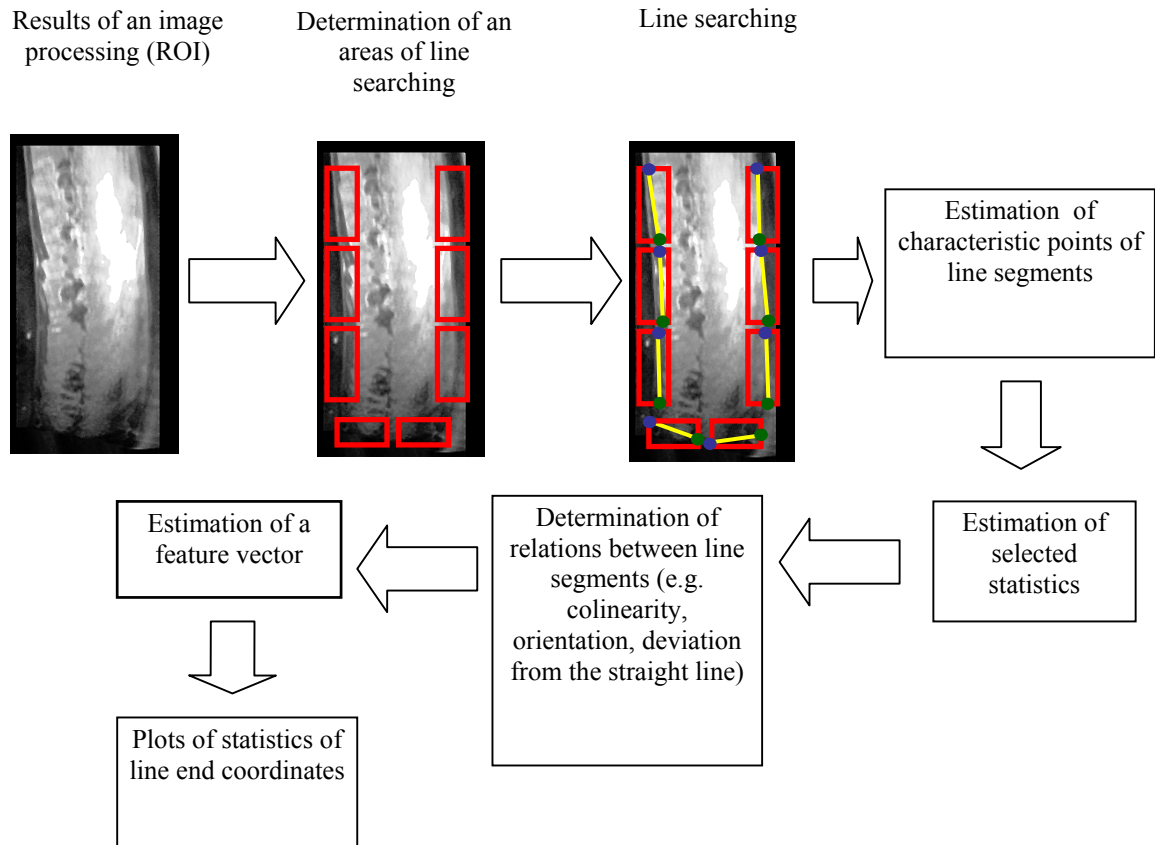


Fig. 7. Schema of the algorithm of identification of lines

In the presented approach the left and right sides of the joint edge were treated separately. In Fig. 8 and Fig. 9 the application of the procedure has been presented. For each edge of the joint within ROI four sections were distinguished.

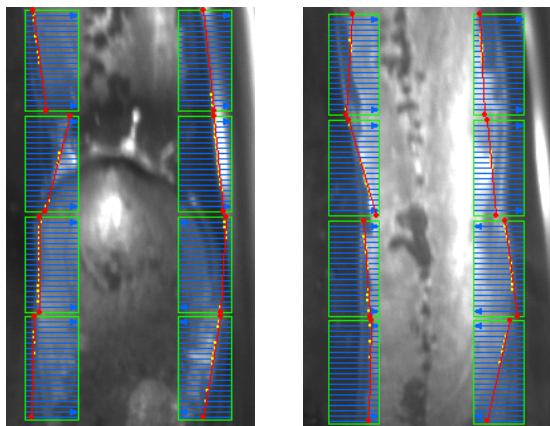


Fig. 8. Sections identified in images of correct welded joints (selected ROIs)

Within each section one straight line was to be detected (indicated by the red line) and coordinates of the line were determined. Further calculations for each single identified sections consisted in estimation of selected statistics such as mean, standard deviation and variance. Results have been

shown in form of the statistics plots in Fig. 9 and Fig. 10.

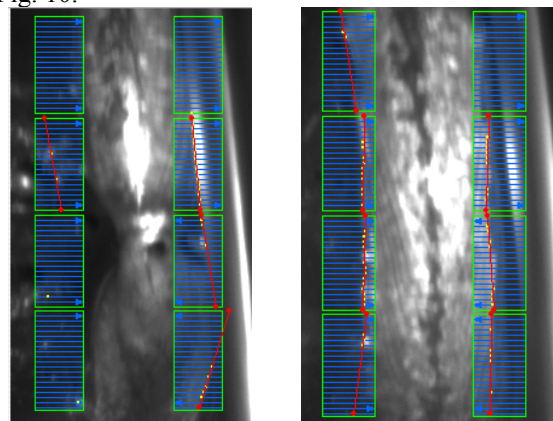


Fig. 9. Sections identified in images of faulty welded joints (selected ROIs)

Differences observed for the left and right sides of the weld let as state about similarity between sides of the weld. The approach allowed also to estimate some incorrectness (such as nonlinearity of the endpoints) on the right and left sides of the joint and also to calculate their dimensions. Moreover other kinds of characteristic coefficients apart from statistics enumerated above such as distance between sections in horizontal direction could be also calculated.

The most crucial problem related to the application of this procedure was to select proper values of parameters of the algorithm. Examples of important parameters were:

- dimensions of ROI divided into sections,
- dimensions of an area of a single section ,
- numbers of sections.

Selected results of observation of the welding process and the application of the algorithm have been presented in Fig. 10 and Fig. 11.

In the plots changes of some statistical values in function of image numbers have been shown. Such results let us s

tate about changes of the process that occurred during the observation In the plots relatively huge fluctuations are visible. They are characteristic for cases the edge has been not identified. The fluctuations are results of fixed parameters of the algorithm (localization of sections and their dimension).

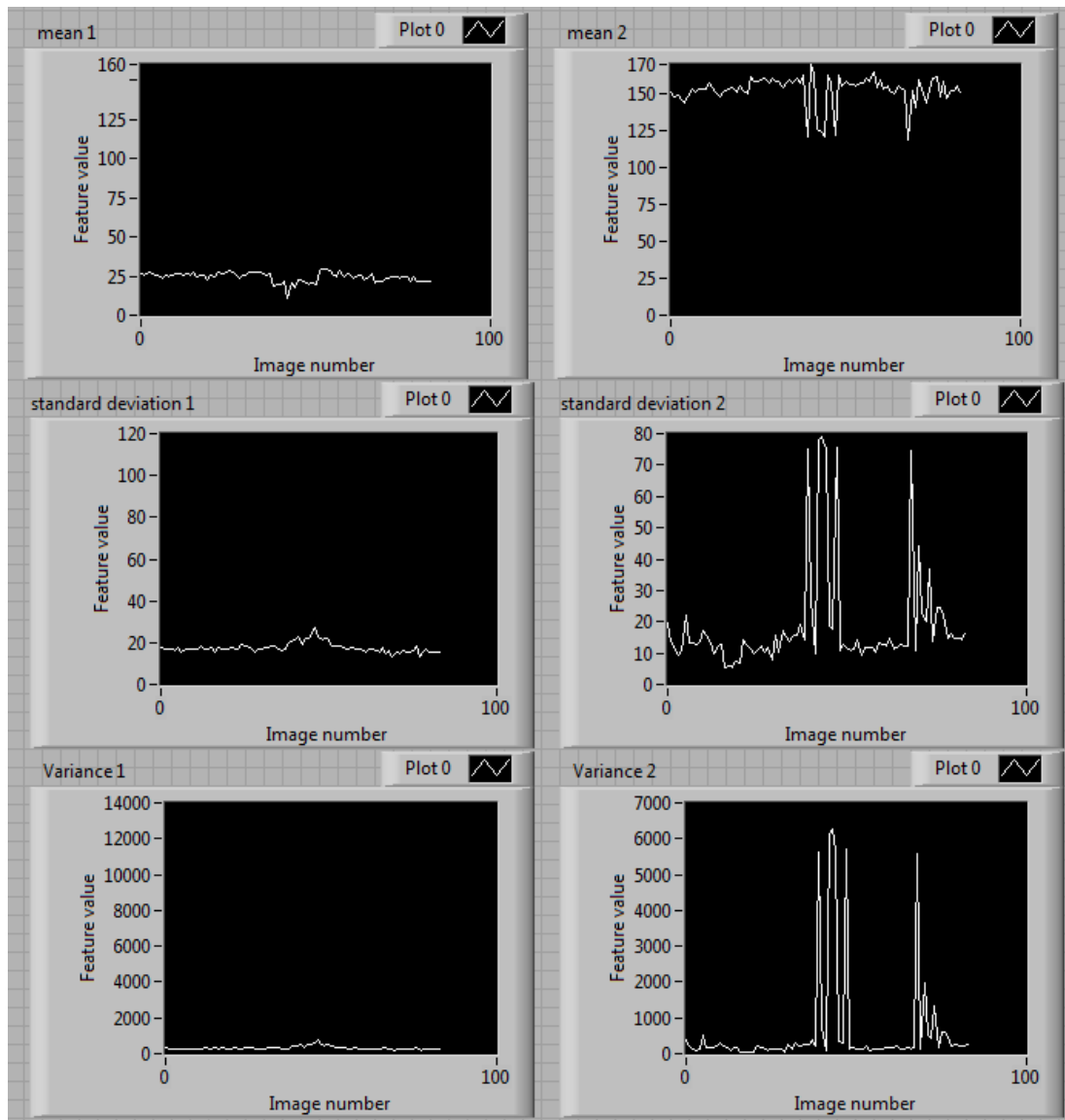


Fig. 10. Results of analysis of line ends coordinates position for correct joint

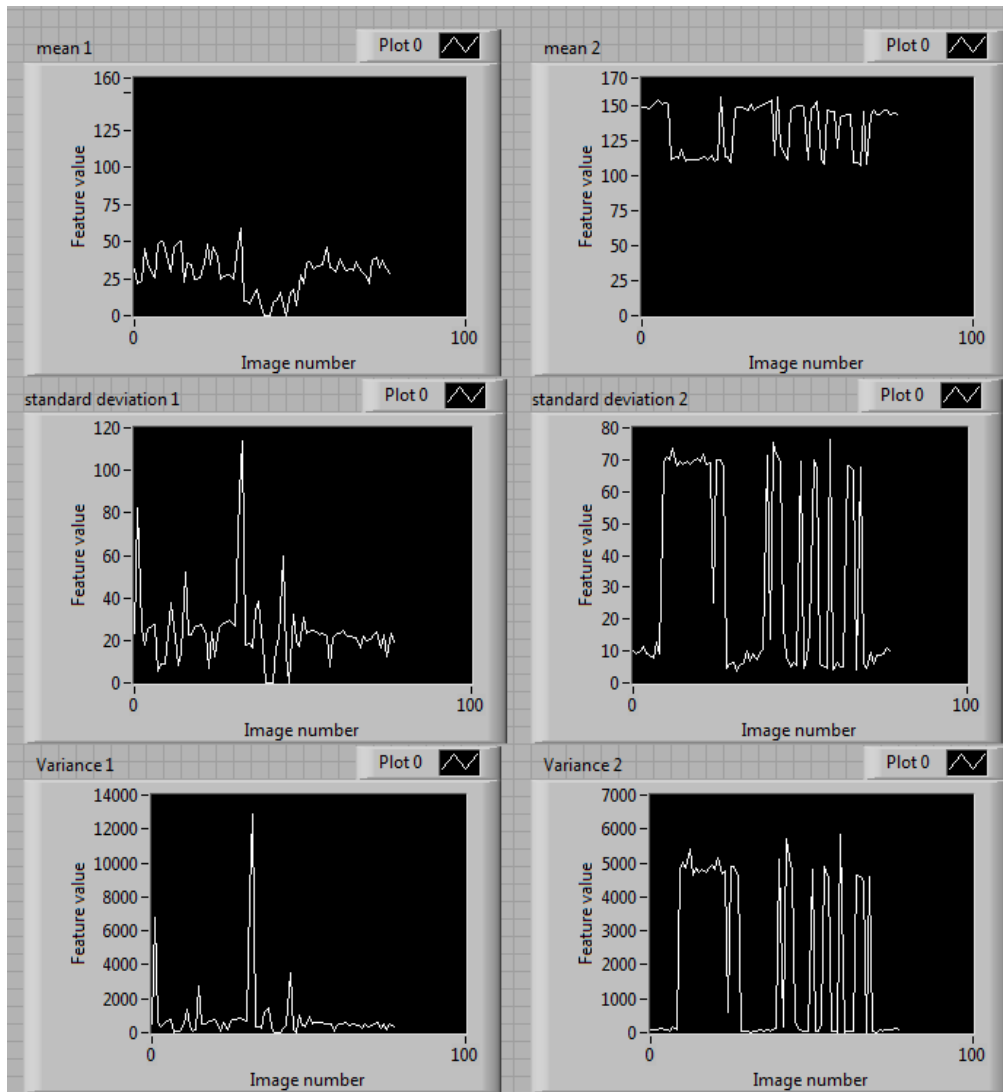


Fig. 11. Results of analysis of line ends coordinates position for faulty joint

In some cases the joint edges are outside the section within they were expected to be. Depending on the goal of the application of the procedure such parameters can be perceived as disadvantage. However, results obtained within the research made it possible to determine relationships between shape and quality of the joint. Improperities of the process and incorrectness of the joint are visible as huge peaks in the plots.

4. DISCUSSION AND CONCLUSIONS

In the paper descriptions of two algorithms applied in the vision system designed for welded process diagnostics have been presented. The first algorithm was based on scanning a selected part of the image recorded by means of a CCD. The second algorithm let us to detect edges of the welded joint within small sections. Some results of the applications of the algorithms have been presented on the basis of images recorded during the welding process performed in automotive industry company. The most important property of both algorithms was

their simplicity. However, their results in form of series of enumerated above parameters can be basis for next steps of the diagnostic process.

The algorithm based on the scanning procedure provided us with result in the form of series of profiles (averaged and characteristic) estimated according to intensity (brightness) level changes. The characteristic profiles were used for overall detection of faults. Localization of the characteristic profiles and relationships between these profiles let us roughly estimate fault localization and in some cases their size. The averaged profiles were used for evaluation of statistical features that characterize the process. These values were evaluated in further parts of the system (recognition and inference modules).

The second algorithm based on identification of characteristic edges in a selected areas of the image (ROIs) provided us with information about short straight sections that represented fragments of edges of the welded joint. Values of coordinates of characteristic points of these sections enabled us to estimate special feature vectors consisting of statistical features. The analysis of these values let

us conclude about faults and their precise dimensions. The proposed procedure have some disadvantages such as: uncertainty associated with the number of sections used for each side of the welded joint, size of the sections and localization of the section within chosen ROI. These parameters, among others [8] have an influence on the efficiency of the line searching algorithm and inappropriate values of the parameters make often finding of the line impossible. Therefore the procedure is to be developed in further research that will be performed in the frameworks of the project "Methodology of diagnosing of welding processes with the use of image fusion" to be realized by the authors.

BIBLIOGRAPHY

- [1] Bzymek A., Fidali M., Jamrozik W., Timofiejczuk A.: *Diagnostic vision system for welded joint and welding process assessment*. Problemy Eksploatacji 4/2008.
- [2] Bzymek A., Czupryński A., Fidali M., Jamrozik W., Timofiejczuk A.: *Analysis of images recorded during welding processes*. QIRT'2008, 9th International Conference on Qualitative InfraRed Thermography, Kraków 2008.
- [3] Bzymek A., Timofiejczuk A.: *Estimation of welding process stability based on image analysis and recognition*. Diagnostyka 4(52)/2009.
- [4] Cook G. E., Barnett R. J.: *Automated visual inspection and interpretation system for weld quality evaluation*, Industry Applications Conference, 1995. Thirtieth IAS Annual Meeting, IAS '95, Conference Record of the 1995 IEEE.
- [5] Fidali M., Bzymek A., Timofiejczuk A., Czupryński A., Jamrozik W.: *Evaluation of welding process state on the basis of image and thermogram analysis*. Biuletyn Instytutu Spawalnictwa w Gliwicach 2/2009 (53), pp 50-56 (in Polish).
- [6] Huang R. S., Liu L. M., Song G.: *Infrared temperature measurement and interference analysis of magnesium alloys in hybrid laser-TIG welding process*. Mater. Sci. Eng. A, 2006, doi:10.1016/j.msea.2006.10.069.
- [7] Kim J. S., Son Y. T., Cho H. S., Koh K.II.: *A robust method for vision-based seam tracking in robotic arc welding*, Proceedings of the IEEE International Symposium on intelligent Control 1995.
- [8] NI Vision Concepts Manual, *National Instrument Corporation*, Austin USA 2008.
- [9] NI Vision for LabView Help
- [10] Smith J.S., Balfour C.: *Real time top-face vision based control of weld pool size*, An international journal Industrial robot, No 32/2/2005.

- [11] Xu D., Wang L., Tan M.: *Image processing and visual control method for arc welding robot*, Proceedings of the IEEE International Conference on Robotics and Biomechanics, Shenyang, China 2004.
- [12] Yamamoto M., Kaneko Y., Fujii K., and others.: *Adaptive Control of Pulsed MiG Welding Using Image Processing System*, IEEE 1988.



Anna Bzymek is PhD. student in the Department of Fundamentals of Machinery Design. Main area of research are vision systems in diagnostics, machine vision, image processing, analysis and recognition, signal processing.



Anna Timofiejczuk, PhD., assistant professor in Department of Fundamentals of Machinery Design. Main area of research: time-frequency signal analysis, diagnostic inference, image processing, analysis and recognition

RELIABILITY ESTIMATION IN PRODUCT CONFIGURATION ISSUE

Izabela KUTSCHENREITER-PRASZKIEWICZ

Department of Industrial Engineering
University of Bielsko-Biała
43-300 Bielsko-Biała, ul. Willowa 2, POLAND
phone +48338279282, fax+48338279300
e-mail: ipraszkiwicz@ath.bielsko.pl

Summary

In the product configuration problem of mechanical product type reliability is one of the most important requirements. Product adjustment to customer expectations, which mean product customization, decides about its commercial success. Development of methods helpful in the early phase of product design is needed to product customization. The early phase of design problems is focused on deriving the optimal solution that satisfies some objective functions like e.g. reliability. The proposed product decomposition method and system reliability estimation were presented.

Keywords: product decomposition, reliability estimation.

SZACOWANIE NIEZAWODNOŚCI W ZARZĄDZANIU KONFIGURACJĄ PRODUKTU

Streszczenie

W problematyce zarządzania konfiguracją produktu przemysłowego niezawodność jest jednym z podstawowych wymagań. Dostosowanie produktu do wymagań klienta, czyli kustomizacja decyduje o sukcesie rynkowym. Rozwój metod wspomagających wczesne etapy projektowania produktu jest niezbędny do jego kustomizacji. Wczesne fazy projektowania produktu wymagają prowadzenia optymalizacji z uwzględnieniem niezawodności jako funkcji celu. W artykule przedstawiono proponowaną metodę dekompozycji produktu oraz szacowania jego niezawodności.

Słowa kluczowe: dekompozycja wyrobu, szacowanie niezawodności.

1. INTRODUCTION

Product customization needs a configuration algorithm, which assures customer satisfaction. The configuration algorithm can use the existing, well known components or redesign them. So, in many cases the core product is the same, designers redesign some product components to fulfill given customer requirements. The question is how to estimate reliability for a modernized product.

One of the most important problems in the product configuration issue is product decomposition which provides a combination of components which give product suitable for a particular client. Product decomposition and functional requirements will help to answer the following question: Which physical element(s) is responsible for the fulfillment of a specific functional requirement? [5]. In literature we can find different approaches to product decomposition [2], [3].

The proposed idea of product decomposition includes three levels of classification attributes and their values. The first classification level includes products portfolio (product line), their attributes and their values, where each product line is

characterized by a set of similar product structures (e.g. helical reducers) which use particular parts' set.

Finding the optimal product profile from a product family for a particular customer is an optimization problem which includes the problem of process modeling related to translating customer requirements into engineering characteristics. One of important goals of configuration algorithm is assure product reliability.

The objective of this paper is to present results of research on modernized product reliability estimation.

2. PRODUCT RELIABILITY DECOMPOSITION

Quality is a property which may change with the age of the product[4]. Customer product acceptability will depend on its reliability, that's mean ability to continue to function satisfactorily over a period of time. Reliability is one of the most important aspects of competitiveness, so in product development it is necessary to take into consideration reliability during product and process design. Designers have to assure product reliability

by using [4]: proven designs, the simplest possible design, components of known or likely high probability of survival, employ redundant parts, design to "fail-safe", specify proven operations and methods.

In product and process design it is necessary to predict possible failures and their effects to increase product reliability. Failures could be caused by different features e.g.: wrong design, material, process, operation. In failure analysis it is necessary to take into consideration experiences from service, technology, design, suppliers and customers. Identification of the failure cause is a key point in decreasing potential problems.

The study of time-variant structural system reliability is still developing. In order to perform a realistic reliability analysis of a structural system, the best approach is to find the probability of system failure over a period of time t [1].

Different reliability measures existed in literature. Reliability which is time dependent $R(t)$ may be calculated as number surviving at time t and number existing at $t=0$ quotient, or based on cumulative distribution of failure calculated as $1-R(t)$ or based on probability density function of failure, or failure or hazard rate or mean time between failures.

Reliability system may be considered to be of two kinds: a series system in which failure of either components causes failure of the whole system, and a parallel system where components operate in parallel.

In product reliability estimation reliability decomposition (allocation) is an important issue. Reliability allocation is understood as the process of assigning reliability requirements to individual components or sub-systems to attain the specified system reliability [5].

To create reliability model it is necessary to achieve a specified reliability goal for the system.

According to [5] most of mechanical systems are designed in a series system, so the series system reliability $R_s(t)$, assuming that the failure of any function i , component j and failure mechanism k will lead to system failure, could be estimated basing on:

$$R_s(t) = \prod_{i=1}^p \left[\prod_{j=1}^q \left\{ \prod_{k=1}^m R_{ijk}(t) \right\} \right] \quad (1)$$

$$R_s(t) = \exp(-\lambda_{t_s} t^\beta) \quad (2)$$

$$R_{ijk}(t) = \exp(-\lambda_{t_{ijk}} t^\beta) \text{ for } t \geq 0 \quad (3)$$

$$\lambda_{t_s} = \sum_{i=1}^p \sum_{j=1}^q \sum_{k=1}^m \lambda_{t_{ijk}} \quad (4)$$

$$\theta_s = \left\{ \sum_{i=1}^p \sum_{j=1}^q \sum_{k=1}^m \frac{1}{\theta_{ijk}^\beta} \right\}^{-\left(\frac{1}{\beta}\right)} \quad (5)$$

$$\lambda(t) = \beta \left(\frac{t^{\beta-1}}{\theta_{111}^\beta} \right) + \dots + \beta \left(\frac{t^{\beta-1}}{\theta_{111}^\beta} \right) = \beta \left(\frac{t^{\beta-1}}{\theta_s^\beta} \right) \quad (6)$$

Where:

- $\lambda(t)$ - The system hazard rate at any time t ;
- λ_{t_s} - The transformed failure rate of the system;
- $R_{ijk}(t)$ - Reliability of k th failure mode for i th function and j th component for mission time t ;
- θ_s - Life of the system;
- β - Shape factor.

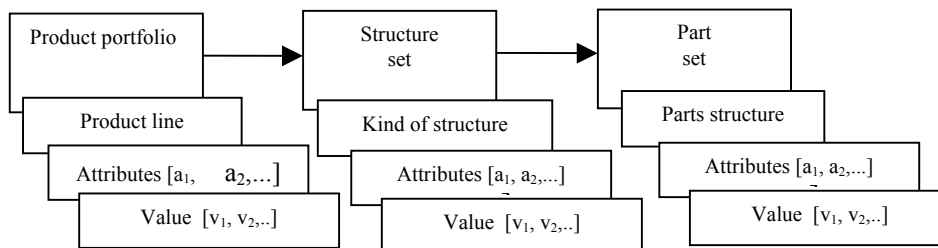


Fig. 1. The idea of product decomposition

3. TOOTHED GEAR EXAMPLE OF PRODUCT RELIABILITY ESTIMATION

3.1. Problem formalization

Producers of machine elements like e.g. toothed gear, besides product portfolio presented in catalogues offer to their clients product adaptation, which means product customization. The goal is to create reliability estimation model which helps in product configuration according to particular customer expectations.

Configuration design is focused on establishing the product based on the pre defined parts' set and could be divided into classes: the first includes pure composition in which a set of parts is already known; in the second class parts could be redesigned in case suitable parts cannot be found. In the presented approach reliability estimation can be based on product decomposition presented in fig. 1. and the decomposition of system level reliability described on p. 2.

3.2. Failure probability estimation

According to the proposed product decomposition method, reliability analysis can be based on reliability matrix (fig.2). For each product decomposition level attributes and a set of values were established. Each product line is characterized by attributes and their values like, e.g. geared motors could be characterized by horizontal and vertical working arrangement, product structures are divided into different kinds which are also characterized by attributes and their values, e.g. double reduction number. A Set of parts includes information like, e.g. nominal modules in toothed elements used in particular kind of product structure. For parts' sets the failure mechanism is specified and estimation of failures could be made. Based on reliability matrix, probability of failure could be estimated on the basis of regression analysis. An example related to toothed elements production process was shown on the fig. 3.

Product line	Attributes	V value	Kind of structure	Attributes	V value	Subsystem / Component reliability	Attributes	V value	Failure mechanism							Reliability
									Transportation failure	Processes failure	Supplier cause failure	Fatigue failure	Construction failure	Unidentified	Wrong selection	
Geared motors	vertical	Helical	Reduction number	Double triple quadruple quintuple	Type	Bearings	Type	1	1	0,989	0,997	1	1	0,989	0,975	0,818
						Housings	Type	0,998	0,999	0,979	1	0,999	1	0,998	0,973	
						Toothed elements	Module	1	0,998	0,997	0,999	1	1	0,969	0,963	
						Shafts	Length/diameter	1	0,999	0,999	0,997	1	1	0,969	0,964	
						Packing	Type	1	1	0,989	1	1	1	0,969	0,958	
						Lubrication	Type	1	1	0,999	1	1	1	0,969	0,968	
		Bevel – helical	Reduction number	Double triple quadruple quintuple	Type	Bearings	Type	1	1	0,999	0,997	1	1	0,989	0,985	0,842
						Housings	Type	0,998	0,999	0,998	1	0,999	1	0,998	0,992	
						Toothed elements	Module	1	0,998	0,997	0,999	1	1	0,969	0,963	
						Shafts	Length/diameter	1	0,999	0,999	0,998	1	1	0,969	0,965	
						Packing	Type	1	1	0,988	1	1	1	0,969	0,957	
						Lubrication	Type	1	1	0,999	1	1	1	0,969	0,968	
	Horizontal	Helical	Reduction number	Double triple quadruple quintuple	Type	Bearings	Type	1	1	0,989	0,997	1	1	0,989	0,975	0,843
						Housings	Type	0,998	0,999	0,999	1	0,999	1	0,998	0,993	
						Toothed elements	Module	1	0,998	0,997	0,999	1	1	0,969	0,963	
						Shafts	Length/diameter	1	0,999	0,999	0,997	1	1	0,969	0,964	
						Packing	Type	1	1	0,999	1	1	1	0,969	0,968	
						Lubrication	Type	1	1	0,999	1	1	1	0,969	0,968	
	Horizontal	Bevel – helical	Reduction number	Double triple quadruple quintuple	Type	Bearings	Type	0,998	0,999	0,979	1	0,999	1	0,998	0,973	0,818
						Housings	Type	1	0,998	0,997	0,999	1	1	0,969	0,963	
						Toothed elements	Module	1	0,999	0,999	0,997	1	1	0,969	0,964	
						Shafts	Length/diameter	1	1	0,989	1	1	1	0,969	0,958	
						Packing	Type	1	1	0,999	1	1	1	0,969	0,968	
						Lubrication	Type	0,998	0,999	0,979	1	0,999	1	0,998	0,973	

Fig. 2. Reliability matrix

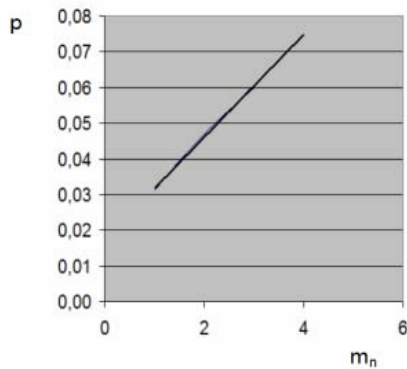


Fig. 3. Estimation of process probability failure (toothed element processing according to Reishauer method)

Nominal module was taken as toothed element attribute. Basing on nominal module, the failure probability of toothed elements processed according to Reishauer method was estimated.

In the Reishauer method a high degree of machine wear affects higher failure rate - the greater cutting resistance, the more likely failures are.

4. CONCLUSION

It is necessary to develop methods useful in product customization, which are helpful in product configuration suitable for a particular client. One of the most important problems in product configuration issue is product decomposition, which provides a combination of components which gives product suitable for a particular client.

The proposed idea of product decomposition is useful is product reliability estimation. The proposed approach joins problems related to product decomposition widely discussed in literature [2], [3] with those related to product configuration issue and theory of reliability [4], [5]. The proposed approach is applicable in mechanical product type and is a useful tool for creating the optimal product configuration. Numerical data used in reliability matrix could be taken from FMEA analysis, complaints analysis or quality assures system.

REFERENCES

- [1] Frangopol D., Maute K.: *Life-cycle reliability-based optimization of civil and aerospace structures*. Computers and Structures 81, 2003, p.397–410.
- [2] Jiao J., Tseng M., Dufty V., Lin F.: *Product family modeling for mass customization*. Computers ind. Engng Vol. 35, Nos 3-4, 1998 p.495-498.
- [3] Lin M, Chen L., Chen M.: *An integrated component design approach to the development of a design information system for customer-oriented product design*. Advanced Engineering Informatics 23, 2009, p.210–221.
- [4] Muhlemann A., Oakland J., Lockyer K.: *Production and operations management*. Pitman Publishing, 1992.
- [5] Yadav O., Singh N., Goel P.: *Reliability demonstration test planning: A three dimensional consideration*. Reliability Engineering and System Safety 91, 2006, p. 882–893.



Izabela

KUTSCHENREITER-PRASZKIEWICZ Ph.D.,

B. Eng. is a lecturer in Department of Industrial Engineering at University of Bielsko-Biala. In her scientific work she deals with application of artificial intelligence in industrial engineering.

CORRELATION ANALYSIS IN STEAM TURBINE MALFUNCTION DIAGNOSTICS

Tomasz GAŁKA

Instytut Energetyki, Pracownia Diagnostyki Urządzeń Ciepłych Elektrowni
02-981 Warszawa, ul. Augustówka 36, fax 22 642 83 78, e-mail tomasz.galka@ien.com.pl

Summary

Rotating machinery condition assessment employs, to a large extent, vibration-based symptoms, characterized by high information content. Diagnostic reasoning is often supported by well-developed qualitative or even quantitative relations. In many cases, however, a situation is encountered wherein several possible malfunction types give similar symptoms. Qualitative diagnosis may thus demand additional diagnostic procedures. The paper concentrates on those employing correlation coefficients, which belong to a broader class of evolutionary symptoms. Such symptoms are sensitive to the malfunction type and thus can substantially enhance qualitative diagnostic capabilities. Moreover, correlation coefficient as a function of time provides valuable quantitative information on lifetime consumption. This is demonstrated by a number of examples, pertaining to large steam turbines operated by utility power plants.

Keywords: technical diagnostics, diagnostic symptom, correlation, prognosis.

ANALIZA KORELACJI W DIAGNOZOWANIU USZKODZEŃ TURBIN PAROWYCH

Streszczenie

Ocena stanu technicznego maszyn wirnikowych opiera się w dużym stopniu na symptomach drganiowych, charakteryzujących się dużą zawartością informacji. Wnioskowanie diagnostyczne często wykorzystuje sprawdzone relacje diagnostyczne, jakościowe, a nawet ilościowe. W wielu przypadkach mamy jednak do czynienia z sytuacją, w której szereg możliwych uszkodzeń daje podobne symptomy. Diagnoza jakościowa wymaga wówczas dodatkowych procedur. Artykuł jest poświęcony zastosowaniu współczynników korelacji, należących do szerszej klasy symptomów ewolucyjnych. Są one wrażliwe na typ uszkodzenia i mogą znacznie poprawić możliwości diagnozowania jakościowego. Współczynniki korelacji w funkcji czasu dostarczają także cennej informacji ilościowej o stopniu wyczerpania żywotności. Jest to zilustrowane kilkoma przykładami, odnoszącymi się do dużych turbin parowych w energetyce zawodowej.

Słowa kluczowe: diagnostyka techniczna, symptom diagnostyczny, korelacja, prognoza.

1. INTRODUCTION

When studying technical diagnostics development, it is useful to have in mind the definition of damage as a 'continuous or sudden loss of integrity and/or operational feature' [1]. At early stages, attention was focused principally on 'sudden' losses, referred to as *random damages*: the aim of diagnostic methods was to detect such occurrences and identify malfunctions. This can be referred to as *qualitative diagnostics*. Next stages were to evaluate damage extent and eventually make a forecast (prognosis) concerning its future development: that, in turn, means focusing on 'continuous' losses, or *natural damages*, and *quantitative diagnostics*. Obviously this corresponds to the generalized damage concept (see e.g. [2,3]), wherein generalized damage can be expressed as $D = \theta/\theta_b$ (θ_b denotes time to breakdown and is determined by object parameters).

Quantitative diagnostic methods have developed considerably in recent years (a concise review for rotating machines can be found in [4]). It has to be kept in mind, however, that a large and complex machine has many possible faults, i.e. its technical condition is described by a multidimensional fault space [5]. At the same time, this condition is assessed on the basis of many diagnostic symptoms. It is convenient to express this in a vector form [6]:

$$\mathbf{S}(\theta) = F[\mathbf{X}(\theta)] \quad (1)$$

wherein $\mathbf{S}(\theta)$ and $\mathbf{X}(\theta)$ denote symptoms and condition parameters vectors, respectively. Now, consider a symptom $S_i(\theta)$. Obviously,

$$S_i(\theta) = f[X_1(\theta), X_2(\theta), \dots, X_n(\theta)] \quad (2)$$

In fact, Eq.(2) may be viewed a more general form of the following relation, derived from the Energy Processor (EP) model (see [2,3]):

$$S(\theta) = \Phi \left[V_0 \left(1 - \frac{\theta}{\theta_b} \right)^{-1} \right], \quad (3)$$

where V_0 denotes the power of residual processes for $\theta = 0$. It is easily seen that Eqs.(2) and (3) become equivalent if only one component of the vector \mathbf{X} , i.e. $X = \theta/\theta_b$, is taken into account (this issue shall be recalled in Section 3.3). In the ideal case, we have¹

$$\partial S_i / \partial X_k > 0 \text{ if } k = j, \quad \partial S_i / \partial X_k \approx 0 \text{ if } k \neq j, \quad (4)$$

which means that, within a reasonable approximation, S_i depends on X_j only. Such assumption is sometimes acceptable for fast-developing faults with very specific representations in the symptom space; in such cases, diagnostic relations of the $S_i = f(X_j)$ type can be determined e.g. by means of regression analysis (see e.g. [8]). Usually, however, a symptom is influenced by a number of condition parameters; synchronous component of vertical vibration in rotating machines provides a good example [9,10]. Therefore, problems arise already at the stage of damage identification.

The problem is further exacerbated by the consequences of the fact that general relation of the type given by Eq.(1) is in most cases only approximate. Usually we have

$$\mathbf{S}(\theta) = F[\mathbf{X}(\theta), \mathbf{R}(\theta), \mathbf{Z}(\theta)], \quad (5)$$

where vectors $\mathbf{R}(\theta)$ and $\mathbf{Z}(\theta)$ describe control and interference, respectively. Control parameters R_i are determined by the operator's purposeful action and their influence can, in principle, be normalized (see e.g. [11]). Influence of interference, in particular non-measurable, cannot be normalized. A good example is provided by two vibration trends, recorded for a 230 MW steam turbine in a utility power plant (see Fig. 1). Both refer to the blade (high) frequency range, wherein vibration components are very sensitive to the \mathbf{R} and \mathbf{Z} vectors components [12]. It is easily seen that, for the 5 kHz component (Fig. 1a), there is a single 'peak', which corresponds to operation at a very low load, about 40% of the rated power. In such situations, pressure distribution over the fluid-flow system cross section, especially immediately downstream the steam inlet, is very uneven and this causes excessive vibration in this frequency range [12,13]. For the 3.15 kHz component (Fig. 1b) the same phenomenon can be observed, but there are two more 'peaks', obviously comparable in magnitude, which are absent in the trend shown in Fig. 1a². The first (indicated by *) can also be attributed to low load (50% of the rated power), but the second (indicated by +) occurred at 87% of

the rated power. Most probably it can be attributed to some interference, but this cannot be resolved on the basis of vibration trends analysis only.

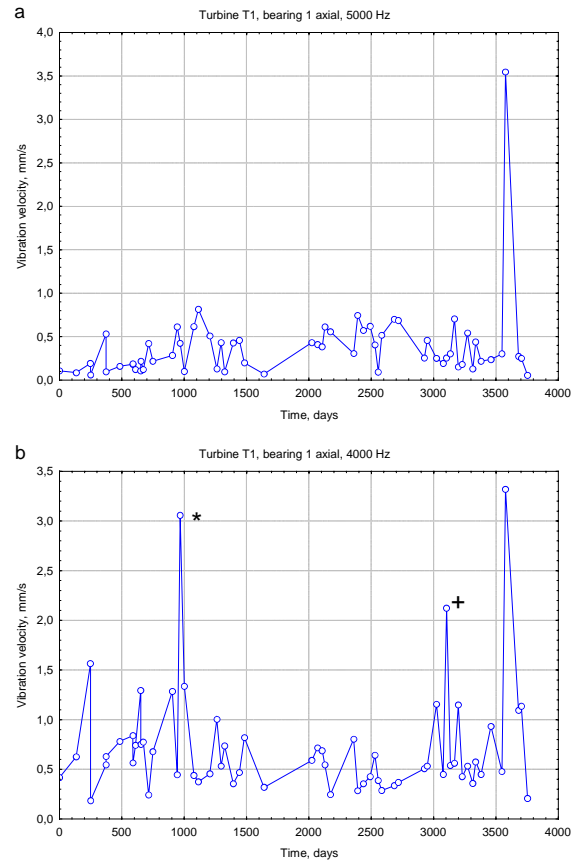


Fig. 1. Vibration velocity trends (23% CPB spectra) for a 230 MW steam turbine, front bearing, axial direction; a, 5 kHz; b, 4 kHz frequency band (see main text for details).

With this all in mind we have to admit that typical procedures, such as analysis of vibration spectra obtained during steady-state operation and even trends analysis, are sometimes not sufficient for a qualitative diagnosis. This draws our attention to additional symptoms that can augment diagnostic reasoning – among them those employing quantitative measures of correlation. In fact, suitability of such symptoms has been pointed out earlier by some authors (see e.g. [10, 15]), albeit in somehow cursory and basically qualitative manner. In the following this issue shall be dealt with in more detail.

Although in this paper attention is focused on steam turbines and vibration-based symptoms, some results and conclusions can obviously be generalized, to cover a broader class of rotating machines or even technical objects and other types of diagnostic symptoms, not necessarily related to vibration.

¹ With the assumption that S_i monotonically increases with damage extent, in accordance with the EP model (for more details, see e.g. [3,7]).

² Influence of 'peaks' such as shown in Fig.1 can be, to some extent, reduced by averaging raw data; for details see e.g. [14].

2. BASIC CONSIDERATIONS

To begin with, let us consider a case wherein observation of turbine condition evolution covers a period from $\theta = 0$ to $\theta = \theta_0$ and furthermore that θ_0 is sufficiently large, typically of the order of magnitude of machine service life – for steam turbines this means at least a few years. In such case we may usually assume that components Z_i of the interference vector have no long-time evolution trends, i.e. do not systematically increase or decrease with time. This can be written as

$$\bigwedge_i \theta \rightarrow \infty \Rightarrow \frac{\Delta Z_i(\theta)}{\theta} \rightarrow 0, \quad (6)$$

where $\Delta Z_i(\theta) = Z_i(\theta) - Z_i(0)$. The same usually applies to the control vector components R_i ,³ which means that, in a similar manner,

$$\bigwedge_i \theta \rightarrow \infty \Rightarrow \frac{\Delta R_i(\theta)}{\theta} \rightarrow 0. \quad (7)$$

The above implies that, when considering symptom evolution between $\theta = 0$ and $\theta = \theta_0$, we may neglect influences of control and interference. This in fact means that we accept approximate relations of the type given by Eq.(2), and forms the basis for diagnostic reasoning based on vibration trends, both $S_i(\theta)$ function types [12,15] and evolution rates [16].

Let us now return to Eq.(2) and assume that the function given by this equation is differentiable with respect to every X_j , $j = 1, 2, \dots, n$. We can thus define a set of partial derivatives $s_{ij} = \partial S_i / \partial X_j$ (cf. Eq. (4)), each representing the ‘sensitivity’ of i -th symptom to j -th condition parameter. Due to non-linearity, s_{ij} in general will change with time. This set can be conveniently written in the $m \times n$ matrix form:

$$[s] = \begin{bmatrix} s_{11} & s_{12} & \dots & s_{1n} \\ s_{21} & s_{22} & \dots & s_{2n} \\ \dots & \dots & \dots & \dots \\ s_{m1} & s_{m2} & \dots & s_{mn} \end{bmatrix}, \quad (8)$$

each row representing a symptom and each column a condition parameter. If we can assume that in each row one element is substantially larger than all other, we have an ideal situation with no ambiguity in *qualitative* diagnosis. This is, however, seldom the case with complex machines, even if we neglect the fact that the s_{ij} elements do change with time. Typically a malfunction (which is equivalent to a condition parameter change) influences a number of symptoms and each symptom can be influenced by a

number of malfunctions. Some additional measures are thus necessary for failure identification.

In general, any symptom will depend on a number of condition parameters, so there will be no deterministic *functional relation* of the $S_i = f(X_j)$ type. We may, however, expect that changes of X_j will affect probability distribution of S_i , which implies a *stochastic relation*. Moreover, it is justified to assume that if X_j changes substantially, then with various values of X_k , $k \neq j$, the value of S_i will fluctuate about some expected value $\hat{S}_i = f(X_j)$. This means a *statistic* or *correlative relation*. If X_j influences a number of symptoms, its changes will affect their probability distributions accordingly. Thus, if two symptoms can be shown to be *correlated*, we may infer that they are *dependent*, i.e. that their changes have been caused by the same condition parameter X_j . The opposite is not true: if two random variables are not correlated, this does not necessarily mean that they are independent [17].

Strength of correlation between symptoms S_1 and S_2 is often described by the Pearson linear correlation coefficient, i.e. a normalized covariance [17]:

$$r = \frac{E\{(S_1 - \eta_1)(S_2 - \eta_2)\}}{\sqrt{E\{(S_1 - \eta_1)^2\}E\{(S_2 - \eta_2)^2\}}}, \quad (9)$$

where E denotes expected value and

$$\eta_1 = E(S_1), \quad \eta_2 = E(S_2). \quad (10)$$

It can be shown that $|r| \leq 1$; $r = 0$ means no correlative relation between S_1 and S_2 , while $|r| = 1$ means a functional relation.

A formal question may be asked whether r can be used as a diagnostic symptom. It should be stressed here that we are speaking of a symptom in the broader sense (a function, usually continuous, rather than an event), in accordance with the EP model [2,3]. We may define such symptom as ‘a measurable quantity which is covariant with object condition’ [5]. Correlation coefficient can be regarded a measure of probability that changes of S_1 and S_2 have been caused by a change of the condition parameter X_j , qualitative relation being determined from the diagnostic model of the object under consideration. We can thus see that r is sensitive to the failure type and conforms to the above diagnostic symptom definition.

According to [10], a measure of correlation between vibration amplitude and an operational parameter is an important diagnostic symptom for steam turbines. This point needs some explanation. In practical applications, correlation (or, more precisely, covariance) between vibration amplitude and turbine load is sometimes used to augment diagnostic reasoning. The same refers to the correlation between vibration amplitude and rotational speed, which can help in identifying malfunctions such as shaft crack or rotor bend; detailed treatment can be found in [9]. In such cases, correlation is usually treated in a purely qualitative manner: investigations are intended to determine whether vibration am-

³ Exceptions to this rule do exist. If a steam turbine is shifted from base-load to peak-load operation, this usually implies that it will be operated in considerably broader load range, hence values of control vector components will also vary within broader limits. In the following we shall neglect such cases.

plitudes change significantly with operational parameters or not. Some remarks on this issue can be found in [18]. In the following, attention shall be focused on the correlation *between two vibration components*.

3. EXAMPLES

All results dealt with in the following have been obtained with large steam turbines, rated between 200 and 260 MW, operated by utility power plants. These machines differ in details, but all are condensing, base-load units; each consists of a high-pressure (HP), intermediate-pressure (IP) and two-stream low-pressure (LP) section and drives a two-pole generator. Absolute vibration velocity (23% constant percentage bandwidth spectra, 10 kHz frequency range) has been recorded on bearing outer casings and LP turbine casing.

3.1. Turbine fluid-flow system failure

This case has been described in detail in references [19,20]. Here we shall concentrate on issues directly related to correlation analysis.

Turbine T9 suffered an IP rotor failure (crack of several last stage blades) and was shut down. It was decided to remove the entire rotor stage blading and keep the turbine in operation until replacement rotor could be supplied. Immediately afterwards, a significant increase of the $4 \times f_0$ component in a number of measurement points (mostly in axial direction) was observed. After opening IP turbine casing during overhaul it was found that steam flow guide fences, mounted inside the outlet part of the casing, were loose and cracked and had to be repaired. Detailed analysis revealed that turbine operation without last stage IP rotor blading resulted in substantial increase of guide fences vibration, probably of resonance nature; this was caused by changes of magnitude and distribution of forces imposed by steam flow. Excited vibration, much higher in amplitude than during normal operation, caused rapid damage of the steam flow guide fences and intensified their vibration; this is a good example of the destructive feedback [3].

Interpretation of higher harmonic components in absolute vibration spectra is by no means straightforward. $3 \times f_0$ and $4 \times f_0$ components are sometimes associated with faulty machining of rotating elements, coupling malfunctions or rotor cracks [10, 15]. They can also result from resonance, which in turn suggests changes in stiffness and/or damping, caused e.g. by substantial material parameters deterioration. It is thus difficult to point out the reason for a dramatic increase of the $4 \times f_0$ component, which became dominant in vibration spectra and caused a substantial increase of overall vibration levels. It can, however, be noticed that this component is, to a high degree, correlated with those from the blade frequency range, which are sensitive to the condition of the fluid-flow system [8]. This can be easily seen

from scatterplots (see Fig.2). In turbine T9, scatterplot clearly indicates correlation, while in turbine T8 (of the same type) vibration components are obviously not correlated.

At the same time, correlation with the f_0 and $2 \times f_0$ components is much weaker than in turbines T8 and T10, which suggests that untypical vibration patterns cannot be attributed to phenomena directly related to the rotational motion (see Table 1) and influence of the fluid-flow system failure is dominant.

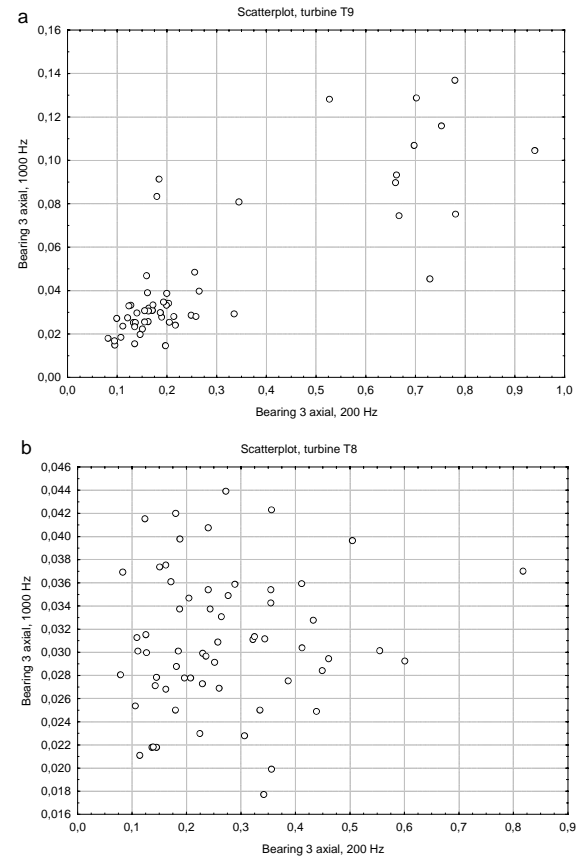


Fig. 2. Scatterplots of 200 Hz vs. 1000 Hz components for turbines T9 (a) and T8 (b); rear IP turbine bearing, axial direction (after [18])

Table 1. Linear correlation coefficients for turbines T8, T9 and T10: rear IP bearing axial (after[18])

Frequency band [Hz]; 23% CPB spectrum	Coefficient of correlation with the $4 \times f_0$ component		
	T8	T9	T10
50	0.19	-0.19	0.77
100	0.23	0.00	-0.35
800	0.16	0.91	0.06
1000	0.11	0.93	0.17
1250	0.07	0.83	0.13
1600	0.22	0.79	0.16
2000	0.04	0.69	0.24
2500	0.06	0.55	0.18

Results for turbine T9 clearly indicate that the $4 \times f_0$ and certain blade range components exhibit strong correlation, i.e. behave in a very similar fashion, which suggests that they probably have the same origin, in terms of object technical condition. In fact, for some frequency bands correlation coefficients are only slightly lower than 1. This facilitates a qualitative diagnosis, as many possible (and more typical) causes can be readily eliminated on this basis.

3.2. IP turbine rotor bow

This case has also received some attention in references [16, 18]. Again, issues relevant to correlation analysis shall be dealt with in the following.

Permanent rotor bow (i.e. involving plastic deformation) is a rare, but serious failure. Repair is costly and time-consuming; in many cases rotor replacement is the only solution. Basically, rotor bow produces symptoms similar to that of a 'plain' unbalance and in fact of many common failure types [9]. Additional tests and measurements are thus required for unambiguous identification. These include vibration monitoring at slow rotational speed [9], monitoring of harmonic components during run-downs in various thermal conditions [21] or phase angle variations at startup [22]. All this requires measurements during transient operation.

IP turbine rotor bow has recently occurred in two steam turbines. Vibration trends shown in Fig.3 reveal that in both cases this has resulted in continuous and rapid increase of the $1 \times f_0$ component of vertical vibration velocity, measured at the rear IP bearing. Rotor balancing, intended as a 'symptom treatment' provided in order to keep turbines in operation until next scheduled overhaul, resulted in some improvement (indicated by arrows), but it is evident that the root cause has not been eradicated. It can be easily seen that, in each cycle, $S_i(\theta)$ is almost linear and $\partial S_i / \partial \theta$ is hardly influenced by rotor balancing. Moreover, influences of interference and control are much weaker than that of the condition parameter (in this case, unbalance resulting from the rotor bow), so trends are fairly regular.

Application of correlation analysis for distinguishing between rotor bow and other possible faults that produce similar behavior of the $1 \times f_0$ component is based on the following reasoning. Normally in a rotating machine with the horizontal shaft line there will always be a rotor sag under its own weight, but resulting rotor shape is maintained during a full rotation [9]. On the other hand, if there is a permanent bow, this shape will change during the period $T = 1/f_0$, so that rotor disks will exhibit a time-dependent tilt in a plane parallel to the rotor axis. For a given disk, the angle α between the disk plane and a vertical plane perpendicular to the rotor axis will behave approximately as [18]

$$\alpha \approx \alpha_s + \alpha_b \sin 2\pi f_0 t, \quad (11)$$

where α_s is the angle resulting from rotor sag due to gravity load and α_b is the amplitude of angle determined by permanent bow. This will result in an additional periodic axial force, with a period of T . We may thus expect axial vibration component with the frequency of f_0 and amplitude increasing with the permanent rotor bow. At the same time, the permanent bow will produce an unbalance with accompanying increase of the f_0 component of vertical vibration. It is therefore justified to suppose that, if this type of fault is present, there will be a correlation of the f_0 components in vertical and axial directions.

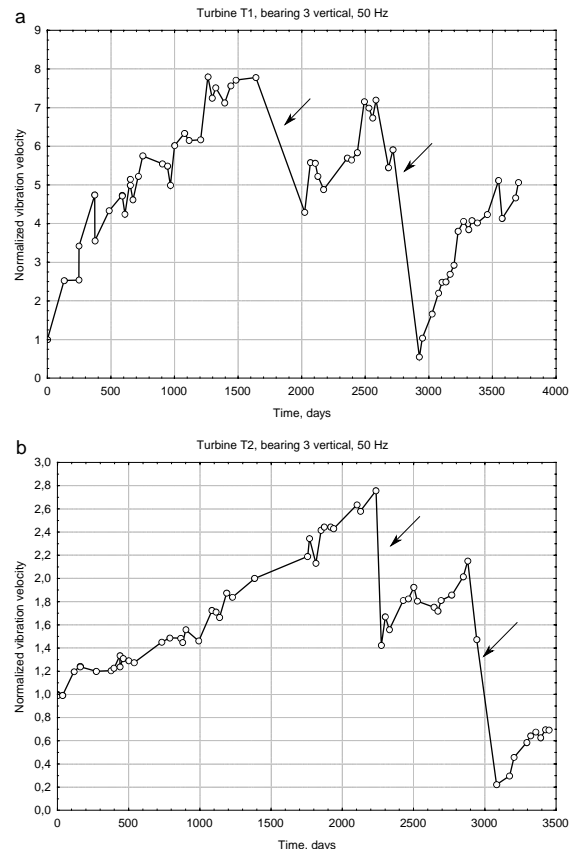


Fig. 3. 50 Hz component of vertical vibration velocity, measured at rear IP rotor bearing in turbines T1 (a) and T2 (b) as a function of time.

Values are normalized with respect to those measured for $\theta = 0$. Arrows indicate IP rotor balancing.

Correlation coefficients calculated for turbines T1 (three cycles, determined by rotor balancing attempts – cf. Fig.3a) and T2 (two cycles – the third one in Fig.3b is too short for a meaningful analysis) are listed in Table 2, together with corresponding values for turbine T3 of the same type, in which no permanent bow has occurred. Values are given for rear IP rotor bearing (i.e. the point at which trends shown in Fig.3 have been recorded) and two adjacent bearings (front IP and front LP), as periodic axial force is transmitted along the shaft line. It is clearly seen that for turbines T1 and T2 correlation is very strong, with seven values of r equal to or

higher than 0.9. All fifteen values are positive. For turbine T3 correlation is much weaker, maximum value of $|r|$ being 0.15; moreover, two values of three are negative, which indicates that an increase of one symptom is accompanied by a decrease of the other. Correlation coefficient thus turns out to be sensitive to the fault type and can be used to provide a reliable qualitative diagnosis. This is accomplished on the basis of steady-state measurement results only.

Table 2. Linear correlation coefficient values for turbines T1, T2 and T3 (see main text for details).

Turbine and cycle	Coefficient of correlation between $1 \times f_0$ components of vertical vibration velocity at rear IP bearing and axial vibration velocity at		
	front IP bearing	rear IP bearing	front LP bearing
T1, cycle 1	0.69	0.90	0.91
T1, cycle 2	0.94	0.79	0.73
T1, cycle 3	0.87	0.91	0.88
T2, cycle 1	0.97	0.97	0.95
T2, cycle 2	0.65	0.60	0.51
T3	-0.15	0.14	-0.04

3.3. Fluid-flow system condition deterioration

As already mentioned, so-called blade components, usually easily distinguished in absolute vibration spectra, convey information on the fluid-flow system condition; details can be found in references [8,12,23]. Amplitudes of these components, with frequencies usually in the range from a few hundred hertz to $10 \div 20$ kilohertz, can be used as diagnostic symptoms. This is particularly useful in old turbines, for which residual lifetime assessment is often of vital importance.

The main problem in vibration patterns assessment in the blade frequency range is in fact a direct consequence of Eq.(5). As already mentioned, influence of interference and control on vibration components in this range is in most cases much stronger than on harmonic (low-frequency) ones. This is illustrated by Fig.4, which shows normalized standard deviation σ/S_a (S_a is the mean value) as a function of frequency for three different turbines and measuring points. Data have been obtained during sessions lasting about 1.5 h each, so that resulting scatter is due mainly to interference. Similar results have been obtained for other measuring points and other turbine types. It is clearly seen that for the harmonic components σ/S_a is of the order of a few percent, while for the blade components σ/S_a is roughly one order of magnitude higher. This explains why vibration trends pertaining to this frequency range are often very irregular (cf. Fig.1).

Moreover, in certain measuring points, there are vibration sources other than turbine fluid-flow system. This refers mainly to front HP bearing, which in typical large steam turbines is usually housed in a casing together with main oil pump drive, speed

governor and several other drives, which generate their own characteristic vibration patterns. Some of these components fall within the blade frequency range and, if spectral resolution is not high enough to distinguish them, which is often the case, interpretation of vibration patterns and trends can be vague.

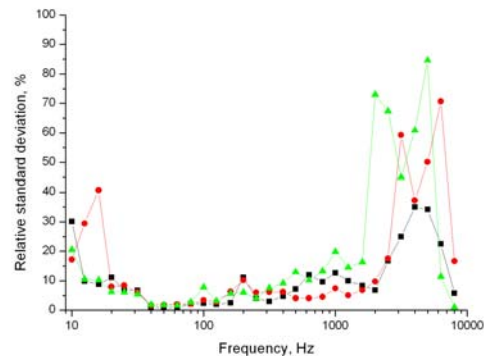


Fig. 4. σ/S_a as a function of frequency, determined from 23% CPB vibration velocity spectra; (squares) K-200 turbine, front LP bearing axial, 58 measurements; (circles) K-200 turbine, front HP bearing horizontal, 55 measurements; (triangles) TK-120 turbine, rear part of the LP casing horizontal, 90 measurements

Can correlation analysis be useful in such cases? It seems reasonable to assume that technical condition deterioration affects the rotor as a whole⁴, although degradation rates will of course be different for individual stages. Thus, if there is a *positive* correlation between vibration amplitudes in spectral bands that contain vibration generated by the fluid-flow system, we can infer that the increasing trend, if present, can be attributed to its technical condition deterioration.

Correlation analysis has been performed for the front HP bearing of turbine T10, which was commissioned in early 1960s and modernized in early 1990s (modernization concerned mainly LP turbine). Two examples of vibration trends, recorded at this point, are shown in Fig.5. Accelerated deterioration of fluid-flow system condition can be suspected, as there is a marked increase and noticeable departure from linearity in $S_i(\theta)$ histories [12,16]. Considerable fluctuations, due to the influences of control and interference, are noteworthy; that of interference is probably dominant, as the turbine in most cases ran at 90 to 100 % of the rated power and in this range load influence is comparatively small [11]. On the basis of these (and also other) vibration trends it is not possible, however, to confirm this conjecture.

In this case there are ten frequency bands in a CPB spectrum that contain blade components, and hence ten symptoms for each measuring direction.

⁴ Of course this refers to 'natural damage' only. With random failures, caused e.g. by foreign objects, this is in general not the case.

Correlation data seem, at a glance, inconclusive. Generally correlation between blade components is not strong and many values are negative (20, 27 and 20 of 45 in vertical, horizontal and axial directions, respectively). If we, however, distinguish those exceeding +0.5 (which is obviously an arbitrary limit), we immediately notice that they fall into two groups: the first one comprises three components (1.6 kHz, 2 kHz and 2.5 kHz) and the second two (5 kHz and 6.3 kHz). Correlation *between* these groups is weak and almost all values (16 of 18) are negative.

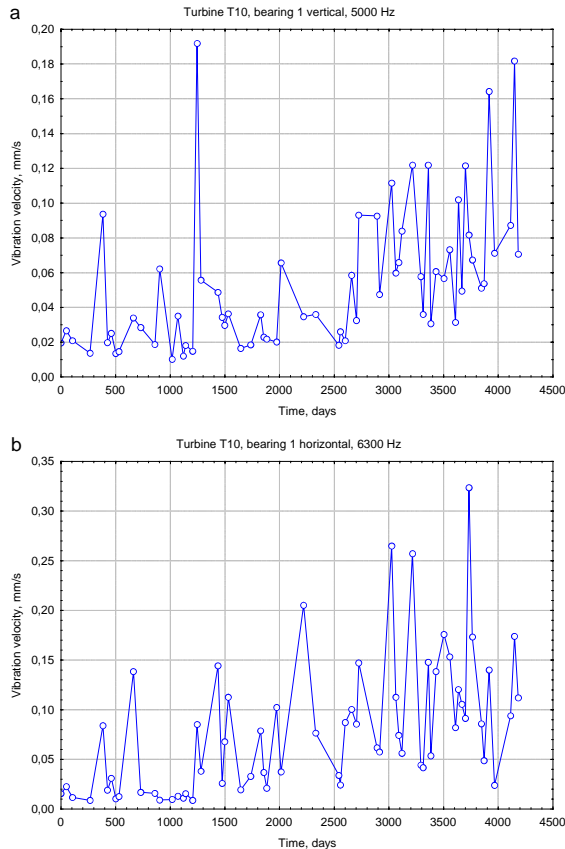


Fig. 5. Vibration velocity trends, recorded at the front HP bearing of turbine T10; a) 5 kHz band, vertical direction; b) 6.3 kHz band, horizontal direction

For this particular turbine type, frequency bands up to 3150 Hz contain components generated by bladed diaphragms, while higher frequency bands contain those generated by rotor stages. It may thus be inferred that both bladed diaphragms and rotor stages exhibit symptoms of substantial lifetime consumption degree, but quantitatively behave in different manners. In general, correlation is stronger for rotor stages, which suggests that their deterioration is more advanced; this is, however, just a conjecture, as quantitative relations still remain to be established.

It may be argued that in all above cases correlation coefficient is treated as a two-value (binary) symptom: in fact the question is whether there is a correlation or not. It seems natural to check how this coefficient changes with time (or, more

precisely, with D). In order to deal with this issue, it is useful to recall the so-called ‘old man syndrome’: as θ_b is approached, all condition symptoms become more and more correlated [24]. This can be understood on the basis of Eq. (5) if we assume – in accordance with suggestions put forward e.g. in [25] – that D should be treated as a condition parameter, i.e. a component of the $\mathbf{X}(\theta)$ vector. For small values of D each symptom is dominated by specific condition parameters (or control and/or interference), so correlation between individual symptoms is expected to be weak. If, however, D is large, or θ is close to θ_b , its influence on all symptoms becomes dominant; note that, according to the EP model, each S_i is a monotonically increasing function of D^5 . This implies that, for a pair of symptoms,

$$\theta \rightarrow \theta_b \Rightarrow r \rightarrow 1 \quad (12)$$

Can this syndrome be observed? Fig. 6 refers to turbine P4 similar to T10 dealt with earlier in this section, in which HP rotor and casing (together with bladed diaphragms) were replaced after about 220,000 hours in operation; last measurements were performed immediately before replacement. A marked increase of vibration velocity amplitudes in frequency bands containing components generated by rotor stages can be observed (Fig. 6a). On the other hand, those that contain components generated by bladed diaphragms show no distinguishable monotonic trend (Fig. 6b). In fact, trend shown in Fig. 6a is qualitatively similar to that shown in Fig. 5 – no wonder, as a similar phenomenon of the HP turbine fluid-flow system lifetime consumption is observed.

Correlation coefficients, shown as functions of time in Figs. 6c and 6d, have been calculated in such a manner that, for a given point on the time axis, they refer to ten preceding measurements. Fig. 6c refers to two velocity amplitudes from the blade frequency range. Initially correlation between them is quite weak and r is negative. Then a fast increase is observed, up to $r = 0.82$, followed by a decrease. Last section of the $r(\theta)$ curve exhibits a monotonic increase, with $r = 0.95$ shortly before the overhaul; the length of this increase period is about three years. Detailed analysis has revealed that after about 1500 days several components of the HP turbine (inlet nozzles and several bladed diaphragms clamping rings) were replaced. This is most probably responsible for the temporary correlation strength decrease. Vital fluid-flow system elements, however, were not affected, so after a comparatively short period the increasing tendency reappeared.

Fig. 6d, on the other hands, shows that correlation between components generated by rotor stages and bladed diaphragms is weak. Time history

⁵ It has to be kept in mind that s_{ij} values (see Eq. (8)) usually increase with D , which intensifies the effect.

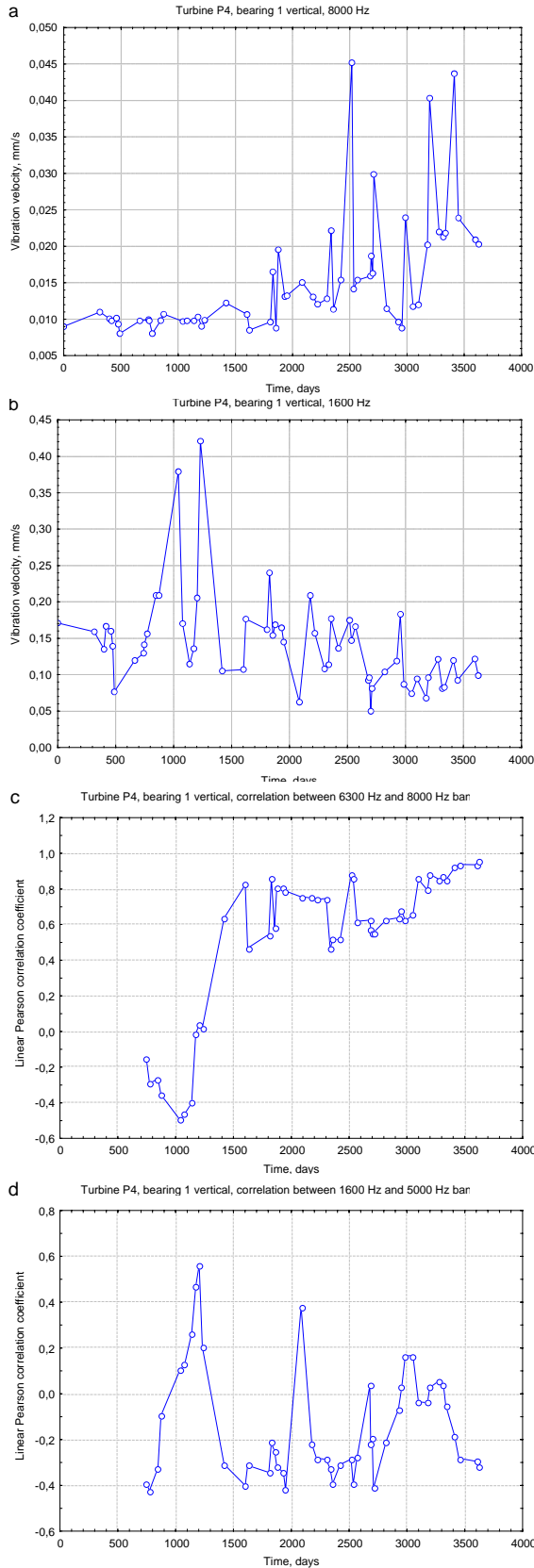


Fig. 6. Vibration velocity amplitudes and correlation coefficients vs. time; turbine P4, front HP bearing vertical. a) vibration, 8 kHz band; b) vibration, 1.6 kHz band; c) correlation between 6.3 and 8 kHz bands; d) correlation between 1.6 and 5 kHz bands

$r(\theta)$ is very irregular and most values fall within the range from $r = -0.4$ to $r = 0.2$. This confirms the observations already mentioned in this section that rotor stages and bladed diaphragms behave in different manners and that rotor condition deterioration is more advanced. It may be added here that, for rotor stages, correlation between results obtained for different measuring directions is weaker, but the ‘old man syndrome’ can nevertheless be observed; two examples are shown in Fig. 7.

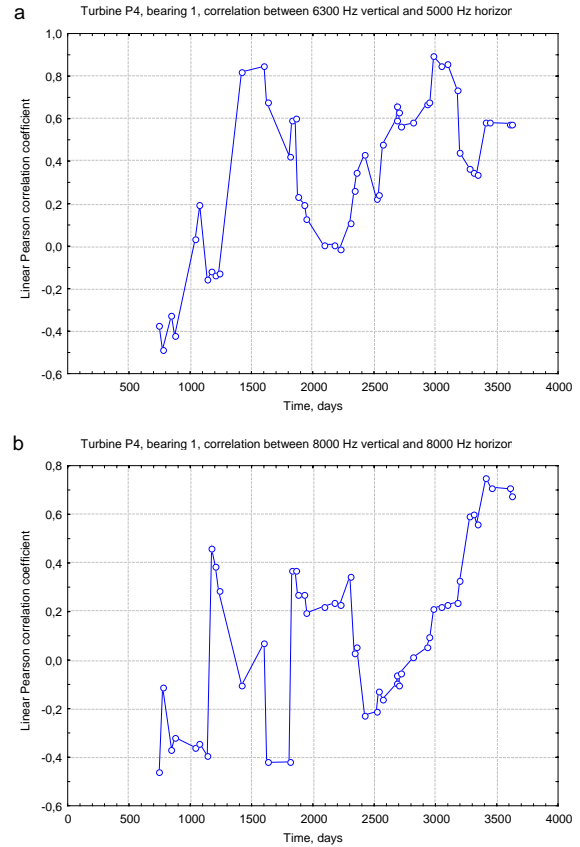


Fig. 7. Correlation coefficients vs. time; turbine P4, front HP bearing. a) correlation between frequency bands 6.3 kHz (vertical) and 5 kHz (horizontal); b) correlation between frequency bands 8 kHz (vertical) and 8 kHz (horizontal)

It should be kept in mind that the above results have been obtained from databases recorded during routine measurements rather than by means of a purpose-designed diagnostic experiment. This is probably responsible for irregularities of the $r(\theta)$ time histories, at least to a certain extent. Similarly, the method employed for determining r as a function of time is responsible for the lag in the correlation coefficient decrease after an overhaul. The potential of the method is, however, clearly demonstrated.

4. CONCLUSION

Vibration-based symptoms, in particular absolute vibration amplitudes in certain frequency bands and their time histories, are widely employed in the diagnostics of rotating machines. It has been shown that correlation between such symptoms contains valuable information on machine technical condition and hence a measure of this correlation can itself be employed as a symptom.

In qualitative diagnostics, presence (or absence) of correlation is indicative of the possible malfunction or damage type and therefore can augment diagnostic capabilities in dubious cases. This is particularly useful in the harmonic (low) frequency range, wherein several phenomena have very similar representations in vibration characteristics. In such approach, correlation can be even treated as a binary symptom.

In quantitative diagnostics, analysis of correlation coefficient as a function of time can reveal the 'old man syndrome', which is indicative of a substantial lifetime consumption degree. This seems particularly important for machines operated beyond their design lifetime (which is by no means an exceptional practice), where residual life assessment becomes vital. In such approach, correlation coefficient is treated as a continuous function of time or of generalized damage.

Examples presented in this paper reveal a substantial potential of diagnostic methods based on correlation analysis. Further research in this field is therefore justified.

ACKNOWLEDGEMENTS

Some of the results used and quoted in this paper have been obtained with the support of the Ministry of Science and Higher Education, within the framework of the N504 030 32/2693 Research Project.

The author wishes to express his gratitude to Prof. Czesław Cempel and Prof. Stanisław Radkowski for inspiration and fruitful discussions.

REFERENCES

- [1] Collacott R. A.: *Structural Integrity Monitoring*, Chapman and Hall, London, 1985.
- [2] Cempel C.: *Theory of Energy Transforming Systems and their Application in Diagnostics of the Operating Systems*, Applied Mathematics and Computer Science, 1993, Vol. 3, No. 3, pp. 533-548.
- [3] Natke H. G., Cempel C.: *Model-Aided Diagnosis of Mechanical Systems*, Springer-Verlag, Berlin-Heidelberg-New York, 1997
- [4] Gałka T., *Large Rotating Machines*, in *Encyclopedia of Structural Health Monitoring*, ed. Boller C., Chang F. and Fujino Y., John Wiley & Sons, Chichester, UK, 2009, pp. 2443-2456.
- [5] Cempel C.: *Multidimensional Condition Monitoring of Mechanical Systems in Operation*, Mechanical Systems and Signal Processing, 2003, vol.17(6), pp. 1291-1303.
- [6] Radkowski S.: *Low-Energy Components of Vibroacoustic Signal as the Basis for Diagnosis of Defect Formation*, Machine Dynamics Problems, vol.12, 1995.
- [7] Gałka T.: *Application of Energy Processor Model for Diagnostic Symptom Limit Value Determination in Steam Turbines*, Mechanical Systems and Signal Processing, 1999, vol. 13(5), pp.757-764.
- [8] Orłowski Z.: *Vibrodiagnostics of Steam Turbines*, Proceedings of the Institute of Power Engineering, vol.18, Warsaw, 1989 (in Polish).
- [9] Bently D. E., Hatch C. T.: *Fundamentals of Rotating Machinery Diagnostics*, Bently Pressurized Bearings Press, Minden, 2002.
- [10] Orłowski Z.: *Diagnostics in the Life of Steam Turbines*, WNT, Warsaw, 2001 (in Polish).
- [11] Gałka T.: *Normalization of Vibration Measurements: Unnecessary Complication or Important Prerequisite?* Proceedings of the Second International Symposium on Stability Control of Rotating Machinery ISCORMA-2, Gdańsk, 2003, pp. 722-731.
- [12] Gałka T.: *Diagnostics of the Steam Turbine Fluid-Flow System Condition on the Basis of Vibration Trends Analysis*, Proceedings of the 7th European Conference on Turbomachinery, Athens, 2007, pp. 521-530.
- [13] Lampart P., Szymaniak M., Kwizdiński R.: *Investigation of Circumferential Non-Uniformity in a Partial Admission Control Stage of a Large Power Turbine*, in *Technical, Economic and Environmental Aspects of Combined Cycle Power Plants*, Domachowski Z. (ed.), Gdańsk University of Technology, 2004, pp. 261-271.
- [14] Cempel C., Tabaszewski M.: *Averaging the Symptoms in Multidimensional Condition Monitoring for Machines in Nonstationary Operation*, Proceedings of the 13th International Congress on Sound and Vibration, Vienna, 2006, paper No.519.
- [15] Morel J.: *Vibration des Machines et Diagnostic de Leur État Mécanique*, Ed. Eyrolles, Paris, 1992.
- [16] Gałka T.: *Evolutional Symptoms in Rotating Machinery Diagnostics*, Proceedings of the International Conference 'Condition Monitoring 2005', King's College, Cambridge, 2005, pp. 255-260.
- [17] Papoulis A.: *Probability, Random Variables and Stochastic Processes*. McGraw-Hill, New York, 1965.
- [18] Gałka T.: *Correlation-based Symptoms in Rotating Machines Diagnostics*, Proceedings of the 21st International Congress COMA-DEM 2008, Praha, 2008, pp. 213-226.

- [19] Gałka T.: *Higher Harmonic Components in Steam Turbine Vibration Velocity Spectra: A Case Study*, Proceedings of the 20th International Congress COMADEM'07, Faro, 2007, pp. 351-359.
- [20] Gałka T., Kiebdój J.: *Untypical Vibroacoustic Symptoms of a Steam Turbine Fluid-Flow System Failure*, Diagnostyka, 2007, vol. 3(43) pp. 5-10.
- [21] Lapini G. L., Zippo M., Bachschmid N., Collina A., Vallini A.: *Experimental Tests and Model Based Calculations for the Diagnosis of a Crack in a 320 MW Generator*, Proceeding of the CISM Symposium 'Diagnostics of Rotating Machines in Power Plants', Springer, Wien-New York, 1994.
- [22] Rao J. S., Sharma M.: *Dynamic Analysis of Bowed Rotors*, Proceedings of VETOMAC-1 Conference, Bangalore, India, 2000.
- [23] Orłowski Z., Gałka T.: *Modeling of the Steam Turbine Fluid-Flow System for Technical Condition Assessment Purposes*, Applied Mechanics in the Americas, vol.9: Proceedings of the 7th Pan American Congress of Applied Mechanics PACAM VII, AAM/ Universidad de la Frontera, 2002, pp. 557-560.
- [24] Cempel C.: *Vibroacoustic Condition Monitoring*, Ellis Horwood, London, 1991.
- [25] Cempel C.: *Generalized Singular Value Decomposition in Multidimensional Condition Monitoring of Systems*, Diagnostyka, 2008, vol. 3(47), pp. 23-30.



Tomasz GAŁKA, Ph.D graduated from Warsaw University of Technology, Faculty of Electronics. Since 1982 he has been employed at the Institute of Power Engineering. His main professional interests are focused on vibration-based diagnostics of large

rotating machines, in particular steam turbines. He has participated in a number of research projects in this field. He has authored or co-authored about 70 publications. His non-professional interests include railways and scuba diving.

METHOD OF EVALUATION OF DEGRADATION OF BIO-MECHANICAL TOOTH-COMPOSITE FILLING SYSTEM

Andrzej NIEWCZAS¹, Daniel PIENIAK², Agata M. NIEWCZAS³

¹ Technical University of Lublin, Department of Combustion Engines and Transport
Lublin 20-608, Nadbystrzycka Str. No 36, Poland, e-mail: a.niewczas@pollub.pl

² Department of Applied Mechanics, Main School of Fire Service
Warsaw 01-629, J. Słowackiego Str. No 52/54, Poland, e-mail: daniel60@poczta.fm

³ Medical University of Lublin, Department of Conservative Dentistry

Lublin 20-081, Karmelicka Str. No 7, Poland, e-mail: agata.niewczas@umlub.pl

Summary

This paper describes a method of an enhanced life evaluation of dental fillings based on the observation of the enlargement of the marginal fissure between the filling and hard tissue of the tooth. A width of marginal fissure was considered as the functional parameter of the whole tooth-filling system in the conducted tests.

In this study development of the fissure influenced by the cyclic changes of thermal loads was analyzed. The extracted human teeth were used in the tests. In which a model lesions with micro-hybrid composite fillings were applied. All tests were conducted on the dedicated test stand. After performance of fatigue tests, measurements of the width of marginal fissure were taken by means of SEM electron scanning microscope and optical microscope with computer image analyzer.

On this basis a risk of functional unfitness of the tooth-filling system was estimated.

Keywords: reliability, laboratory tests, dental composite.

METODA OCENY DEGRADACJI SYSTEMU BIOMECHANICZNEGO ZĄB - WYPEŁNIENIE KOMPOZYTOWE

Streszczenie

W artykule opisano metodę przyspieszonej oceny trwałości wypełnień stomatologicznych na podstawie obserwacji rozbudowy szczeliny brzeżnej pomiędzy wypełnieniem a twardą tkanką zęba. W warunkach prowadzonych badań jako miarę zdatności czynnościowej całego systemu zęb – wypełnienie przyjęto szerokość szczeliny brzeżnej.

Autorzy przeprowadzili analizę rozwoju szczeliny pod wpływem cyklicznie zmiennych obciążeń cieplnych. Do badań wykorzystano usunięte zęby ludzkie. W zębach wypreparowano modelowe ubytki i założono wypełnienia z kompozytu mikrohybrydowego. Badania zostały przeprowadzone na specjalnie opracowanym stanowisku badawczym. Po wykonaniu testów zmęzeniowych przeprowadzono pomiary szerokości badanej szczeliny brzeżnej, wykorzystując elektronowy mikroskop skaningowy SEM. Na tej podstawie oszacowano ryzyko niezdatności użytkowej układu zęb – wypełnienie.

Słowa kluczowe: niezawodność, testy laboratoryjne, kompozyty stomatologiczne.

1. INTRODUCTION

Materials used in a conservative dentistry nowadays need to meet strict fatigue resistance requirements in the tooth-filling system. Fatigue resistance of dental fillings is limited by the development of marginal fissure between the lesion walls and the filling.

The consequence of the occurrence of marginal fissure is a microleakage. Bacterial microleakage consists in penetration of microorganisms and their proliferation in the space between the filling and the wall of lesion. Microleakage results in secondary caries occurring along the walls of filling, which ultimately leads to the physical and biological

degradation of the filling and determines the end of the filling's life. Due to the time consuming testing of this phenomenon in clinical conditions, the development of marginal fissure was studied in laboratory conditions.

To fill the lesion a polymer photo-cured composite was used, always demonstrating polymerization shrinkage leading to the initiation of marginal fissure in the process of polymerization [3, 16, 20, 5, 14, 2]. In order to obtain a resistant bond of the filling with the wall of the lesion, bonding systems with indirect raisins or indirect liquids were applied [13, 15].

Fluctuations of the conditions in the oral cavity (particularly changes of temperature and pH) may

lead to the progress in the degradation of the tooth-composite filling system [6, 9]. The literature presents a common view that changes in temperature of the oral cavity environment may constitute the main factor affecting the placement of stresses and their changes in the bordering area of the filling and tooth tissues [19]. The previous tests have also demonstrated a relation between the temperature in which polymer composites based on resins are used and the loss of filling mass, as well as decomposition and depolymerization of its structure [1]. A consequence of this phenomenon is possible expansion of marginal fissure accompanied by the microleakage of liquids. The wedging activity of the liquids, during the act of chewing, leads to further expansion of the volume of fissure together with the weakening of its structure.

In vitro thermal fatigue simulation of the tooth-composite filling system should correspond to physiological conditions of the human oral cavity. The most important parameters of simulation environment are the following: 1) temperature of working liquid (in most cases it is an artificial saliva), 2) the retention time of working liquid in the vessel containing teeth specimens or the retention time of the examined specimen in the vessel with working liquid and 3) the number of thermal load cycles (thermal shocks).

In the previous studies, various different assumptions have been made with regards to the experimental parameters. Bottom temperature of working liquids used in the experiments varied between 2 and 24°C [7], while the temperatures of heated liquid ranged from 45°C to 60°C [21]. The applied retention time of conditioning liquid in the vessel containing specimens varied from 15 to even 180 seconds, and the number of cycles oscillated between 25 and 1 000 000 thermal cycles [7].

Today, the most frequently used experimental parameters are as follows:

- Temperature of cooled working liquid, 5 °C,
- Temperature of heated working liquid, 55°C,
- Retention time of working liquid in the vessel containing specimen, 30 seconds,
- Number of thermal cycles – from a few thousand to several dozen thousand cycles.

The evaluation of the influence of thermal cycles on resistance of the tooth-filling system was performed by the analysis of marginal untightness, mainly based on quality scales related to the enlargement of the marginal fissure. According to the authors' knowledge, up till now no quantitative evaluation of the process of degradation of the system resulting from the cyclic fluctuations of temperature has been made.

The examined tooth-dental filling system, based on the theory of reliability, is a series system [11]. Thus, its performance is determined by the functioning of all its elements such as tooth hard tissue, bonding layer and the body of the filling material.

The observed marginal fissure in the tooth-filling system indicates lack of continuity in the structure of specific size and shape. On the surface of these discontinuities the forces of atomic bonds do not act. In the unloaded state the edges of the fissure may contact with each other, whereas when loaded – they may spread or even move against each other [12].

In the presented studies it was assumed that the marginal fissure contributes to the functional unfitness of the tooth-filling system, while its parameters are the basis of evaluation of the limit state of the whole studied system.

2. METHOD

2.1. Objective of the study

The developed method consisted in application of the extracted human teeth (removed due to orthodontic reasons) as specimens in the fatigue degradation laboratory tests. In the specimens, model lesions were prepared of the identical size and lateral walls perpendicular to their bottoms (Fig. 1).

The lesions were filled with photo-cured composite with micro-filler according to manufacturer's instructions. In order to ensure a contact of the filling with the enamel and dentine, the lesions were 3 millimeter deep. The enamel and dentine were etched with 37% ortho-phosphoric acid. In the next stage, the bonding material was applied to all walls and the bottom of the lesion. Composite material was applied to the lesion as 2 millimeter layers and heated with halogen lamp for 40 seconds [8].

The tooth specimens were fixed in special holders.

Next, the tooth specimens were submitted to the thermal loads at the test stand simulating load cycles reflecting physiological processes in the oral cavity (Fig. 2).

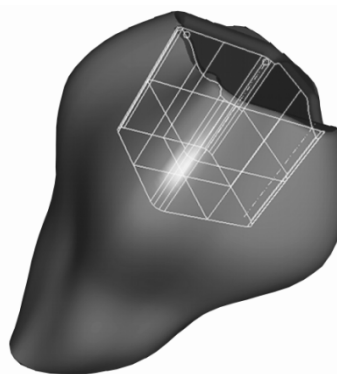


Fig. 1. Geometrical model of the tooth with the prepared lesion

2.2. Simulator of thermal loads

The test stand used for simulation of thermal shocks (Fig. 2) consisted of microprocessor control system and hydraulic system. The equipment assured the realization of thermal shocks in the specimens placed inside the measurement vessel, located in the mastication simulator. The operation of the simulator consisted in periodical pumping in and out of the working liquid into the measurement vessel with set temperature. The vessel was alternately filled with heated (temperature 328K) or cooled (temperature of 278K) working liquid from the two independent temperature conditioning systems.

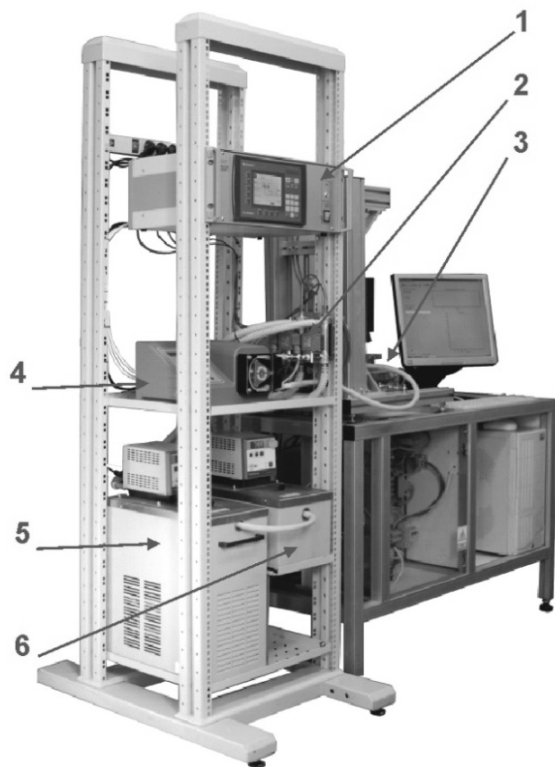


Fig. 2. Test stand for thermal shocks: 1 – microprocessor control module, 2 – control valves, 3 – mastication simulator, 4 – peristaltic pump, 5 – cooling thermostat, 6 – heating ultra thermostat

During thermal shocks performance, programmable times of the individual actions of the control were applied. Figure 3 presents the course of the procedure of one cycle of thermal shocks.

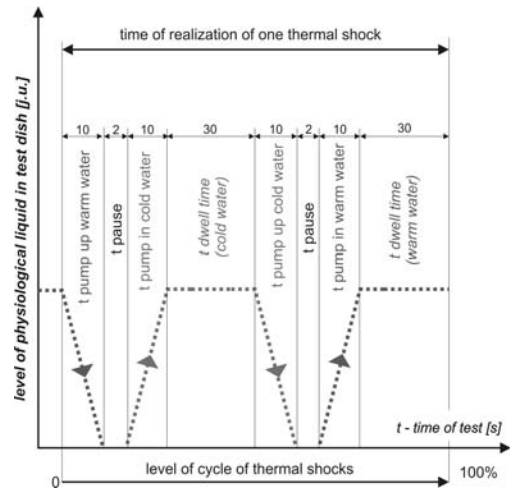


Fig. 3. Graphical presentation of thermal shock cycle with single pumping of working liquid

2.3. Microscope observations

After series of cyclic loads the teeth were cut along their long axis into two halves (Fig. 4).

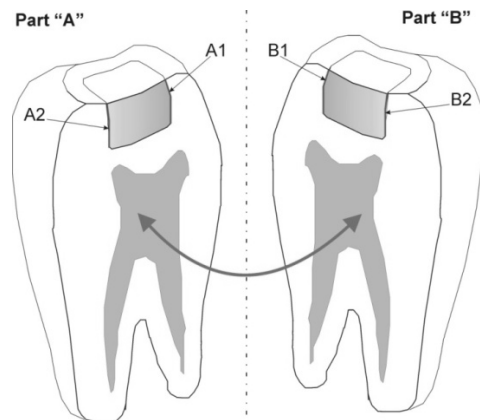


Fig. 4. Diagram of the tooth specimens: A1, A2, B1, B2 – marginal fissure observation areas

A surface of the prepared specimens was grinded with a few types of fine-grained abrasive paper, and next it was polished.



Fig. 5. Intersection of the tooth – the specimen for geometrical measurements of marginal fissure

The nature of the tooth tissue adherence to the surface of the composite filling was investigated by means of microscopic observation. Electron scanning microscope (LEO 1430 VP), optical microscope (Neophot 2) and image analysis software (Image-ProPlus, Media Cybernetics) were applied. Figure 6 presents the enamel, dentine and composite filling bordering area. Marginal fissure is visible between the enamel (2) and composite filling (1) and between dentine (3) and composite. The shape of the fissure is irregular along its whole length. The fissure ends with a crater-like lesion of parabolic intersection by the chewing surface (Fig. 6).

Figure 7 clearly shows irregular marginal fissure between the composite filling and the enamel on the chewing surface. The shape of the border line of the filling and the tooth hard tissue takes a different form. The border of the lesion is more linear, whereas that of the filling is more irregular.

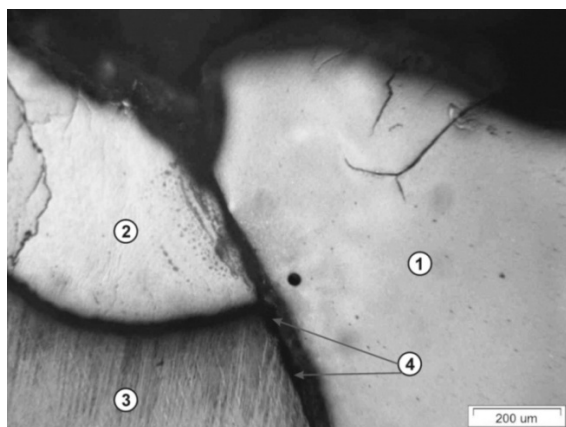


Fig. 6. Image of marginal fissure: 1 – polymer composite, 2 - enamel, 3 - dentine, 4 – marginal fissure

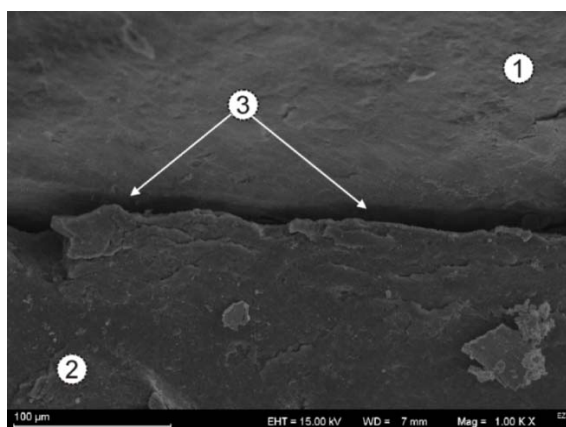


Fig. 7. SEM image of marginal fissure on the chewing surface: 1 – enamel, 2 – composite filling, 3 – marginal fissure

3. TESTS RESULTS AND RESULTS ANALYSIS

3.1. Parameters of marginal fissure

The results of the measurements of the marginal fissure width in *Heliomolar Radiopaque* material with regards to the number of thermal cycles are presented in Figure 8.

In the diagram (Fig.8) values from x1 to x10 show the depth of the measurement. Value x10 refers to the point of measurement by the chewing surface, whereas value x1 indicates the lowest point of measurement, near the filling's bottom. The shape of the diagram demonstrates different dynamics of changes in the width of marginal fissure in various depth zones. The most significant variability of fissure parameters can be observed on the chewing surface.

3.2. Evaluation of differences between means

The evaluation of differences between the mean widths of the fissure in individual groups of measurements was carried out on the basis of T student test. Significance of differences in mean values of the fissure between the subsequent thermal load ranges was estimated (number of thermal cycles – TC): 2 000 cycles, 20 000 cycles, 40 000 cycles, 60 000 cycles, 90 000 cycles (Table 1).

Level p given in the results of T test represents error probability associated with the acceptance of the hypothesis on the existence of differences between the averages. This is error probability consisting in the rejection of the hypothesis about the lack of differences between averages in the two studied categories of observation belonging to the general population (represented by the studied groups) in the situation when actual state in the population is that this hypothesis is true [10]. Sign of t function, in the same way as in the case of standardized variable, indicates negative or positive deviation from the average [18].

Table 1. Comparison of values of the width of the fissure for the increasing number of thermal shocks

Gr. 1 vs. Gr. 2	t	p
2000 TC vs. 20000 TC	0,91452	0,361027
2000 TC vs. 40000 TC	-0,01398	0,988856
2000 TC vs. 60000 TC	-0,05215	0,958451
2000 TC vs. 90000 TC	-5,12049	0,000001
20000 TC vs. 40000 TC	-0,92713	0,354587
20000 TC vs. 60000 TC	-0,84739	0,397483
20000 TC vs. 90000 TC	-6,80944	0,000000
40000 TC vs. 60000 TC	-0,05115	0,959269
40000 TC vs. 90000 TC	-5,38188	0,000000
60000 TC vs. 90000 TC	-4,56952	0,000012

Figure 9 shows graphical presentation of variability measures and mean values of analyzed groups of variables.

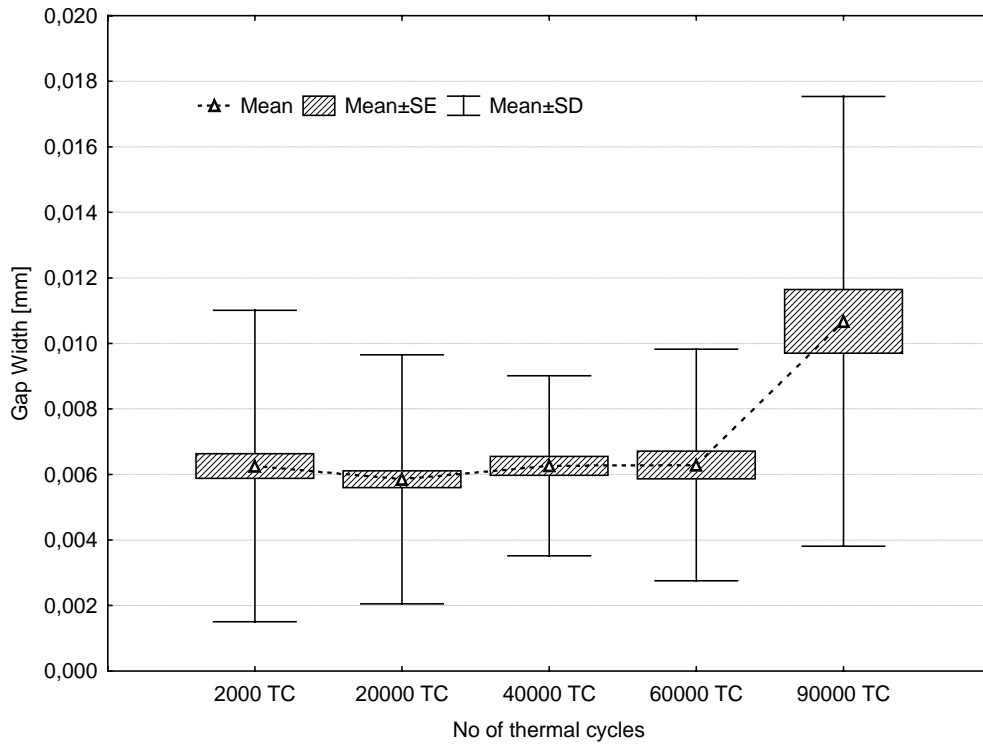


Fig. 9. Box & whiskers diagram of the width of marginal fissure for different number of thermal cycles

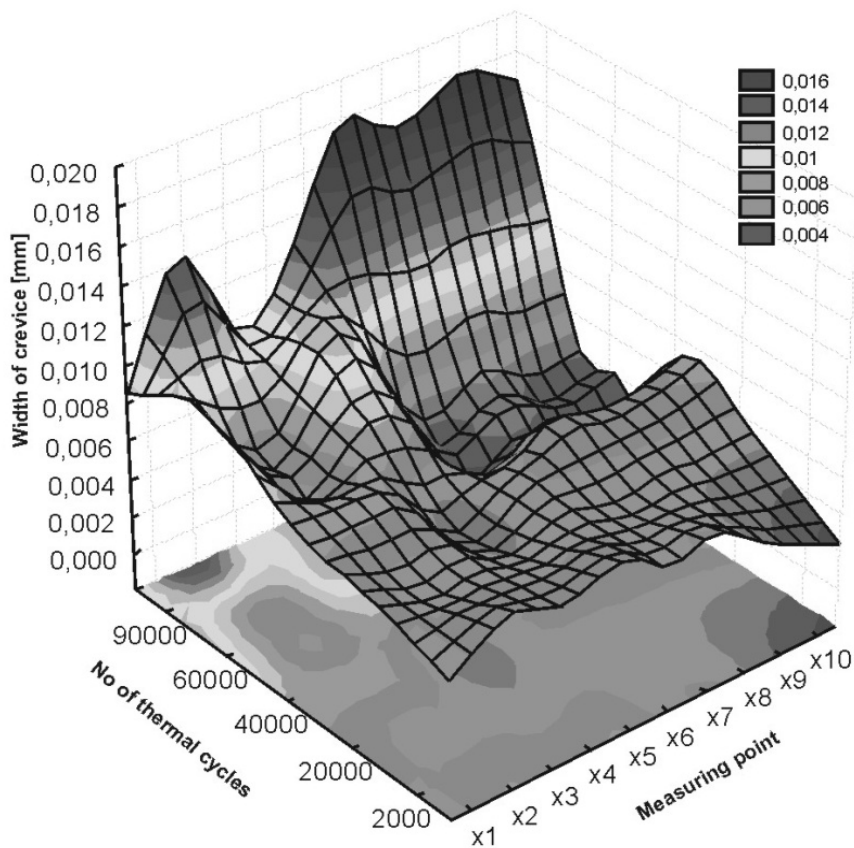


Fig. 8. The width of marginal fissure

3.3. Analysis of the predicted durability („survival time”)

In order to determine predicted durability („survival time”), so-called life table was prepared (Table 2). It is an expanded table of the quantity distribution. Distribution of survival times was divided into a certain number of ranges. For each range a number and proportion of cases which did not reach the limit state were calculated as well as the number and proportion of the cases reaching the limit state.

The percentage of the specimens reaching the limit state (Fig.10a) constitutes the proportion of the observed cases – specimens. This proportion was calculated as the ratio of the number of cases reaching limit state in a given range to the number of cases observed in this range. After initial number of the load cycles (2000TC), 37.5% of specimens reaching limit state were identified. In the subsequent ranges the percentage of those specimens was decreasing. After 90 000 load cycles, the highest percentage of cases reaching limit state was noticed.

Survival function (Fig.10b) describes the ratio of the number of teeth specimens, remaining in the state of usability during the operation time t to the initial number of specimens. This is a cumulated proportion of cases which did not reach limit condition from the initial moment till the analyzed moment.

In the next stage of durability analysis hazard function $h(t)$ was determined. Hazard function is described by the probability per unit of time, that the case which “survived” since the beginning of the tests will undergo failure in the studied interval of time. Hazard function $h(t)$ was estimated according to the following formula:

$$h(t) = \frac{\frac{dF}{dt}}{R(t)} \quad (1)$$

where:

$F(t)$ - unreliability,

$R(t)$ – reliability,

t - generalized usage time (No of thermal cycles).

Figure 10c presents the hazard function which takes the shape of bathtub curve. Thus, a failure risk (reaching limit condition) is the highest in the initial and final periods of usage.

Durability of the filling was approximated by the Weibull distribution, in which density of probability was described by the following relation [11]:

$$a = \frac{c}{b} \left(\frac{t}{b}\right)^{c-1} \exp\left(-\left(\frac{t-\theta}{b}\right)^c\right) \quad (2)$$

Whereas distribution function (with positive parameters b , c and θ) is given by:

$$F(t) = 1 - \exp\left(-\left(\frac{t-\theta}{b}\right)^c\right) \quad (3)$$

where:

x – time,

b – scale parameter,

c – shape parameter,

θ – location parameter,

e – constant ($e = 2.71828...$)

Hollander-Proschan test was used in order to estimate the most probable shape of reliability function $R(t)$ of the examined fillings (Fig. 10d). On the basis of $R(t)$ function the durability of the fillings described in this paper can be determined. Assuming a probability criterion of 0.9 (90%), in the sense of not exceeding the limit value of marginal fissure (0,015 mm [17]), predicted durability of fillings can be estimated to 58 000 thermal cycles.

Table 2. Life table of the examined dental fillings

Parameters	Parameter values						
	0	15000	30000	45000	60000	75000	90000
Load level	0	15000	30000	45000	60000	75000	90000
Central point	7500	22500	37500	52500	67500	82500	-
Interval width	15000	15000	15000	15000	15000	15000	-
Number of the observed	32	16,5	13	12	12	9	9
Number of reaching limit condition	12	2	1	0	3	0	9
Proportion of reaching limit condition	0,375	0,1212	0,0769	0,0416	0,25	0,055556	0,9444
Proportion of the surviving	0,625	0,8787	0,9230	0,9583	0,75	0,944444	0,0555
Cumulated proportion of the surviving	1	0,625	0,5492	0,5069	0,4858	0,364401	0,3441
Probabilist density	0,000025	0,000005	0,000003	0,000001	0,000008	0,000001	0,000024
Hazard	0,000031	0,000009	0,000005	0,000003	0,000019	0,000004	0,00002

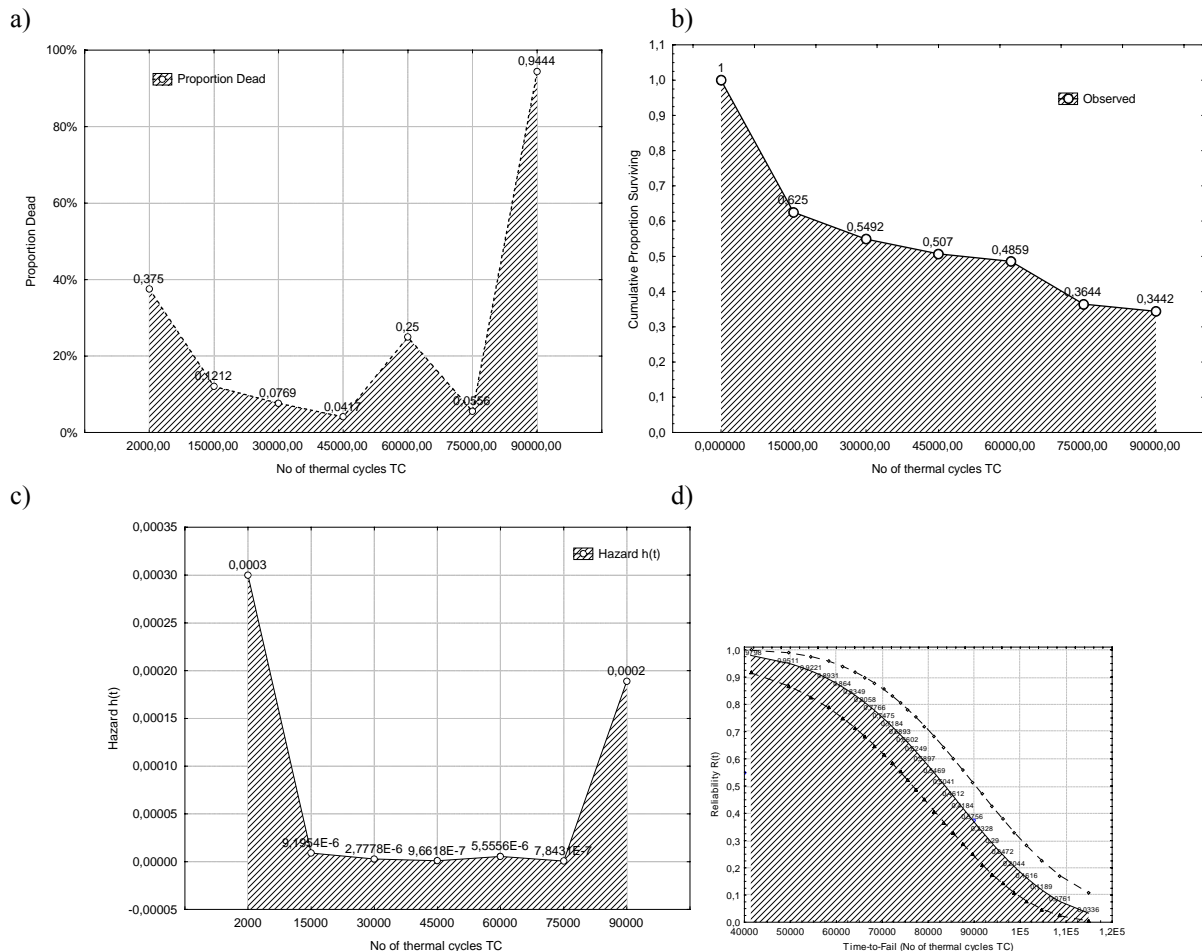


Fig. 10. a) Percentage of specimens reaching limit state, b) Survival function, c) Hazard function of dental fillings, d) Reliability function of greatest significance

4. SUMMARY

The tests have demonstrated that the marginal fissure in the bio-mechanical tooth-composite filling system, resulting from the polymerization shrinkage, grows under the influence of cyclic changes of temperature. Furthermore, the enlargement of the fissure has a multi-stage character. After exceeding the limit number of cycles (in the test conditions the limit was about 60 000 thermal cycles) a rapid growth of fissure width occurs, accompanied by the formation of micro-cracks in the enamel and filling material.

The observed shape of the hazard curve $h(t)$ (Fig. 10c) indicates a significant increase in the probability of functional degradation occurrence (reaching critical marginal fissure width in the tooth-composite filling system) after 75 000 thermal cycles.

It can be concluded that the developed method shows high applicability for evaluating durability of the filling as well as testing new dental materials.

REFERENCES

- [1] Achilias D.S., Karabela M.M., Sideridou I.D. *Thermal degradation of light-cured dimethacrylate resins Part I. Isoconversional kinetic analysis*. Thermochemica Acta (2008) 472, p.74–83.
- [2] Braga R.R., Boaro L.C.C., Kuroe T., Azevedo C.L.N., Singer J.M. *Influence of cavity dimensions and their derivatives (volume and 'C' factor) on shrinkage stress development and microleakage of composite restorations*. Dental Materials (2006) 22, p.818–823.
- [3] Calheiros C.F., Sadek F.T., Boaro L.C.C., Braga R.R. *Polymerization stress related to radiant exposure and its effect on microleakage of composite restorations*. Journal of Dentistry (2007) 35, p.946–952.
- [4] Chan K.C, Swift E.J. *Marginal seal of new generation dental bonding agents*. Journal of Prosthet. Dent. (1994) 72, p.420–423.

- [5] Fleming G.J.P., Hall D.P., Shortall A.C.C., Burke F.J.T. *Cuspal movement and microleakage in premolar teeth restored with posterior filling materials of varying reported volumetric shrinkage values*. Journal of Dentistry (2005) 33, p.139–146.
- [6] Geis-Gerstorfer J. *In vitro corrosion measurements of dental alloys*. Journal of Dentistry (1994) 22, p.247–51.
- [7] Gale M.S., Darvell B.W. *Thermal cycling procedures for laboratory testing of dental restorations*. Journal of Dentistry 27 (1999), p.89–99.
- [8] Hunicz J, Niewczas A, Kordos P, Pieniak D. *Experimental test stand for analysis of composite dental fillings degradation*. Eksploatacja i Niezawodność - Maintenance and Reliability (2007) 2, p.37 – 43.
- [9] Joyston-Bechal A., Kidd E., Joyston-Bechal S. *Essentials of dental caries: the disease and its management*. 2nd ed. Oxford: Oxford University Press (1998), p. 66–78.
- [10] Kendall M. G., Buckland W. R. *Słownik terminów statystycznych*, wyd. PWN, Warszawa (1986).
- [11] Migdalski J (red.). *Inżynieria niezawodności. Poradnik*. Wyd. ATR and ZETOM, Warszawa (1992).
- [12] Neimitz A. *Mechanika pękania*, wyd. PWN, Warszawa (1999).
- [13] Walczak M., Niewczas A., Hunicz J. *Propagacja szczeliny brzeżnej w kompozytach stomatologicznych – próba laboratoryjnej symulacji cyklu żucia*. Przegląd Mechaniczny (2007) 5, p. 149–151.
- [14] Piemjai M., Watanabe A., Iwasaki Y., Nakabayashi N. *Effect of remaining demineralised dentine on dental microleakage accessed by a dye penetration: how to inhibit microleakage?*. Journal of Dentistry (2004) 32, p.495–501.
- [15] Qingshan L., Jepsen S., Albers H.K., Eberharda J. *Flowable materials as an intermediate layer could improve the marginal and internal adaptation of composite restorations in Class-V-cavities*. Dental Materials (2006) 22, p.250–257.
- [16] Rosin M., Urban A.D., Gartner C., Bernhardt O., Spleith C., Meyer G. *Polymerization shrinkage-strain and microleakage in dentin – border cavities of chemical and light-cured restorative materials*, Dental Materials (2002) 18, p.521–528.
- [17] Szenowski H., Kupka T., Twardawa H., Skaba D. *Analiza szczelności brzeżnej materiałów do wypełnień stałych zewnętrznych*. Stomatologia Zachowawcza (1997) 2, p.15 – 19.
- [18] Volk W. *Statystyka stosowana dla inżynierów* wyd. WNT, Warszawa (1973),.
- [19] Sanders-Tavares da Cunha Mello F., Feilzer A.J., de Gee A.J., Davidson C.L. *Sealing ability of eight resin bonding systems in a Class II restoration after mechanical fatiguing*. Dental Materials (1997) 13, p.372–376.
- [20] Wilder Jr. A.D., Swift Jr. E.J., May Jr. K.N., Thompsona J.Y., McDougal R.A. *Effect of finishing technique on the microleakage and surface texture of resin-modified glass ionomer restorative materials*. Journal of Dentistry (2000) 28, p.367–373.
- [21] Yoshida K., Matsumura H., Atsuta M. *Monomer composition and bond strength of light-cured 4-META opaque resin*. Journal of Dental Restoration (1990) 69, p.849–851.



Andrzej NIEWCZAS
Prof. PhD eng., is the Head of the Department of Combustion Engines and Transport at the Technical University of Lublin.



Daniel PIENIAK
PhD eng., he works at the Department of Applied Mechanics at the Fire Safety Engineering Faculty at Main School of Fire Service.



Agata NIEWCZAS
MD PhD, she works at the Department of Conservative Dentistry, Medical University of Lublin.

AN EXAMPLE OF SURFACE FAULT ESTIMATION ON THE BASIS OF SUPER-RESOLUTION APPROACH¹

Wojciech JAMROZIK

Silesian University of Technology at Gliwice, Department of Fundamentals of Machinery Design
18A Konarskiego Str., 44-100 Gliwice, Poland, wojciech.jamrozik@polsl.pl

Summary

The paper presents an image processing (fusion) technique for resolution enhancement. The technique can be applied to detection of product and process faults. Obtaining images with desired resolution is one of the most important stages in a whole vision system applied to industrial applications. A group of techniques which allows to enhance the image spatial resolution is a super resolution. This group differs from simple interpolation approaches. The application of this technique to the surface fault estimation of concrete stones has been presented in the paper. A set of images was acquired on a fully automatic production line between stones forming and curing stages with the use of CCD camera and then processed. Several super resolution methods have been investigated. Afterwards simple analysis of synthetic images was carried out. Provided results of experiments has shown that super resolution approach is promising when image resolution enhancement is necessary for reliable product diagnostic.

Keywords: image fusion, super-resolution, image processing, paving stones.

PRZYKŁAD ESTYMACJI WAD POWIERZCHNIOWYCH Z ZASTOSOWANIEM NADROZDZIELCZOŚCI

Streszczenie

Artykuł prezentuje technikę przetwarzania (fuzji) obrazów pozwalającą na zwiększanie ich rozdzielczości. Technika ta może zostać zastosowana w procesie detekcji uszkodzeń produktów i procesów. Uzyskanie obrazów o żądanej rozdzielczości jest jednym z najważniejszych zadań w systemie wizyjnym zastosowanym w przemyśle. Grupa technik, które pozwalają na zwiększenie rozdzielczości obrazów, nazywana jest nadrozdzielczością i w znacznym stopniu różni się od podejść interpolacyjnych. Zastosowanie tej techniki do estymacji wad powierzchniowych betonowej kostki brukowej została zaprezentowana w artykule. Na w pełni zautomatyzowanej linii produkcyjnej, pomiędzy fazą formowania, a dojrzewania kostek, przy użyciu kamery CCD zarejestrowany został zbiór obrazów. W następnej kolejności zbiór ten został przetworzony. Proste metody analizy obrazów zostały zastosowane do otrzymanych obrazów syntetycznych. Przedstawione wyniki eksperymentów, dowodzą, że nadrozdzielczość jest obiecującą techniką, kiedy wymagane jest zwiększenie rozdzielczości obrazów w procesie diagnozowanie produktów.

Słowa kluczowe: fuzja obrazów, nadrozdzielczość, przetwarzanie obrazów, kostka brukowa.

1. INTRODUCTION

In recent years there has been an increasing interest in detection of product faults at an early stage of the production process. Because the complexity of continuous technical processes has also grown significantly, many advanced techniques have been worked out, including the application of a vision system to fault detection of products, processes as well as machines. Frequently, during simultaneous monitoring of the product and process

a direct relationship between machinery wear or faults and properties of a final product can be revealed. This relationship could be identified only in a case when products are observed with the appropriate sensors. In some cases to obtain reliable data that is suitable for further analysis, applications of more sophisticated techniques are required. This problem is clearly noticeable in case of cameras (e.g. CCD) used to product and process observation.

When spatial dimensions of potential symptoms, representing faults on the product surface or in its

¹ All research data was collected at Betra (Racibórz) member of the Awbud Group

geometrical structure, are relatively small in comparison to the whole product dimensions, and moreover it is not certain that the failure appears at a fixed place, the area observed by the camera is often insufficient. In such cases resolution of acquired images is often too low. One of possible solutions is the use of expensive high performance cameras. However, there is also an alternative solution for these kinds of problems. To obtain images with a sharp and unequivocal representation of desired objects, instead of expensive acquisition devices, proper image processing methods can be applied to images of lower resolution.

An example of image processing methods useful in fault detection is a super resolution (SR), which enhance the image spatial resolution. The paper deals with the application of SR to detect some small surface faults, which could be symptoms of machine wear or incorrectnesses of production process parameters.

2. SUPER-RESOLUTION

The super-resolution (SR) approach is a process of generating images characterized by higher resolution in comparison to source images. The source can consist of one or more images. As opposed to interpolation, the images which are generated by super-resolution techniques are characterized not only by a higher pixel number but also by more resolving power. The next advantage of SR methods is minimization of blur, which is a common effect of image interpolation.

There are two main steps all SR approaches. First is the image registration, which should be understood as the process of geometrical aligning of two or more images. The second step is the image reconstruction. It is the fusion of previously aligned images in order to generate new synthetic high resolution image. This process is shown in Fig. 1.

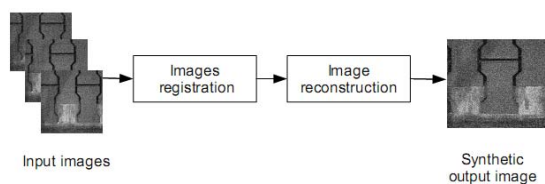


Fig. 1. Generation of high resolution image

2.1. Image registration

In the paper image registration was carried out using Fourier-Mellin transform [3, 13]. It was based on Fourier Shift Theorem [1], which was proposed for registration of translated images, because Fourier Transform (FT) was translation invariant. The Mellin transform is very close to Fourier transform but it uses polynomial kernel. It gives a transform-space image that is invariant to translation, rotation and scale. A similar effect can be obtained using FT

when input data is converted to log-polar coordinates, thus scale and rotation are changed to vertical and horizontal of sets can be measured.

2.2. Image reconstruction

Image reconstruction is a phase of the SR method. Previously registered images are aggregated in a new synthetic image. This image is characterized by higher spatial resolution than input images used in the reconstruction process. Several image reconstruction methods have been taken into consideration. Details of these methods are discussed below.

Iterated backprojection This SR algorithm was introduced by Irani and Peleg in [4]. In this method the key element solving the following equation is defined:

$$g_k(m, n) = \sigma_k(h(f(x, y))) + \eta_k(x, y) \quad (1)$$

where:

- g_k is an acquired k th image,
- f is a high resolution image after reconstruction,
- h is a blurring operator,
- η_k is an additive noise term,
- σ_k is a downsampling operator. It provides transformation between SR image dimensions and low resolution image dimensions.

The SR image estimation process starts with initial guess $f^{(0)}$ of the high resolution image. Set of low resolution images $g^{(0)}$ is obtained from HR guess. The difference between the original LR image and simulated ones is computed. If $f^{(0)}$ is the ideal guess of the HR image the difference equals to zero. In another case it is used to improve the HR image quality, by backprojecting each value of the difference image into its place on the HR image. The process is repeated iteratively to minimize an error function, given by Eq. 2:

$$e^{(n)} = \sqrt{\sum_k \sum_{(x,y)} (g_k(x,y) - g_k^{(n)}(x,y))^2} \quad (2)$$

Projection onto convex sets In POCS technique [9, 11] blurring caused by camera PSF (point spread function), as well as effects of undersampling are taken into account. The low resolution sequence is described for each frame $g(x, y, k)$. It is assumed that the estimated HR image for frame k is desired at time t_r . For each pixel, within the LR image set a convex set can be defined by Eq. 3:

$$C_{t_r}(x, y, t) = \{y(p, q, t_r) : |r^{(d)}(x, y, k) - \delta_0|\} \quad (3)$$

where:

$$r^{(d)}(x, y, k) \doteq g(x, y, k) - \sum_{(p,q)} d(p, q, t_r) h_{t_r}(p, q, x, y, k) \quad (4)$$

is the residuum, associated with d - member of the constrained set, h_{t_r} is the blur PSF and the combination of relative motion of object and camera. The quantity δ_0 reflects statistical confidence of actual image membership to the C_{t_r} set. An estimation of the high-resolution version of the reference image is determined iteratively starting from some arbitrary initialization. Successive iterations are obtained by projecting the previous estimated image into the consistency set with an amplitude constraint set that restricts the grey levels of the estimated image to the range [0, 255].

Papoulis-Gerchberg Papoulis-Gerchberg algorithm [2, 7] is a special case of the POCS method. This method is based on two assumptions: some pixel values on a high resolution grid are known, the high frequency components in the high resolution image are equal to zero. To obtain the HR image the hi-res grid is formed. Then after position conversion known pixel values are placed on the high resolution grid. Next, the high frequency components are set to zero in the frequency domain. Then in spatial domain known pixel values are set on the high resolution grid. Setting the high frequency components equal to zero, this method interpolate the unknown values, thus corrects the aliasing for low frequency components. The entire procedure is repeated until all pixel values are found and corrected.

Structure adaptive normalized convolution The method is based on the framework of normalized convolution (NC), in which an image is approximated through projection onto a subspace [8]. The window function of adaptive NC is adapted to local linear structures. This leads to more samples of the same modality that are gathered for the analysis.

The normalized convolution is a method for image analysis that takes into account uncertainties in pixel values and at the same time allows spatial localization of possibly unlimited analysis functions. The projection into the subspace which is spanned by analysis functions is equivalent to a weighted least square problem, where the weights are induced from the certainty of the image and the desired localization of analysis functions. The result of Normalized Convolution is in each image pixel a set of expansion coefficients, one for each analysis function.

The normalized convolution can be considered as a local operator because it works in a finite neighborhood. When the area of application is relatively large the result is blurred. The use of an adaptive applicability function increases the quality of fusion from sparsely sampled data. The applicability function is an anisotropic Gaussian kernel with ability to adapt its shape and orientation

to the local image structure. It ensures that only samples with similar intensity and gradient information are used for the local expansion. That avoids blurring along lines and edges.

3. ERROR MEASURES

Two error measures have been proposed in order to assess evaluated image reconstruction algorithms.

3.1. Peak signal to noise ratio

The peak signal to noise ratio (PSNR) is commonly used for image quality assessment [5, 10]. It is based on the mean squared error (MSE), which can be obtained using Eq. 5:

$$MSE = \frac{1}{mn} \sum_{i=1}^n \sum_{c=1}^m (x_{ic} - y_{ic})^2 \quad (5)$$

where: x_{ic} and y_{ic} are values of a pixel i in a channel c of the original and compared image respectively, n is the number of pixels in each channel and is m number of channels. The PSNR can be obtained from MSE and the maximum signal (pixel) value s with the use of Eq. 6:

$$PSNR = 10 \lg \frac{s^2}{MSE} \quad (6)$$

The PSNR is expressed in dB. Higher values indicate that there are lower errors and according to that higher quality.

3.2. Structural similarity

The mean squared error measures have been widely used, but obtained results are characterized by insufficient correlation with the visual degradation [6, 10]. Wang et al. described in [10] the mean structural similarity (MSSIM) error measure. They stated that it has greater correlation with visual degradation than MSE and is not so computational demanding. The structural similarity (SSIM) error measure calculates the similarity in a local window. It combines differences in average, variation and correlation.

The input for SIMM are two intensity value sets, with n elements each, from corresponding windows in the original and compared image. The first averages μ_x and μ_y are calculated using Eq. 7:

$$\mu_x = \frac{1}{n} \sum_{i=1}^n x_i \quad (7)$$

Next, the calculation of variances σ_x and σ_y for two sets of the intensity values is conducted using Eq. 8:

$$\sigma_x = \sqrt{\frac{1}{n-1} \sum_{i=1}^n (x_i - \mu_x)^2} \quad (8)$$

The last operation is correlation calculated between two sets of the intensity values using Eq. 9:

$$\sigma_{xy} = \frac{1}{n-1} \sum_{i=1}^n (x_i - \mu_x)(y_i - \mu_y) \quad (9)$$

Previously calculated averages, variances and correlation are used to obtain the SSIM (Eq. 10):

$$SSIM_{xy} = \frac{(2\mu_x\mu_y + c_1)(2\sigma_{xy} + c_2)}{(\mu_x^2 + \mu_y^2 + c_1)(\sigma_x^2 + \sigma_y^2 + c_2)} \quad (10)$$

Constants c_1 and c_2 (small values) are used to prevent dividing by zero. SSIM values calculated for all windows are then averaged to obtain the mean structural similarity measure.

MSSIM takes into account the image luminance, contrast and structure comparison measures.

4. CONCRETE STONE PRODUCTION PROCESS

Nowadays, concrete stones are produced by fully automatic machines. Stones are formed on a special reinforced wooden product plate. On the plate a hollow mould is lowered. The whole forming set is laying on a vibrating table. Because each stone consists of two layers of concrete, the more robust in the lower part and more even (smooth) at the top, the mould is filled in two steps. Each of these steps is followed by vibration. That ensures proper mould fulfillment. The concrete in mould is tighten from above with the tightening stamp and the main vibration takes place. Fresh, wet stones are transported to curing racks. The curing racks can be enclosed as well as insulated and equipped with heating systems. Once the curing is completed stones are transported to the dry site of the line and packed. Simplified scheme of the process is presented in Fig. 2.

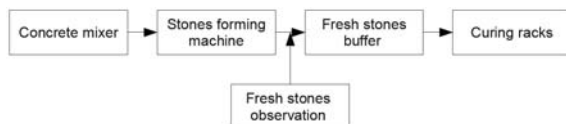


Fig. 2. Paving stones production process scheme

Because constant monitoring of the inner side of mould holes and the lower stamp side is difficult due to limited space and large amount of dust, the crucial place, in which the most of defects of stones (and indirectly of machine) can be identified, is located between the forming machine and the buffer before curing racks. There, the newly formed stones can be

measured and their surfaces can be examined. When some defects, mostly small-sized ones, are identified at this stage, decisions about further correction of process parameters, either presence of machine faults or excessive wear can be taken.

Among many different techniques proper for shape measurements and surface monitoring the choice of the vision system for fresh concrete stones observation is justified. The hardware side of this kind of system is relatively uncomplicated because the camera can be directly connected to the computer using USB or FireWire protocol. The main disadvantage of this approach is, in most cases, the small resolution of obtained images. Because of that some methods for image resolution enhancement are necessary to be applied.

5. IMAGE ACQUISITION AND PROCESSING

Image acquisition has been performed with the use of a CCD camera. A test stand near the fresh stones conveyor is presented in Fig. 3. The acquisition speed was 30 fps, and the exposure time was set to 1/4000 s. The resolution of acquired images were 1024x768 or 640x480 pixels and it depended on a type of camera used. During the research about 3 millions images, from the side and from above the production plate, were acquired, but only 10000 most valuable ones were processed. To obtain the reference images required for comparison with estimated synthetic images, only a fragment of the production plate (with fresh stones) was observed. Images were downsampled to generate input data for the resolution enhancement process. These downsampled images resolutions were 256x192 and 160x120 pixels, thus the upasampling factor was 4.

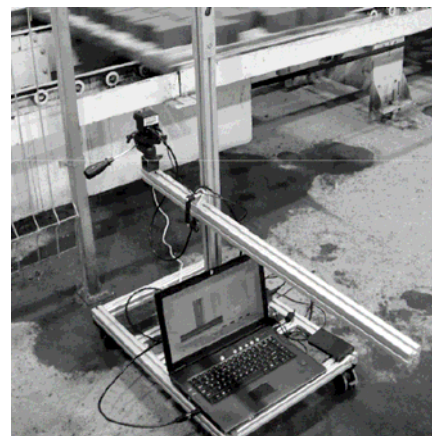


Fig. 3. The image acquisition stand

For the test purposes the normalization of images was performed. It consisted in the equalization of the histogram and gamma correction.

To detect faults on the concrete stone surface a simple processing of the interpolated and super resolved images was applied. The image before processing is presented in Fig. 4(a). At first,

a lookup table was used for histogram equalization (Fig. 4(b)). Then image binarization using adaptive thresholding was accomplished and the result of the operation is shown in Fig. 4(c). Next, the binary image was eroded (Fig. 4(d)). At last small objects were removed, to reduce the noise in the image. The image which was result of the whole processing procedure is presented in Fig. 4(e).

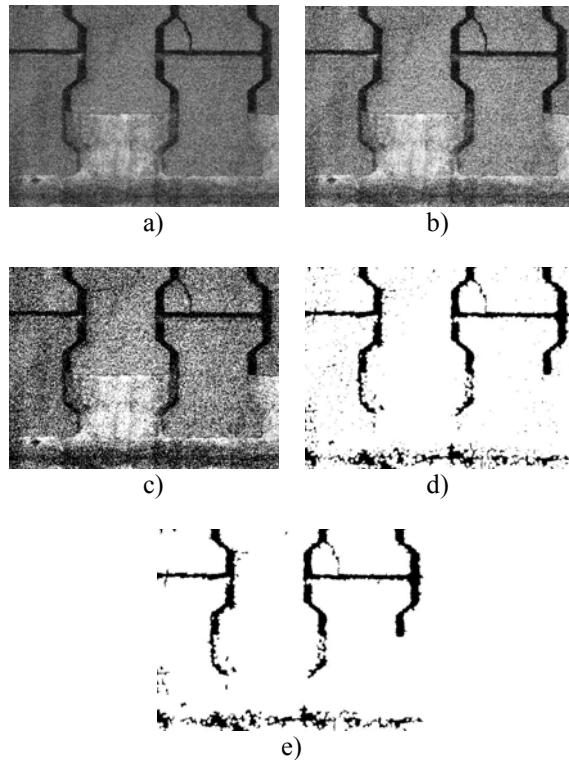


Fig. 4. Results of processing of synthetic images at particular procedure stages

6. RESULTS

In this subsection, the results of four SR reconstruction algorithms described in Sec. 2.2 were compared. The comparison was based on the error metrics described in Sec. 3. In Table 1 the obtained values of PSNR measure are gathered. It was stated that a typical PSNR value for the reconstructed image is greater than 20 dB [12]. PSNR values obtained for two and six frames were nearly equal, and it could be stated that during the reconstruction process the synthetic images of sufficient quality were possible to be generated. The lower value of PSNR obtained when eight frames were taken into consideration could be caused by too high translation between particular frames.

Tab. 1. PSNR values for proposed reconstruction methods

		Frames		
		2	6	8
SR method	Backprojection	17,63	17,72	17,91
	Normalized convolution	19,63	18,63	18,45
	Papoulis-Gerchberg	18,72	19,09	11,91
	POCS	19,63	19,45	19,36

The mean structural similarity values were presented in Table 2. Based on the results in Table 2, it could be stated that the MSSIM values analysis led to similar conclusions as it was in the case of the PSNR. Also it could be perceived that the image normalization led to better reconstruction results, through minimization of the influence of lightening conditions. Owing obtained result one stated that among all tested methods POCS was the most promising. The PSNR and especially MSSIM values confirmed that images reconstructed by the projection onto convex sets have the lowest visual degradation and noise. That made them a sufficient input for further image processing and analysis.

Exemplary results of synthetic image processing are presented in Fig. 5. The main difference between the superresolved and interpolated images is in the presence of noise.

Tab. 2. MSSIM values for proposed reconstruction methods

		Frames			
		2	6	8	
SR method	Real image	Backprojection	0,348	0,348	0,348
		Normalized convolution	0,408	0,400	0,400
		Papoulis-Gerchberg	0,392	0,372	0,101
		POCS	0,380	0,372	0,380
	Normalized image	Backprojection	0,832	0,836	0,836
		Normalized convolution	0,888	0,888	0,888
		Papoulis-Gerchberg	0,876	0,880	0,464
		POCS	0,896	0,892	0,893

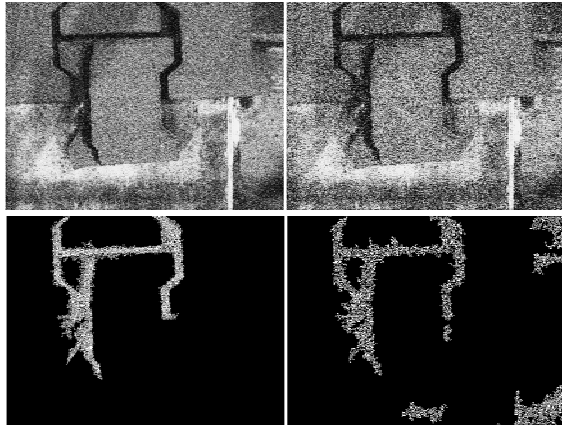


Fig. 5. Results of processing of synthetic images: SR (left), interpolated (right)

When analyzing the superresolved images the degree of noise is considerably lower as in comparison to the corresponding interpolated one. The noise reduction can lead to better selectivity in fault detection tasks. When dealing with relatively small faults in interpolated images they can be reduced to the noise level and removed. In this manner some valuable information can be lost.

7. CONCLUSIONS

As the result of the performed investigations one concluded that SR could be a promising method when sharp and clear small details are required to be found in a low resolution image. In the case of estimation of faults appearing during a production process SR methods provide images with minimized blur, which is a common effect of image interpolation.

The main disadvantage of presented methods is their computational complexity. High reconstruction time (exceeding 30 sec) makes the application in a real production process very difficult. The solution could be implementation of high efficiency and specialized DSP processors or elaboration of dedicated platforms based on FPGA chips.

REFERENCES

- [1] Bracewell R. N., editor. *The Fourier Transform and Its Applications*. McGraw-Hill, New York, 1965.
- [2] Gerchberg R. W. *Super-resolution through error energy reduction*. Journal of Modern Optics, 21(9), pp. 709-20, 1974.
- [3] Xiaoxin Guo, Zhiwen Xu, Yinan Lu, and Yunjie Pang: *An application of Fourier-Mellin transform in image registration*. In CIT '05: Proceedings of the The Fifth International Conference on Computer and Information Technology, pp. 619-623, Washington, DC, USA, 2005. IEEE Computer Society.

- [4] Irani M., Peleg S.: *Improving resolution by image registration*. CVGIP: Graph. Models Image Process., 53(3), pp. 231-239, 1991.
- [5] Mrak M., Grgic S., Grgic M.: *Picture quality measures in image compression systems*. In EUROCON 2003. Computer as a Tool. The IEEE Region 8, vol. 1, pp. 233-236, September 2003.
- [6] Muresan D. D., Parks T. W.: *Image interpolation using adaptive linear functions and domains*. IEEE 2001 Western New York Image Processing Workshop.
- [7] Papoulis A.: *A new algorithm in spectral analysis and band-limited extrapolation*. IEEE Trans. Circuits Syst, vol. 22, pp. 735-742, 1975.
- [8] Pham T. Q., van Vliet L. J., Schutte K.: *Robust fusion of irregularly sampled data using adaptive normalized convolution*. EURASIP J. Appl. Signal Process., 2006(1), pp. 236-236, 2006.
- [9] Stark H., Oskoui P. *High-resolution image recovery from image-plane arrays, using convex projections*. J. Opt. Soc. Am. A, 6(11), 1715-1726, 1989.
- [10] Zhou Wang, Bovik A. C., Sheikh H. R., Simoncelli E. P.: *Image quality assessment: From error measurement to structural similarity*. IEEE Trans. Image Processing, 13, pp.600-612, 2004.
- [11] Wheeler F. W., Hocror R. T., Barrett E. B.: *Super-resolution image synthesis using projections onto convex sets in the frequency domain*. In IS&T/SPIE Symposium on Electronic Imaging, volume 5674 of Conference on Computational Imaging, pages 479_490, January 2005.
- [12] Wu H. R. and Rao K. R.: *Digital Video Image Quality and Perceptual Coding (Signal Processing and Communications)*. CRC Press, Inc., Boca Raton, FL, USA, 2005.
- [13] Zieliński T. P.: *Cyfrowe przetwarzanie sygnałów. Od teorii do zastosowań*. W.T, Warszawa, 2007.



Wojciech JAMROZIK

is, since 2007, PhD student in the Department of Fundamentals of Machinery Design at Silesian University of Technology at Gliwice. The main areas of his interest are applications of vision system in diagnostic systems,

image processing, analysis and recognition. He deals also with the fusion of images and information.

**PRÓBKOWANIE SYGNAŁÓW DIAGNOSTYCZNYCH
 CZĘŚĆ V
 PRÓBKOWANIE SYGNAŁÓW O NIEOGRANICZONYM PAŚMIE ZA POMOCĄ
 NIEKLASYCZNYCH JĄDER**

Zenon SYROKA
 Uniwersytet Warmiński – Mazurski, Wydział Nauk Technicznych
 ul. Oczapowskiego 11, 10 –717 Olsztyn

Streszczenie

W pracy przedstawiono matematyczny opis próbkowania sygnałów diagnostycznych posiadających nieograniczone pasmo przy pomocy nieklasycznych jąder oraz próbkowania sygnałów określonych na zbiorach mierzalnych.

Słowa kluczowe: próbkowanie sygnałów, przestrzenie sygnałów, twierdzenie Shanona, zbiory mierzalne jądra reprodukujące.

SAMPLING OF THE DIAGNOSTIC SIGNALS
 PART V
 SIGNAL SAMPLING WITH INFINITE FREQUENCY BAND USING NON CLASICAL KERNELS

Summary

In this article is presented mathematical description of diagnostic signals sampling with infinite frequency band using non clasical kernels and sampling of signals defined on measurement sets.

Keywords: sampling signals, signals space, Shanon theorem,. measure sets reproducing kernel.

1. WPROWADZENIE

Istnieje bardzo duża grupa sygnałów diagnostycznych, która w dziedzinie czasu posiada informację zawartą w kształcie sygnału. Istotne są załamania, ostre wierzchołki, szybkie zmiany amplitudy i fazy. Takie zachowanie się sygnału w czasie powoduje, iż sygnał w dziedzinie częstotliwości posiada bardzo szerokie pasmo, teoretycznie nieskończone. Należy się zastanowić czy próbować sygnał w dziedzinie czasu a później transformować go do dziedziny częstotliwości czy też postępować odwrotnie.

W pracy przedstawione zostaną podstawy matematycznego podejścia do rozwiązania tych problemów.

**2. PRÓBKOWANIE SYGNAŁÓW
 O NIEOGRANICZONYM PAŚMIE**

Określimy na początku **twierdzenie Shannona –Nyquista w euklidesowej n-wymiarowej przestrzeni R^n** .

Jeżeli sygnał $s(t)$ spełnia warunek:

$$s(t) \in L^2(R^n) \cap C(R^n), \quad (1)$$

i jego transformata Fouriera jest ograniczona w n- wymiarowym przedziale:

$$[-\Pi B, +\Pi B], \quad (2)$$

dla pewnego $B \in R^n$, $B_j > 0$, $j = 1, 2, 3, \dots, n$, wtedy sygnał może być całkowicie odtworzony z próbek w punktach $\frac{k}{B}$, $k \in Z^n$, w następującej postaci:

$$s(t) = \sum_{k \in Z^n} s\left(\frac{k}{B}\right) \prod_{j=1}^n \text{sinc}(B_j t_j - k_j), \quad (3)$$

$$(t \in R^n).$$

Powyższy szereg jest absolutnie i jednostajnie zbieżny.

Pojawia się pytanie, czy możliwe jest odtworzenie sygnału z jego próbek gdy szerokość pasma dąży do nieskończoności. Zapiszemy ten warunek w postaci:

$$s(t) = \lim_{B \rightarrow \infty} \sum_{k \in Z^n} s\left(\frac{k}{B}\right) \prod_{j=1}^n \text{sinc}(B_j t_j - k_j) \quad (4)$$

$$(t \in R^n)$$

Ciągłość sygnału nie wystarcza, potrzebne są jeszcze inne ograniczające warunki.

Należy się zastanowić, czy istnieje sygnał $\varphi : R^n \rightarrow C$ dla, którego będzie spełniona zależność:

$$s(t) = \lim_{B \rightarrow \infty} \frac{1}{(\sqrt{2\Pi})^n} \sum_{k \in \mathbb{Z}^n} s\left(\frac{k}{B}\right) \varphi(Bt - k),$$

$$(t \in \mathbb{R}^n), \quad (5)$$

dla każdego ciągłego sygnału.

Warunkiem koniecznym i wystarczającym aby powyższy szereg był absolutnie i jednostajnie zbieżny na zwartych podzbiorach \mathbb{R}^n jest:

$$\sum_{k \in \mathbb{Z}^n} \varphi(t - k) = (2\Pi)^{n/2}. \quad (6)$$

W tym przypadku, funkcja $\varphi: \mathbb{R}^n \rightarrow \mathbb{C}$ nazywana jest **jądrem**.

Szereg (5) jest dyskretnym spłotem sygnału $s(t)$ i jądra φ . Klasycznym przykładem jądra [1] jest:

$$\varphi(t) := \sqrt{2\Pi}(1 - |t|), \quad t \in (-1, 1). \quad (7)$$

Wprowadzimy pojęcie **uogólnionego szeregu próbkującego**, określonego w następujący sposób [1]:

$$(S_B^\varphi s)(t) := \frac{1}{(\sqrt{2\Pi})^n} \sum_{k \in \mathbb{Z}^n} s\left(\frac{k}{B}\right) \varphi(Bt - k),$$

$$(8)$$

oraz **uogólnionej całki spłotowej**:

$$(I_B^\varphi s)(t) := \frac{\prod_{j=1}^n B_j}{(\sqrt{2\Pi})^n} \int_{\mathbb{R}^n} s(u) \varphi(B(t - u)) du,$$

$$(t \in \mathbb{R}^n; B \in \mathbb{R}_+^n). \quad (9)$$

I_B^φ jest ograniczonym, liniowym odwzorowaniem $C(\mathbb{R}^n)$ w siebie, i spełnia warunki:

$$\|I_B^\varphi\|_{[C, C]} = \|\varphi\|_{L^1}, \quad (B > 0), \quad (10)$$

$$\lim_{B \rightarrow \infty} \|I_B^\varphi s - s\|_C = 0, \quad (s \in C(\mathbb{R}^n)). \quad (11)$$

Określimy szczegółowe właściwości nieklasycznych jąder w przypadku nieograniczonego pasma.

Jeżeli $\varphi: \mathbb{R}^n \rightarrow \mathbb{C}$ jest ograniczoną funkcją taką, że szereg

$$\frac{1}{(\sqrt{2\Pi})^n} \sum_{k \in \mathbb{Z}^n} |\varphi(t - k)| < \infty, \quad (t \in \mathbb{R}^n), \quad (12)$$

jest absolutnie i jednostajnie zbieżny na zwartych podzbiorach \mathbb{R}^n i

$$\frac{1}{(\sqrt{2\Pi})^n} \sum_{k \in \mathbb{Z}^n} \varphi(t - k) = 1, \quad (t \in \mathbb{R}^n), \quad (13)$$

wtedy φ jest nazywane **jądrem** (dla **uogólnionych szeregów próbkujących**)

Moment rzędu $r \in \mathbb{N}_0$ jądra wynosi:

$$m_r(\varphi) := \max_{|j|=r} \sup_{t \in \mathbb{R}^n} \frac{1}{(\sqrt{2\Pi})^n} \sum_{k \in \mathbb{Z}^n} (t - k)^j \varphi(t - k)$$

$$(14)$$

Twierdzenie 1

Jeżeli $\varphi \in C(\mathbb{R}^n)$ jest jądrem, to spełnione są następujące warunki:.

1. Jeżeli $s: \mathbb{R}^n \rightarrow \mathbb{C}$ jest sygnałem ograniczonym na \mathbb{R}^n , to

$$\lim_{B \rightarrow \infty} (S_B^\varphi s)(t_0) = s(t_0) \quad (15)$$

dla wszystkich punktów $t_0 \in \mathbb{R}^n$, gdzie sygnał s jest ciągły.

2. $\{S_B^\varphi\}_{B>0}$ definiuje rodzinę ograniczonych, liniowych odwzorowań $C(\mathbb{R}^n)$ w siebie, mających normę:

$$\|S_B^\varphi\|_{[C, C]} = m_0(\varphi), \quad (B > 0), \quad (16)$$

i spełniających

$$\lim_{B \rightarrow \infty} \|S_B^\varphi s - s\|_C = 0,$$

$$(s \in C(\mathbb{R}^n)). \quad (17)$$

Dowód

Jednostajna zbieżność szeregu (12) na zwartych zbiorach powoduje, iż

$$m_0(\varphi) < \infty, \quad (18)$$

stąd funkcja

$$\frac{1}{(\sqrt{2\Pi})^n} \sum_{k \in \mathbb{Z}^n} |\varphi(t - k)|, \quad (19)$$

jest okresowa.

Odnosnie części pierwszej, jeżeli s jest ciągłe w t_0 , wtedy dla $\varepsilon > 0$ istnieje takie $\delta > 0$, że $|s(t) - s(t_0)| < \varepsilon$ dla każdego $t \in \mathbb{R}^n$ spełniającego $-\delta < t - t_0 < \delta$.

Stąd:

$$\begin{aligned} & (\sqrt{2\Pi})^n |s(t_0) - (S_B^\varphi s)(t_0)| \leq \\ & \leq \left\{ \sum_{k \in S_1} + \sum_{k \in S_2} \right\} \left| s(t_0) - s\left(\frac{k}{B}\right) \right| |\varphi(Bt_0 - k)| \\ & \leq \varepsilon (\sqrt{2\Pi})^n m_0(\varphi) + 2 \sup_{t \in \mathbb{R}^n} |s(t)| \sum_{k \in S_2} |\varphi(Bt_0 - k)| \end{aligned}$$

$$(20)$$

gdzie

$$S_1 := \{k \in \mathbb{Z}^n; -\delta B < Bt_0 - k < \delta B\}, \quad (21)$$

$S_2 := Z^n - S_1 = \{k \in Z^n \text{ istnieje najmniejsze } j \in \{1, \dots, n\} \text{ z } |B_j t_{0_j} - k_j| \geq \delta B_j\}$. (22)

Należy pokazać, iż ostatnia suma (20) jest zbieżna do 0 dla $B \rightarrow \infty$. Z (12) wynika, iż dla każdego $1 \leq j \leq n$ jest spełniona zależność:

$$\sum_{k \in Z^n} |\varphi(t - k)| = \sum_{k_j = -\infty}^{\infty} \left\{ \sum_{k_{[j]} \in Z^{n-1}} |\varphi(t - k)| \right\} < \infty, \quad (23)$$

gdzie:

$$k_{[j]} := (k_1, \dots, k_{j-1}, k_{j+1}, \dots, k_n), \quad (24)$$

i stąd zbieżność jest jednostajna na zwartych podzbiorach $K_j \in N$. Spełniony jest warunek:

$$\sum_{|k_j| \geq K_j} \left\{ \sum_{k_{[j]} \in Z^{n-1}} |\varphi(t - k)| \right\} < \varepsilon, \quad (t \in [0, 1]^n). \quad (25)$$

Zbiór K jest określony w następujący sposób:

$$K := \max_{1 \leq j \leq n} \{K_j\}. \quad (26)$$

Możemy zapisać:

$$\begin{aligned} \sum_{k \in S_2} |\varphi(Bt_0 - k)| &\leq \sum_{j=1}^n \left\{ \sum_{|B_j t_{0_j} - k_j| \geq \delta B_j} \sum_{k_{[j]} \in Z^{n-1}} |\varphi(Bt_0 - k)| \right\} \\ &= \sum_{j=1}^n \left\{ \sum_{|B_j t_{0_j} - k_j| \geq \delta B_j} \sum_{k_{[j]} \in Z^{n-1}} |\varphi(Bt_0 - \lfloor Bt_0 \rfloor - (k - \lfloor Bt_0 \rfloor))| \right\} \end{aligned} \quad (27)$$

Oznaczając:

$$m := k - \lfloor Bt_0 \rfloor \in Z^n, \quad (28)$$

mamy:

$$Bt_0 - \lfloor Bt_0 \rfloor \in [0, 1]^n. \quad (29)$$

Stąd:

$$\begin{aligned} \sum_{k \in S_2} |\varphi(Bt_0 - k)| &\leq \\ &\leq \sum_{j=1}^n \left\{ \sum_{|m| \geq \delta B - 1} \sum_{m_{[j]} \in Z^{n-1}} |\varphi(Bt_0 - \lfloor Bt_0 \rfloor - m)| \right\} \leq n\varepsilon \end{aligned} \quad (30)$$

dla każdego $W \geq \frac{k+1}{\delta}$, otrzymujemy więc (25).

Odnosnie części drugiej najpierw pokażemy, że $S_B^\varphi s$ jest jednostajnie ciągłe na R^n i pokażemy, że zależność:

$$(S_B^\varphi s)(t) = (S_1^\varphi g)(Bt), \quad (31)$$

gdzie

$$g(t) = s\left(\frac{t}{B}\right), \quad (32)$$

wystarczy rozważyć w przypadku $B = (1, \dots, 1)$. Wtedy szereg (12) będzie zbieżny jednostajnie w $[-1, 2]^n$. Weźmiemy $\varepsilon > 0$, $K_0 \in N$ i otrzymamy:

$$\sum_{k \in Z^n} |\varphi(t - k)| - \sum_{-K_0 \leq k \leq K_0} |\varphi(t - k)| < \frac{\varepsilon (\sqrt{2\Pi})^n}{3\|s\|_C}, \quad (33)$$

dla każdego $t \in [-1, 2]^n$. Jeżeli $\varphi \in C(R^n)$, to istnieje $0 < \delta < 1$ taka, że:

$$|\varphi(t) - \varphi(\dot{t})| \leq \frac{\varepsilon (\sqrt{2\Pi})^n}{3(2K_0 + 1)^n \|s\|_C}, \quad (34)$$

dla każdego $t, \dot{t} \in R^n$ i $-\delta \leq t - \dot{t} \leq \delta$. Teraz niech $t, \dot{t} \in R^n$ oraz spełnia warunek $-\delta < t - \dot{t} < \delta$, wtedy $t - \lfloor t \rfloor$ i $\dot{t} - \lfloor \dot{t} \rfloor = (\dot{t} + t) + t - \lfloor t \rfloor$ należy do $[-1, 2]^n$ i stąd $\lfloor t \rfloor - k \in Z^n$.

W związku z tym zapiszemy:

$$\begin{aligned} &(\sqrt{2\Pi})^n \|S_1^\varphi s(t) - S_1^\varphi s(\dot{t})\| \leq \\ &\leq \sum_{k \in Z^n} |s(k)| |\varphi(t - \lfloor t \rfloor - (k - \lfloor t \rfloor)) - \varphi(\dot{t} - \lfloor \dot{t} \rfloor - (k - \lfloor \dot{t} \rfloor))| \\ &\leq \|s\|_C \sum_{m \in Z^n} |\varphi(t - \lfloor t \rfloor - m) - \varphi(\dot{t} - \lfloor \dot{t} \rfloor - m)| \\ &\leq \|s\|_C \left\{ \sum_{-K_0 \leq k \leq K_0} |\varphi(t - \lfloor t \rfloor - k) - \varphi(\dot{t} - \lfloor \dot{t} \rfloor - k)| + \right. \\ &\quad \left. + \sum_{k \in Z^n} \sum_{-K_0 \leq k \leq K_0} \left\{ \varphi(t - \lfloor t \rfloor - k) + \varphi(\dot{t} - \lfloor \dot{t} \rfloor - k) \right\} \right\} \\ &\leq \|s\|_C \left\{ \sum_{-K_0 \leq k \leq K_0} \frac{\varepsilon (\sqrt{2\Pi})^n}{3(2K_0 + 1)^n \|s\|_C} + \frac{2\varepsilon (\sqrt{2\Pi})^n}{3\|s\|_C} \right\} \\ &\leq (\sqrt{2\Pi})^n \varepsilon. \end{aligned} \quad (35)$$

W przypadku gdy $j = 0$ i $c = 1$ można będzie w prosty sposób zweryfikacji zależności (13)

Jeżeli $\varphi \in C(R^n)$ będzie spełniać warunek $m_r(\varphi < \infty)$ dla pewnego $r \in N_0$ i niech $j \in N_0^n$ będzie stałą spełniającą warunek $|j| \leq r$. Wtedy następujące stwierdzenia są równoważne dla $c \in R$:

$$1. \frac{1}{(\sqrt{2\Pi})^n} \sum_{k \in \mathbb{Z}^n} (t-k)^j \varphi(t-k) = c \text{ p.w. w } R^n. \quad (36)$$

$$2. D^j \hat{\varphi}(2k\Pi) = \begin{cases} (-i)^{|j|} c & \text{dla } k = 0 \\ 0 & \text{dla } k \in \mathbb{Z}^n - \{0\} \end{cases}$$

$$\text{Szereg} \sum_{k \in \mathbb{Z}^n} \left| (t-k)^s \varphi(t-k) \right|, \quad (38)$$

jest jednostajnie zbieżny na wszystkich zwartych podzbiórach R^n , dla wszystkich $s \in N_0^n$, oraz dla $|s| = r$ ograniczenie p.w. ze stwierdzenia 1 zanika.

Przykładowymi nieklasycznymi jądrami są:

1. Jądro Fejera:

$$F(t) := \frac{1}{(\sqrt{2\Pi})^n} \prod_{j=1}^n \left(\frac{\sin\left(\frac{t_j}{2}\right)}{\frac{t_j}{2}} \right)^2, \quad (39)$$

$$(t \in R^n).$$

2. Jądro de la Vallee Poussina:

$$VP(t) := \left(\frac{4}{\sqrt{2\Pi}} \right)^n \prod_{j=1}^n \left(\frac{\sin\left(\frac{t_j}{2}\right) \sin\left(\frac{3t_j}{2}\right)}{t_j^2} \right) \quad (40)$$

$$(t \in R^n)$$

3. Jądro Bochnera – Rieszca :

$$BR(t) := 2^\gamma \Gamma(\gamma + 1) \|t\|_2^{-\left(\frac{n}{2} + \gamma\right)} J_{\frac{n}{2} + \gamma} \left(\|t\|_2 \right) \quad (41)$$

$$(t \in R^n).$$

dla $\gamma > \frac{n-1}{2}$. J_λ jest funkcją Bessela rzędu λ .

4. Jądro klinowe jednowymiarowe rzędu $r \geq 2$:

$$M_r(t) := \begin{cases} \sqrt{2\Pi} \sum_{v=0}^{\lfloor \frac{r}{2} - |t| \rfloor} \frac{(-1)^v r \binom{r/2 - |t| - v}{v}^{-1}}{v!(r-v)!}, & \text{dla } |t| \leq \frac{r}{2} \\ 0, & \text{dla } |t| > \frac{r}{2} \end{cases} \quad (42)$$

3. PRÓBKOWANIE SYGNAŁÓW W ZBIORACH MIERZALNYCH

Uogólniając przestrzenie Bernsteina B_σ^2 zdefiniujemy przestrzeń:

$$L_A^2 := \left\{ s \in L^2(R); \hat{s}(v) = 0 \text{ dla } v \notin A \right\}, \quad (1.37) \quad (43)$$

gdzie A jest mierzalnym podzbiorem R.

Sygnały należące do tej przestrzeni nazywane są pasmowo ograniczonymi do mierzalnego zbioru A.

Ponadto będziemy jeszcze używać przestrzeni zdefiniowanej następująco:

$$L^2(A) := \left\{ s \in L^2(R); s(u) = 0 \text{ dla } u \notin A \right\} \quad (44)$$

Zakładamy, że zbiór A spełnia warunek:

$$A \cap (A + 2k\Pi V) = \emptyset, (k \in \mathbb{Z} - \{0\}). \quad (45)$$

dla pewnego $V > 0$. Warunek ten implikuje, że A ma miarę skończoną:

$$m(A) \leq 2\Pi V. \quad (46)$$

Jeżeli A jest zbiorem ograniczonym to istnieje takie $|x| < M$, że dla każdego $x \in A$, zależność (46) jest spełniona dla każdego $V \geq \Pi^{-1}M$.

Jeżeli $s \in L_A^2$ i zbiór A spełnia warunek (45), wtedy taki sygnał można przedstawić w postaci:

$$s(t) = \frac{1}{\sqrt{2\Pi}} \int_A \hat{s}(v) e^{-ivt} dv \text{ p.w.} \quad (47)$$

Sygnał spełniający (47) jest ciągły.

Jeżeli sygnał $s \in L^2(A)$ gdzie A i $V > 0$, spełnia (45), to:

$$s(x + 2\Pi kV) \overline{s(x + 2\Pi lV)} = 0, \text{ dla } k \neq l. \quad (48)$$

Normy sygnałów w powyższych przestrzeniach można określić w poniższy sposób:

1. Jeżeli sygnał $s \in L^2(A)$ i $V > 0$ spełnia (45), wtedy norma sygnału wynosi:

$$\|s\|_{L^2} = \left\{ \frac{1}{\sqrt{2\Pi V}} \sum_{k=-\infty}^{\infty} \left| \hat{s}\left(\frac{k}{V}\right) \right|^2 \right\}^{1/2} \quad (49)$$

2. Jeżeli sygnał $s \in L_A^2$ i $V > 0$ spełnia (45), wtedy norma sygnału wynosi:

$$\|s\|_{L^2} = \left\{ \frac{1}{\sqrt{2\Pi V}} \sum_{k=-\infty}^{\infty} \left| s\left(\frac{k}{V}\right) \right|^2 \right\}^{1/2} \quad (50)$$

Poniższe dwa lematy są wprowadzeniem do twierdzenia o próbkowaniu sygnałów w zbiorach mierzalnych.

Lemat 2

Jeżeli $s, g \in L_A^2$ i $V > 0$ spełnia (45), wtedy:

$$\int_{-\infty}^{\infty} s(u) \overline{g(u)} du = \frac{1}{V} \sum_{k=-\infty}^{\infty} s\left(\frac{k}{V}\right) \overline{g\left(\frac{k}{V}\right)}. \quad (51)$$

Powyższa suma jest absolutnie zbieżna.

Lemat ten jest uogólnieniem lematu dotyczącego splotu w przestrzeni Bernsteina na sygnały należące do L_A^2 .

Lemat 3

Jeżeli $s, g \in L_A^2$ i $V > 0$ spełnia (45), wtedy:

$$(s * g)(t) = \frac{1}{\sqrt{2\Pi V}} \sum_{k=-\infty}^{\infty} s\left(\frac{k}{V}\right) g\left(t - \frac{k}{V}\right), \quad (52)$$

$(t \in R).$

Powyższy szereg jest absolutnie i jednostajnie zbieżny.

Dowód.

Zmienną $t \in R$, występującą w g (lemat (3)) zapiszemy w postaci $\overline{g(t -)}$. Stąd

$$\widehat{[\overline{g(t -)}]}(v) = e^{-ivt} \widehat{g}(v). \quad (53)$$

Absolutna i jednostajna zbieżność wynika z:

$$\begin{aligned} & \sum_{|k|>n} \left| s\left(\frac{k}{V}\right) \right| \left| g\left(t - \frac{k}{V}\right) \right| \leq \\ & \leq \left\{ \sum_{|k|>n} \left| s\left(\frac{k}{V}\right) \right|^2 \right\}^{1/2} \left\{ \sum_{|k|>n} \left| g\left(t - \frac{k}{V}\right) \right|^2 \right\}^{1/2} = \\ & = (2\Pi V^2)^{1/4} \left\{ \sum_{|k|>n} \left| s\left(\frac{k}{V}\right) \right|^2 \right\} \left\| g \right\|_{L^2}. \end{aligned}$$

Twierdzenie 4. O próbkowaniu w L_A^2

Jeżeli sygnał $s \in L_A^2$ i $V > 0$ spełnia (lemat 3), wtedy możemy odtworzyć sygnał z ciągu próbek $s\left(\frac{k}{V}\right)$ w następującej postaci :

$$s(t) = \frac{1}{\sqrt{2\Pi V}} \sum_{k=-\infty}^{\infty} s\left(\frac{k}{V}\right) \overset{\vee}{\chi}_A\left(t - \frac{k}{V}\right), \quad (54)$$

$(t \in R).$

$\overset{\vee}{\chi}$ oznacza odwrotną transformatę Fouriera funkcji charakterystycznej zbioru A. Szereg (2.13) jest absolutnie i jednostajnie zbieżny.

Dowód.

Zbiór A ma skończoną miarę oraz $\hat{s} \in L^1(R)$, stąd:

$$s(t) = \frac{1}{\sqrt{2\Pi}} \int_{-\infty}^{\infty} \hat{s}(v) \overset{\vee}{\chi}_A(v) e^{ivt} dv = \left[\hat{s} \overset{\vee}{\chi}_A \right] (t) = (s * \overset{\vee}{\chi}_A)(t) \quad (55)$$

$(t \in R).$

Dla $V = B$ i $A = [-\Pi B, \Pi B]$ oraz $\overset{\vee}{\chi}_{[-\Pi B, \Pi B]} = \sqrt{2\Pi} \operatorname{sinc}(BT)$ otrzymamy **klasyczne twierdzenie o próbkowaniu.**

BIBLIOGRAFIA

- [1] J. R Higgins, *Sampling Theory in Fourier and Signal Analysis - Foundations*. Clarendon Press, Oxford 1996.
- [2] A Jakubowski, *Repetitorium z przedmiotu „Miara i prawdopodobieństwo”*, UMK Toruń 2001.
- [3] A Kufner, J Kadlec, *Fourier Series*, Academia Prague 1971.
- [4] E. H Lieb, M Loss, *Analysis, Graduate Studies in Mathematics*, American Mathematical Society, 1998.
- [5] L Shwartz, *Sous espaces hilbertiens d'espaces vectoriels topologiques et noyaux associés*, Journal d'Analyse Mathematique, pp. 115-256, 1964.
- [6] E. M Stein, G Weiss, *Fourier Analysis on Euclidean Spaces*. Princeton University Press 1971.
- [7] Z. Syroka, *Próbkowanie sygnałów diagnostycznych. CzI. Próbkowanie w przestrzeni Hilberta z reprodukującym jądrem Shanona*. Diagnostyka Nr2(42)2007,s19-26.
- [8] Z. Syroka, *Próbkowanie sygnałów diagnostycznych. CzII. Próbkowanie w przestrzeni Hilberta z bazami harmonicznymi za pomocą nieklasycznych jąder*. Diagnostyka Nr2(42)2007,s27-34.
- [9] Z. Syroka, *Próbkowanie sygnałów diagnostycznych. CzIII. Próbkowanie*

w przestrzeni Hilberta z bazami wielomianowymi za pomocą nieklasycznych jąder. Diagnostyka Nr2(42)2007,s35-41.

Nadanie "Medalu im. Profesora Stefana Ziemby" prof. dr. hab. inż. Bogdanowi ŻÓŁTOWSKIEMU

Z przyjemnością informujemy, że Medal im. Profesora Stefana Ziemby za rok 2009 przyznany został przez Kapitułę medalu prof. dr. hab. inż. Bogdanowi ŻÓŁTOWSKIEMU.



Prof. B. Żółtowski ukończył studia w Wyższej Oficerskiej Szkole Samochodowej (inż.) oraz UAM w Poznaniu (mgr fizyki). Stopień naukowy doktora nauk technicznych uzyskał w 1979 na Wydziale Budowy Maszyn Politechniki Poznańskiej, stopień doktora habilitowanego nauk technicznych w 1985

na Wydziale Budowy Maszyn Politechniki Poznańskiej. Tytuł profesora nauk technicznych uzyskał w 1997r. W 1992 został prof. nadzw. ATR, a 1999 – profesor zwyczajny UTP.

Główne zainteresowania naukowe profesora obejmują rozwój najnowszej techniki, w szczególności dynamika i diagnostyka maszyn, budowa i eksploatacja maszyn ze szczególnym uwzględnieniem transportu. Posiada ponad 40 letni staż pracy naukowej i dydaktycznej. Równoległe z pracą naukowo-badawczą pełnił odpowiedzialne stanowiska:

- 1986 - 1988 docent w WOSWR i A w Toruniu,
- 1988 – 1992 docent w Akademii Techniczno-Rolniczej w Bydgoszczy,
- 2001 - 2002 prorektor ds. Nauki i Rozwoju PWSZ w Pile.
- 2008 – 2012 dziekan Wydziału Inżynierii Mechanicznej UTP.

Obecnie jest profesorem zwyczajnym UTP i dziekanem Wydziału Inżynierii Mechanicznej UTP w Bydgoszczy.

Jako uczoney i specjalista wniósł istotny wkład do interdyscyplinarnej nauki o eksploatacji złożonych obiektów technicznych, w szczególności w obszarze diagnostyki technicznej, posiadający niekwestionowany autorytet w naukowym środowisku krajowym i zagranicznym.

O jego autorytecie świadczy bezspornie liczba wykonanych:

- recenzji rozpraw habilitacyjnych: 9,
- recenzji rozpraw doktorskich: 19,
- opinii na tytuł profesora: 2,
- opinii na stanowisko profesora zwyczajnego: 2,
- opinii na stanowisko profesora nadzwyczajnego: 3

Należy też do wielu stowarzyszeń i komitetów jako:

- członek Institution of Diagnostic Engineers, Leicester, England – od 1989r.,
- członek EUROMECH (European Mechanics Society) od 2003,
- **Sekcja Podstaw Eksploatacji KBM PAN – członek od 1988, już drugą kadencję v-ce przewodniczący,**
- Członek Sekcji Dynamiki Układów Komitetu Mechaniki PAN od 2003,
- Zespół Diagnostyki SPE KBM PAN – od założenia (1992), sekretarz naukowy, v-ce przewodniczący, członek zarządu,
- **Polskie Towarzystwo Diagnostyki Technicznej** – od 1994, v-ce prezes, członek prezydium, członek,
- Sekcja Transportu Komitetu Transportu PAN – członek od 1996,
- redaktor działu „Diagnostyka” w Zagadnieniach Eksploatacji Maszyn PAN, od 1995 - 2006r.
- członek Rady Programowej wydawnictwa PTDT „DIAGNOSTYKA” od 2000r.,
- członek Komisji Motoryzacji Rolnictwa, filia PAN w Lublinie, od 2001r,
- członek komitetu naukowego ZEM od 2005r.,
- członek komitetu naukowego CIMAC od 2008r.

Dorobek naukowy Profesora dotyczy dziedziny: budowa i eksploatacja maszyn, specjalność: *diagnostyka techniczna, wibroakustyka, transport, eksploatacja maszyn.*

Bardzo aktywny w naukowym kształceniu młodej kadry:

- liczba zakończonych przewodów doktorskich – 11,
- otwarte przewody doktorskie – 3 ,
- opieka nad doktorantami – 3,
- udział (opiekun) w promocjach naukowych (habilitacyjnych) – 8 .

Był i jest nadal głównym organizatorem, cyklicznej, ogólnopolskiej konferencji naukowej: „*Diagnostyka maszyn roboczych i pojazdów*”, która jest organizowana co 3 lata. Zorganizowanych zostało już 13 konferencji, ostatnia była w 2009r.

Ma także bogaty dorobek wydawniczy, mianowicie:

- wydania zwarte, książki, skrypty – 26, w tym: 1 poz. w j. rosyjskim i 1 poz. w j. hiszpańskim,
- publikacje: 400 w tym 35 w j. ang. Nadal wykazuje dużą aktywność publikacyjną. W 2009 roku ukazały się między innymi opracowania książkowe których prof. B. Żółtowski jest współautorem:

1. **Żółtowski B., Castaneda Heredia L. F.: Estudio de explotación de vehículos ferroviarios.** EAFIT University, Colombia, 2009 s. 298. - udział własny 80%.

2. **Żółtowski B.,** Castaneda Heredia L. F.: **Badania pojazdów szynowych. Transport.** Wydawnictwo UTP, Bydgoszcz, 2009 s.220. - udział własny 90%.

oraz opracowanie zwarte pod jego redakcją **Elementy diagnostyki maszyn roboczych i pojazdów.** Zbiór materiałów, Radom – Bydgoszcz – Borówno, WN ITE – PIB.

Brał udział w 32 konferencjach zagranicznych i 100 krajowych. Zrealizował 9 różnych projektów badawczych własnych i promotorskich. Aktualnie realizuje 2 projekty badawcze (promotorski, POIG - badania rozwojowe).

Za swoją działalność był wielokrotnie wyróżniany w formie nagród i odznaczeń. Do najważniejszych można zaliczyć: Złoty Krzyż Zasługi – 1986 r., Krzyż Kawalerski Orderu Odrodzenia Polski – 2002r., Medal Komisji Edukacji Narodowej – 2004, wiele medali za zasługi dla obronności kraju, 2 nagrody naukowe (zespołowe) Ministra Nauki, wiele nagród Rektora ATR/UTP.

Uzasadnienie wniosku o nadanie „Medalu”

W okresie dotychczasowej działalności prof. Bogdan Żółtowski wniósł istotny wkład do nauki w formie bardzo wielu publikacji książkowych, monografii i artykułów o zasięgu krajowym i międzynarodowym, referatów wydanych w zwartych materiałach konferencyjnych, zarówno krajowych jak i zagranicznych. Dorobek ten ma nie tylko walory poznawcze, istotne dla nauki, lecz także walory użyteczne o istotnym znaczeniu praktycznym.

Prof. Bogdan Żółtowski ma także ogromne zasługi na niwie organizacyjnej jako kierownik katedry, dziekan wydziału i prorektor ds. nauki a także organizator wielu konferencji naukowych, dzięki czemu stworzył sprzyjające warunki do rozwoju młodych kadr naukowych. Prowadził bardzo wiele różnych projektów badawczych, w tym własne i promotorskie, a aktualnie realizuje 2 projekty badawcze (promotorski, POIG - badania rozwojowe). Wypromował przy tym 11 doktorów, jest aktualnie promotorem 3 przewodów doktorskich i opiekunem 3 osób pragnących uzyskać stopień naukowy doktora nauk technicznych.

Cieszy się niekwestionowanym autorytetem w środowisku krajowym i zagranicznym. Jest członkiem wielu prestiżowych towarzystw i komitetów zarówno krajowych jak i zagranicznych. Został za swoją działalność wielokrotnie wyróżniony odznaczeniami, medalami i nagrodami.

I co ważne, prof. B. Żółtowski wiele lat blisko współpracował z prof. Stefanem Ziębą.

W podsumowaniu stwierdzam, że osiągnięcia publikacyjne w 2009r. prof. dr hab. inż. Bogdana Żółtowskiego zasługują na wielką uwagę. Osiągnięcia te można uznać za wybitne, mające nie tylko walory poznawcze ważne dla nauki, lecz także użyteczne istotne dla praktyki. Wobec tego uważam, że prof. Bogdan Żółtowski w pełni zasługuje na wyróżnienie „Medalem im. Profesora Stefana Ziemby”.

*Prof. dr hab. inż. Jerzy GIRTLEK, prof. zw. PG
Zespół Niezawodności
Sekcji Podstaw Eksploatacji
Komitetu Budowy Maszyn
Polskiej Akademii Nauk*

**Żółtowski B.,
Castaneda Heredia L. F.**
Estudio de explotación de vehículos ferroviarios.
EAFIT University, Colombia, 2009

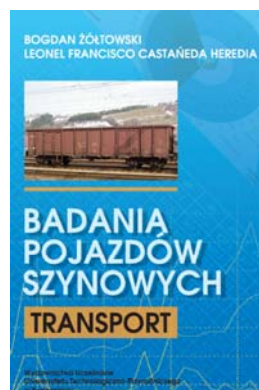


Umiejscowienie problematyki książki w obrębie nauki eksploatacja maszyn jest zgodne z poglądami o składowych dziedzinach eksploatacji maszyn, na którą składają się: niezawodność, tribologia, diagnostyka techniczna, bezpieczeństwo i teoria eksploatacji.

Procesy starzenia i zużycia są źródłem (przyczyną) generowania różnych procesów, a następnie sygnałów diagnostycznych, które coraz częściej wykorzystuje się do sterowania systemem eksploatacji pojazdów szynowych. Nieodłącznym istnieniu pojazdów szynowych destrukcja wymaga prowadzenia uzasadnionych czynności obsługowych, przywracających ich zdolność użytkową. Problemowi temu poświęcono wiele miejsca w tym opracowaniu wskazując na czynności i procedury konieczne w praktycznym działaniu podczas użytkowania pojazdów szynowych.

Wiele z poruszonych powyżej zagadnień zostało szczegółowo omówionych w opracowaniach wybitnych eksploatorów, a przedstawione w monografii stanowią ich ważne uzupełnienie. Publikacja jest przeznaczona dla szerokiego grona odbiorców: użytkowników pojazdów szynowych, studentów wydziałów mechanicznych, inżynierów mechaników i młodych pracowników naukowych oraz pracowników zaplecza technicznego zakładów pracy. Treści tej książki stanowią o zakresie programowym DIAGNOSTYKI TECHNICZNEJ MASZYN wprowadzonej, dużymi staraniami autorów, w Kolumbii do programów kształcenia.

**Żółtowski B.
Castaneda Heredia L. F.**
Badania pojazdów szynowych. Transport.
Wydawnictwo UTP, Bydgoszcz, 2009



Dla zapewnienia trwałości, niezawodności i gotowości środków systemów transportu kolejowego i zmniejszenia ryzyka zagrożenia bezpieczeństwa w czasie użytkowania, niezbędna jest implementacja metod diagnostyki technicznej. Metody i środki nowoczesnej

diagnostyki technicznej pozwalają utrzymywać stan zdatności środków transportu kolejowego poprzez ciągłe monitorowanie ich stanu technicznego. Pozwalają także na badania spełniania wymagań stawianym środkom transportu kolejowego w zakresie obowiązujących standardów bezpieczeństwa i komfortu jazdy.

W pracy przedstawiono metodykę badania i opisu zmian stanu dynamicznego pociągu oraz zasady kształtowania bezpieczeństwa i komfortu systemów kolejowych, według obowiązujących norm fabrycznych (dla obiektów nowych, badanych w fabryce).

Podczas realizacji poszczególnych zadań wykorzystano dostępne i opracowano nowe procedury akwizycji i przetwarzania sygnałów diagnostycznych i oceny stanu, zweryfikowano praktycznie metodę wyboru punktów pomiarowych w diagnostyce drganiowej, zaproponowano zmodernizowane procedury w obszarze badania wrażliwości diagnostycznej i wyznaczania wartości granicznych mierzonych sygnałów, zweryfikowano wybrane modele diagnostyczne oraz przeanalizowano wybrane metody prognozowania dla potrzeb wyznaczania terminu następnego diagnozowania.

Opisane dokonania w badaniach eksploatacyjnych pojazdów szynowych skupiają się na opracowanym i wdrożonym do eksploatacji przenośnym systemie diagnostycznym.

Materiał zawarty w tej książce w dużej mierze opiera się na opisie metodologii badań zrealizowanych we współpracy zespołu UTP z Bydgoszczy oraz EAFIT – GEMI z Kolumbii, w których to badaniach autorzy tej książki uczestniczyli jako wykonawcy.

Diagnostyka

Obszar zainteresowania czasopisma to:

- ogólna teoria diagnostyki technicznej
- eksperymentalne badania diagnostyczne procesów i obiektów technicznych;
- modele analityczne, symptomowe, symulacyjne obiektów technicznych;
- algorytmy, metody i urządzenia diagnozowania, prognozowania i genezowania stanów obiektów technicznych;
- metody detekcji, lokalizacji i identyfikacji uszkodzeń obiektów technicznych;
- sztuczna inteligencja w diagnostyce: sieci neuronowe, systemy rozmyte, algorytmy genetyczne, systemy ekspertowe;
- diagnostyka energetyczna systemów technicznych;
- diagnostyka systemów mechatronicznych i antropotechnicznych;
- diagnostyka procesów przemysłowych;
- diagnostyczne systemy utrzymania ruchu maszyn;
- ekonomiczne aspekty zastosowania diagnostyki technicznej;
- analiza i przetwarzanie sygnałów.

Topics discussed in the journal:

- General theory of the technical diagnostics,
- Experimental diagnostic research of processes, objects and systems,
- Analytical, symptom and simulation models of technical objects,
- Algorithms, methods and devices for diagnosing, prognosis and genesis of condition of technical objects,
- Methods for detection, localization and identification of damages of technical objects,
- Artificial intelligence in diagnostics, neural nets, fuzzy systems, genetic algorithms, expert systems,
- Power energy diagnostics of technical systems,
- Diagnostics of mechatronic and antropotechnic systems,
- Diagnostics of industrial processes,
- Diagnostic systems of machine maintenance,
- Economic aspects of technical diagnostics,
- Analysis and signal processing.

Wszystkie opublikowane artykuły uzyskały pozytywne recenzje wykonane przez niezależnych recenzentów.

All the published papers were reviewed positively by the independent reviewers.

Druk:

Centrum Graficzne „GRYF”, ul. Pieniężnego 13/2, 10-003 Olsztyn, tel. / fax: 089-527-24-30

Oprawa:

Zakład Poligraficzny, UWM Olsztyn, ul. Heweliusza 3, 10-724 Olsztyn
tel. 089-523-45-06, fax: 089-523-47-37



XXXVIII
Ogólnopolskie Sympozjum
DIAGNOSTYKA MASZYN

Wisła 28.02 ÷ 05.03.2011 r.

organizatorzy:

Wydział Transportu Politechniki Śląskiej
Polskie Towarzystwo Diagnostyki Technicznej
Zespół Diagnostyki Sekcji Podstaw
Eksploatacji KBM PAN

KOMUNIKAT NR 1

Wszystkie opublikowane w czasopiśmie artykuły uzyskały pozytywne recenzje, wykonane przez niezależnych recenzentów.

Redakcja zastrzega sobie prawo korekty nadesłanych artykułów.

Kolejność umieszczenia prac w czasopiśmie zależy od terminu ich nadesłania i otrzymania ostatecznej, pozytywnej recenzji.

Wytoczne do publikowania w DIAGNOSTYCE można znaleźć na stronie internetowej:

<http://www.diagnostyka.net.pl>

Redakcja informuje, że istnieje możliwość zamieszczania w DIAGNOSTYCE ogłoszeń i reklam.

Jednocześnie prosimy czytelników o nadsyłanie uwag i propozycji dotyczących formy i treści naszego czasopisma.

Zachęcamy również wszystkich do czynnego udziału w jego kształtowaniu poprzez nadsyłanie własnych opracowań związanych z problematyką diagnostyki technicznej. Zwracamy się z prośbą o nadsyłanie informacji o wydanych własnych pracach nt. diagnostyki technicznej oraz innych pracach wartych przeczytania, dostępnych zarówno w kraju jak i zagranicą.